ДОКЛАДЫ
АКАДЕМИИ НАУК СССР

SOVIET PHYSICS

"Doklady"

VOLUME 2 NUMBER 4

A Translation
of the
"Physics Section"
of the

Proceedings of the Academy of Sciences of the USSR

(RUSSIAN ORIGINAL VOL. 115, NOS. 1-6)

Published by the
AMERICAN INSTITUTE OF PHYSICS
INCORPORATED

SOVIET PHYSICS

"Doklady"

A translation of the "Physics Section" of the Proceedings of the Academy of Sciences of the USSR.

A publication of the

AMERICAN INSTITUTE OF PHYSICS

Governing Board

ALLEN V. ASTIN
WALTER S. BAIRD
JESSE W. BEAMS
HANS A. BETHE
RAYMOND T. BIRGE
RICHARD H. BOLT
FRANKLIN D. DEXTER
IRVINE C. GARDNER
SAMUEL A. GOUDSMIT
CHARLES KITTEL
HUGH S. KNOWLES
WINSTON E. KOCK
R. BRUCE LINDSAY
WILLIAM F. MEGGERS
WALTER C. MICHELS
R. RONALD PALMER
ROBERT F. PATON
JOSEPH B. PLATT
RALPH A. SAWYER
HENRY D. SMYTH
MARK W. ZEMANSKY

Officers and Staff

FREDERICK SEITZ
Chairman, Governing Board
ELMER HUTCHISSON
Director
HENRY A. BARTON
Associate Director
WALLACE WATERFALL
Executive Secretary
MARK W. ZEMANSKY
Treasurer
THEODORE VORBURGER
Advertising Manager
RUTH F. BRYANS
Publication Manager
KATHRYN SETZE
Assistant Treasurer
ALICE MASTROPIETRO
Circulation Manager
EUGENE H. KONE
Director of Public Relations

American Institute of Physics Advisory Board on Russian Translations

ROBERT T. BEYER, *Chairman*

FREEMAN DYSON, DWIGHT GRAY, MORTON HAMERMESH, VLADIMIR ROJANSKY

Advisory Editor, Soviet Physics—"Doklady": VLADIMIR ROJANSKY, Ramo-Wooldridge Corporation, Los Angeles, California

SOVIET PHYSICS—"Doklady" is a bi-monthly journal published by the American Institute of Physics for the purpose of making available in English reports of current Soviet research in physics as contained in the "Physics Section" of the Proceedings of the Academy of Sciences of the USSR. The Proceedings appears thirty-six times per year and the "Physics Sections" are accumulated and English translations of them are published in six issues per year.

Transliteration of the names of Russian authors follows the system employed by the Library of Congress.

This translating and publishing project was undertaken by the Institute in the conviction that dissemination of the results of research everywhere in the world is invaluable to the advancement of science. The National Science Foundation of the United States encouraged the project initially and is supporting it in large part by a grant. Translation and printing are being handled by Consultants Bureau, Inc.

The American Institute of Physics and its translators propose to translate faithfully all of the scientific material in the "Physics Section" of the Proceedings of the Academy of Sciences of the USSR appearing after January 1, 1956. The views expressed in the translated material, therefore, are intended to be those expressed by the original authors, and not those of the translators nor of the American Institute of Physics.

One volume is published annually. Volume 2 will consist of six issues and will contain all scientific material published in the "Physics Section" of the original Russian journal during the 1957 calendar year.

Subscription Prices:

Per year (6 issues)	
United States and Canada	$25.00
Elsewhere	27.50
Back Numbers	
Single copies	$ 5.00

Subscriptions should be addressed to the American Institute of Physics, 335 East 45th Street, New York 17, New York.

Copyright by American Institute of Physics 1958

SOVIET PHYSICS

"Doklady"

VOLUME 2, NUMBER 4 JULY-AUGUST, 1957

MEASUREMENT OF THE PRIMARY COSMIC-RAY FLUX AT 31° N LATITUDE

K. I. Alekseeva, S. I. Brikker, N. L. Grigorov,
F. D. Savin and N. A. Shcherbakov

(Presented by Academician D. B. Skobeltsin on January 15, 1957)

During the measurement of the cross section for the inelastic interaction of cosmic-ray particles with hydrogen and carbon nuclei we have measured the intensity of the hard component in the stratosphere. These measurements have enabled a determination to be made of the primary-particle flux at the top of the atmosphere. This paper contains a description of the equipment used for measuring the interaction cross section and the results of measurement of the hard-component intensity (the results of cross section measurements will be published in papers to follow).

A diagram of the arrangment of counters and absorbers in the equipment is given in Fig. 1b. The telescope, accepting vertical cosmic-ray particles, consists of three rows A, B and C of self-quenching counters connected into a triple-coincidence circuit and a row D of hodoscope counters covering nearly all the solid angle of the apparatus. To separate the penetrating component of the cosmic rays an absorber, consisting of 8 cm Pb and 0.9 cm Al, was placed between rows B and C of counters. The absorber Σ of the material studied (the solid line indicates the outline of the graphite absorber, the dashed line that of the paraffin absorber), for example graphite, was placed on a trolley and every three minutes was automatically moved into the space between the rows A and B of counters or removed from it, so that the measurements with graphite and the measurements of the background (as also measurements with paraffin and graphite) were made in turn. The telescope and absorbers were surrounded by a large number of hodoscope counters which were used to register the secondary particles produced by the interaction of protons with nuclei of carbon, hydrogen and lead. In addition, all three rows A, B, C of telescope counters were also connected to the hodoscope.*

---

*Counter dimensions: A, B, C: diameter 22 mm, geometric length 200 mm, 5 counters in every row; D, K, L, M, N: diameter 33 mm, length 300 mm; G, H: diameter 33 mm, length 550 mm; K_1, L_1, M_1, N_1: diameter 22 mm, length 300 mm. The thickness of the glass walls of the counters was 1.0-1.5 mm.

The pulse, controlling the operation of the apparatus, was a triple coincidence of the counter rows, A, B and C. However, in processing the results we always took into account only those cases where the triple coincidence was accompanied by a discharge of one of the counters in row D (quadruple coincidence). To register showers we used a valve hodoscope with thyratrons MTH-90, connected into the valve anode circuits, indicating the discharge of a given hodoscoped counter. All the data from the equipment were telemetered to earth and recorded on a moving photographic film. During the transmission of the hodoscope data the Rossi valves were blocked by means of a special circuit to avoid the superposition of signals referring to different control pulses. The resolving time of the telescope was equal to $3 \cdot 10^{-6}$ sec, that of the hodoscope varied from $1 \cdot 10^{-5}$ to $2 \cdot 10^{-5}$ sec depending on the group of counters discharged.

In 1954-1955 seven telescopes were flown by us in the stratosphere: two with a graphite absorber (16 $g\,cm^{-2}$) and an absorber of 8 cm Pb+ 0.9 cm Al; four with absorbers of paraffin (18.8 $g\,cm^{-2}$) and graphite (16.0 $g\,cm^{-2}$) and an absorber of 8 cm Pb+ 0.9 cm Al; one with absorbers of paraffin (18.8 $g\,cm^{-2}$) and graphite (16.0 $g\,cm^{-2}$) without any lead absorber in the telescope.*

To determine the primary-particle flux it was adequate to determine the altitude dependence of the total counting rate of the equipment (subtracting only the non-local showers) and to extrapolate to the top of the atmosphere. Nevertheless, since the investigation of the altitude dependence for the electron-nuclear showers produced in lead under conditions of good geometry was of interest by itself, we carried out the data processing as follows:

1. Single particle – a discharge of one counter in each of the four rows D, A, B and C of the telescope without a shower discharge of the hodoscope counters K, K_1, L, L_1, M, M_1, N, N_1, B, C, E.

2. A shower produced outside the absorbers (non-local shower). We considered events to fall into this category when, for example, more than one counter in row A or D was discharged. In addition, a considerable number of non-local showers were also recorded by the counters immediately surrounding the graphite (paraffin) absorber (counters K, K_1, B, L, L_1). These showers, whose number remained practically unchanged when Σ was placed in the telescope, were eliminated by taking into account the different results obtained with graphite – background and paraffin – graphite.

3. A shower in the upper part of the apparatus – a discharge of one counter in rows A and D due to the particle producing the shower and, in addition, a discharge of at least two counters from those immediately surrounding the graphite (paraffin) absorber (counters K, K_1, B, L, L_1) independently of a discharge of counters near the lead. Cases of interaction in the graphite (paraffin) were included in the class of showers produced in the class of showers produced in the upper part of the apparatus.

4. A shower in the lower part of the apparatus (a shower produced in lead) – the discharge of one counter in rows D, A, B and C and a discharge of counters M, M_1, N, N_1 or the discharge of one counter in rows D, A and B and a discharge of at least two counters in one of the rows C or E. Therefore, in the lower part of the apparatus we recorded only those showers produced in lead which did not contain particles moving upwards. An examination of the hodoscope pictures of such showers showed that in 96% of the cases a straight line could be drawn through the discharged counters within the acceptance angle of the apparatus corresponding to the path of the particle producing the shower in the lead. This means that the contribution from non-local showers does not exceed 4%. For the determination of the total particle flux at the top of the atmosphere we used the measure-

---

* We determined the geometrical factor of the apparatus by comparing the measured intensity at the starting point (geomagnetic latitude 31° N, atmospheric depth 900 g/cm^2) with the absolute intensity of the cosmic rays at the same point determined by calculation. In the calculations we used the following data: 1) the absolute intensity of the penetrating component at sea level at 51° latitude under 15 cm Pb (0.500 ± 0.006 particles $\cdot\, cm^{-2} \cdot min^{-1} \cdot sterad^{-1}$) [1], converted to the value for an absorber of 8 cm Pb (0.534 particles $\cdot\, cm^{-2} \times min^{-1} \cdot sterad^{-1}$); 2) the magnitude of the latitude effect between 51° N and 31° N – 0.95 [2]; 3) the altitude dependence for altitudes between 1000 and 900 $g \cdot cm^{-2}$ – 1.20 ± 0.01 (according to the data of N. L. Grigorov). From these data it follows that the absolute intensity at the starting point is equal to $0.534 \times 1.20 \times 0.95 = 0.609$ particles $\times\, cm^{-2} \times min^{-1} \times sterad^{-1}$. The geometrical factor for the various telescopes did not differ by more than ± 5 percent from the mean value of 16.5.

ments of the penetrating component of the cosmic rays without the graphite (paraffin) absorber. A correction was made to the results for the effect of δ-showers and chance coincidences).*

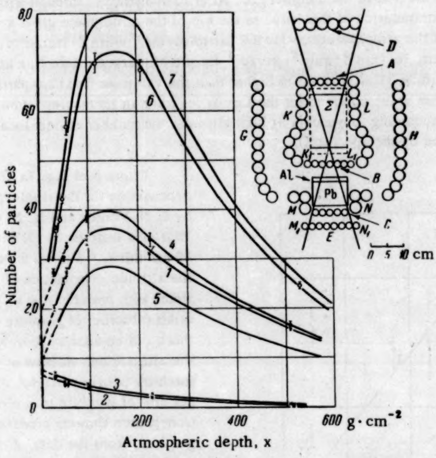

Fig. 1. a) The altitude dependence of the c. r. intensity at geomagnetic latitude 31° N. 1) 5) Hard component, 6, 7) total intensity; b) diagram of the arrangement of counters and absorbers.

Figure 1a gives in absolute units the altitude dependence of the flux of particles which did not produce a nuclear interaction in the Pb + Al absorber (single particles, curve 1) and the altitude dependence for the nuclear interactions produced in the absorber Pb + Al, registered in the lower part of the apparatus (curve 2).

An analysis of the showers observed in the upper part of the apparatus, with and without the lead in the telescope, showed that the number of showers produced in the lead having particles discharging counters K, K_1, B, L, L_1 was about 30% of the number of showers registered by the lower part of the apparatus. Taking into account the possibility of a small error in the counting with our equipment and also the data available in the literature on the angular distribution of shower particles obtained with nuclear emulsion [3], we took the magnitude of the correction for the "backward flux" in the case of showers produced in lead to be 15% of the number of showers registered in the lower part of the apparatus. Curve 3 gives the number of nuclear interactions in the absorber Pb + Al corrected for the showers produced in lead with upward-moving particles.

---

*During 1949-1950 K. I. Alekseeva and S. N. Vernov carried out special experiments to study the production of δ-electrons by the total component of the cosmic rays in a graphite absorber (area of absorber 20×20 cm^2, thickness 1.0 g $\times$ cm^{-2}) at various altitudes. It was found that the ratio of the number of δ-showers (mainly showers with not more than three counters discharged) to the number of single particles recorded at all altitudes from sea level to 20 km remains practically constant. A small increase in the ratio for heights above 20 km was mainly caused by an admixture of electron-nuclear showers produced in the absorber used.

In our equipment the δ-showers, registered by the counters surrounding the lead (M, M_1, N, N_1, C and E), were (6.85 ± 0.12) percent of the number of single particles registered. The number of δ-showers produced in the upper part of the apparatus in the absence of the absorber Σ was (3.00 ± 0.15) percent. The particles accompanied by δ-showers we included in the class of single particles which did not produce a nuclear interaction in the absorbers.

Curve 4 is the sum of curves 1 and 3, i. e., represents the total flux of particles of the hard component (particles which either interacted in the absorber Pb + Al or passed straight through without interaction) at various altitudes. The extrapolation of this curve to the top of the atmosphere gives a value of the primary particle flux at the top of the atmosphere equal to 2.0 particles $\cdot$ cm$^{-2}\cdot$ min$^{-1}\cdot$ sterad^{-1}. Foreign authors [4] give the value 2.7-2.8 particles $\cdot$ cm$^{-2}\cdot$ min$^{-1}\cdot$ sterad^{-1} for the primary-particle flux at the top of the atmosphere at geomagnetic latitude 31° N, about 30% higher than the value we find (2.0 particles $\cdot$ cm$^{-2}\cdot$ min$^{-1}\cdot$ sterad^{-1}). It is possible that the higher value obtained for the flux arises from an incomplete subtraction of the contribution from non-local showers (according to our data at high altitudes the number of non-local showers is about 30% of the total number registered by the apparatus).

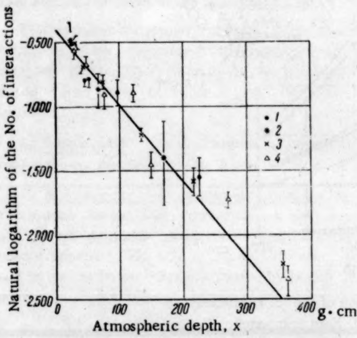

Fig. 2. The altitude dependence of the number of electron-nuclear showers produced in lead. Geomagnetic latitude 31° N: 1) electron-nuclear showers from 8cm Pb + 0.9 cm Al (1955, the authors of this paper); 2) 8 cm Pb (1954, the authors of this paper); 3) 10 cm Pb (1951, S. N. Vernov and A. N. Charakhchyan); 4) 8 cm Pb (1951, S. N. Vernov and A. M. Kulikov).

Curve 5 of Fig. 1a also gives the altitude dependence for the single-particle flux obtained by S. N. Vernov and A. N. Charakhchyan [5] in 1951 at a latitude 31° N with a lead absorber 10 cm thick.* Curves 6 and 7 of Fig. 1a give the altitude dependence of the flux of single particles with path lengths > 20 g/cm^2 of light materials (absorber of graphite (paraffin) 17.4 g/cm^2 thick and counter walls ~ 2.6 g/cm^2) and Curve 7 the altitude dependence of the total cosmic-ray intensity (single particles with path lengths > 20 g per cm^2 of graphite plus electron-nuclear and electron-photon showers produced in 20 g per cm^2 of graphite) from the data of the apparatus without the lead absorber.

A comparison of the results referring to the altitude dependence of the electron-nuclear showers obtained by us and other authors [5] at geomagnetic latitude 31° N is given in Fig. 2. In this Figure, the atmospheric depth $\underline{x}$ is plotted along the abscissa in g per cm^2 and along the ordinate the natural logarithm of the number of interactions produced in lead. All the data given are normalized to our data of 1955. We see that, within the limits of statistical accuracy indicated in the figure (the statistical error is shown for all points), the altitude dependence of the electron-nuclear showers, obtained with a large number of "additional counts" [5] and without these (our data) are in agreement. From these data, the absorption mean free path for charged particles of the shower-producing component in the stratosphere at a latitude of 31° N is equal to 150-170 g/cm^2.

The authors express their thanks to V. P. Grigorov for carrying out the balloon flights into the stratosphere during the expedition.

M. V. Lomonosov Moscow State University

Received January 12, 1957.

---

* The discrepancy between Curves 5 and 1 can be partly explained by the fact that in the experiments of S. N. Vernov and A. N. Charakhchyan the value for the absolute vertical flux of the penetrating component at sea level and latitude 51° N, under 10 cm Pb was taken to be 0.46 particles $\cdot$ cm$^{-2}\cdot$ min$^{-1}\cdot$ sterad^{-1}.

LITERATURE CITED

[1] K. I. Greisen, Phys. Rev. 61, 212 (1942).

[2] M. A. Pomerantz, Phys. Rev. 98, 105 (1955).

[3] U. Camerini, J. H. Davies, et al., Phil. Mag. 42, 1241 (1951).

[4] J. Wilson (ed.), Cosmic Ray Physics (Moscow, 1954), vol. 1, p. 254.

[5] S. N. Vernov and A. N. Charakhchian, Doklady Akad. Nauk, 91, 487 (1953).

ON THE LINES ASSOCIATED WITH THE $L\alpha_{1,2}$ AND $L\beta_1$ LINES OF THE GERMANIUM SPECTRUM

G. P. Borovikova and M. I. Korsunsky

(Presented by Academician G. V. Kurdiumov February 6, 1957)

In paper [1] data were given on the lines $L\beta_3$ and $L\beta_4$ of the germanium L-spectrum corresponding to the transitions $L_I \rightarrow M_{III}$ and $L_I \rightarrow M_{II}$. The discovery of the lines $L\beta_3$ and $L\beta_4$ confirmed the statement made in that paper that the L-series of the germanium spectrum has not been fully investigated. Since germanium is one of the most important semiconductor materials we have considered it necessary to continue the study of the L-series of the germanium spectrum with the aim of establishing the presence of lines not found earlier, particularly, the lines $L\beta_6$ ($L_{III} \rightarrow N_I$ transition), $L\gamma_5$ ($L_{III} \rightarrow N_I$ transition) and $L\gamma_{2,3}$ ($L_I \rightarrow N_{II-III}$ transition). The experimental arrangement used was described in paper [1].

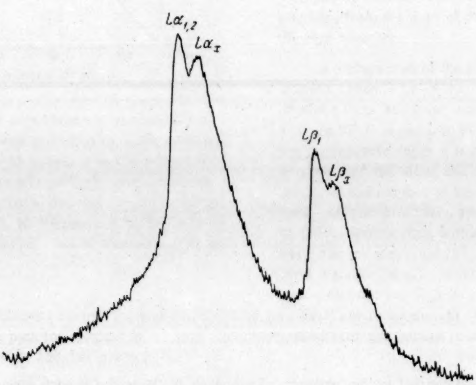

Fig. 2.*

The L-series x-ray spectrum of germanium, obtained for the range of wavelengths 10150 to 10400 XU, containing the lines $L\alpha_{1,2}$ ($L_{III} \rightarrow N_{IV-V}$ transition) and $L\beta_1$ ($L_{II} \rightarrow M_{IV}$ transition) was found to be very different from the spectrum given in the literature [2]. Bright lines were found in our photographs in the vicinity of the lines $L\alpha_{1,2}$ and $L\beta_1$, on the short wavelength side. Figure 1 shows a photograph of this region of the spectrum, while Fig. 2 gives the corresponding microphotogram. In the photograph of Fig. 1 the image density is greater than one so that this photograph does not give a correct representation of the relative intensities of the lines. The image density of the photograph from which the microphotogram was taken does not exceed 0.5. At this image density, according to the data in the literature and our control photographs, the ratio of the relative intensities of the separate lines remains constant for different exposure times.

---

*(Fig. 1 and the caption to Fig. 2 are missing from the Russian text – Publisher.)

As seen from the microphotogram given, the double-peaked line obtained from the superposition of $L\alpha_{1,2}$ and an unknown line ($L\alpha_X$) is asymmetric. This shows that the width of the unknown line $L\alpha_X$ is greater than the width of $L\alpha_{1,2}$. If we take into account that the magnitudes of the maximum intensity of these lines are comparable then it must be recognized that in the L-series spectrum of germanium the number of transitions producing the line $L_{\alpha X}$ is greater than the number of those producing the line $L\alpha_{1,2}$ (considered the brightest line of the L-series). A similar situation is found in the case of the line associated with $L\beta_1$.

The considerable intensity of the lines $L\alpha_X$ and $L\beta_X$ makes the assumption that these lines are the satellite lines of $L\alpha_{1,2}$ and $L\beta_1$ very improbable. For this reason it was decided to see whether these indistinct lines $L\alpha_X$ and $L\beta_X$ could be normal diagram lines whose presence in the L-series germanium spectrum could be expected, but which for some reason were not discovered up to the present. The fact that the lines associated with $L\alpha_{1,2}$ and $L\beta_1$ are separated from the latter by approximately the same distance makes it probable that these lines are connected with the transition from the levels L_{II} and L_{III} to the level N_I. To verify this, the graph of Fig. 3 was constructed giving the dependence of ΔE, the difference in energy between the levels M_{IV} and N_I, on the atomic number Z. It can be seen that ΔE, in the range of atomic numbers from 35(Br) to 42(Mo), is approximately a linear function of Z. The value of ΔE for germanium, determined by us from the photographs, falls on the extrapolated part of this line. Therefore, it may be concluded that the positions of the lines $L\alpha_X$ and $L\beta_X$, found by us, coincide with the positions of the lines $L\beta_6$ ($L_{III} \rightarrow N_I$ transition) and $L\gamma_5$, ($L_{II} \rightarrow N_I$ transition). From this, we consider that the discovered lines, associated with the $L\alpha_{1,2}$ and $L\beta_1$ lines of germanium, to be the diagram lines $L\beta_6$ and $L\gamma_5$, respectively.

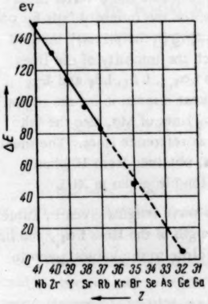

Fig. 3. The dependence of the energy interval ΔE between the M_{IV} and N_I levels on the atomic number Z.

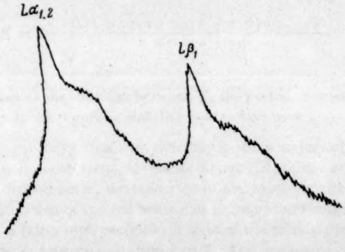

Fig. 4. Microphotogram of the GeO_2 spectrum.

We obtained a further confirmation of this conclusion by comparing the L-series spectra of germanium and GeO_2, whose microphotogram is given in Fig. 4. As can be seen from the comparison of Figs. 2 and 4, the relative intensities of the $L\alpha_{1,2}$ and $L\beta_1$ lines in the case of germanium dioxide is considerably less than in the case of pure germanium. This is to be expected, since the germanium in the GeO_2 molecule is tetravalent and donates four electrons to the oxygen. These four electrons include both N_I electrons. We also observed the weakening of the lines $L\beta_6$ and $L\gamma_5$ of pure germanium as the result of long exposures with the primary method for exciting the spectrum. Apparently, in this case the surface of the germanium becomes oxidized. It must be noted that, the photographs of the germanium L-series spectrum obtained by Gwinner [2] are similar to our photographs in the case of germanium dioxide. Since Gwinner excited the spectrum by the primary method he had to deal with oxidized and not pure germanium. This is confirmed also by the fact that Gwinner did not observe any significant difference between the spectra of pure germanium and its dioxide. Because the L-series radiation of germanium is produced in the surface layer (the thickness of the layer in which the intensity falls by one-half is 2.5×10^{-5} cm), it is obvious that with the strong heating of the anode occuring in the primary method of excitation the surface of the anode becomes oxidized, as a consequence of which the intensity of the lines $L\beta_6$ and L_{γ_5} markedly decreases. We have measured the wave lengths of the lines $L\alpha_{1,2}$, $L\beta_1$, $L\beta_6$ and $L\gamma_5$ The calculation of the wave lengths was made from the microphotograms. The linear dispersion for the region of reflection angles used is approximately 32 XU/mm. The 5th order $K\alpha_1$ and $K\alpha_2$ lines of Mn, also the 7th order Cu $K\alpha_1$ and $K\alpha_2$ lines, served as reference lines. The mean values of the measured wave lengths, obtained from 10 photographs, are given in Table 1 (wave lengths given in XU).

TABLE 1

	$L\alpha_{1,2}$	$L\beta_6$	$L\beta_1$	$L\gamma_5$
Ge	10408	10365	10146	10103
GeO_2	10415		10155	

The error in the values for the wave lengths given in Table 1 is 2 XU. The values for the wave length of the lines $L\alpha_{1,2}$ and $L\beta_1$ in the case of germanium oxide are close to the values given in reference books for pure germanium.

In addition to the lines $L\beta_6$ and $L\gamma_5$, we have discovered in the L-series spectrum of germanium a faint line with a wave length (8709 ± 5) XU, corresponding, because of its position, to the line $L\gamma_{2,3}$ ($L_I \rightarrow N_{II-III}$ transition). The presence of this line in the germanium spectrum shows that in solid germanium the level N_{II-III} is partially filled by electrons (this is confirmed by the presence of the line $K\beta_2$ in the germanium spectrum). On this basis it can be considered that the level N_I must be filled in germanium and, consequently, the transitions $L_{III} \rightarrow N_I$ and $L_{II} \rightarrow N_I$ must take place.

V. I. Lenin Kharkov Polytechnical Institute

Received February 5, 1957.

LITERATURE CITED

[1] G. P. Borovikova, and M. I. Korsunskii, Doklady Akad. Nauk 114, 6, 1192 (1957).*

[2] E. Gwinner, Z. Physik 108 (1938).

---

*[Soviet Physics — Doklady, p. 281].

ON NEW POSSIBILITIES TO RAISE THE EFFICIENCY OF CHARGED-PARTICLE ACCELERATORS

E. M. Moroz

(Presented by Academician D. B. Skobeltsin February 27, 1957)

In this paper a new type of accelerator with a magnetic field constant in time is proposed – an accelerator with touching stable particle trajectories. The magnetic system of this accelerator consists of three or more sectors with uniform magnetic fields.

Figure 1 shows one of the variants of the system considered. The magnet consists of four sectors having equal magnetic field strengths $H_1 = H_2 = H_3 = H_4 = H$. In the gaps between the sectors the magnetic field is absent. In one of the gaps, at the point A through which pass the trajectories of particles of any energy, a small accelerating element of small dimensions is situated. The stability of the particle motion is secured by the action of the magnetic field at the edges of the magnetic sectors where the particles enter and leave the magnetic sectors. The vertical ω_z, and the horizontal ω betatron-oscillation frequencies, depend on φ_1, the deflection angle of the particles in the first sector, on the angle φ between the boundary of the second sector and the line of symmetry of the magnetic field, on the length of the linear interval $l_{BB'} = 2rx$ between the symmetric halves of the magnetic system, on the length $l_{BG} = rkx$ between the points of intersection of the magnetic-sector boundaries BC and DG with the boundary JG parallel to the line of symmetry and, also, on the adjustable angles γ_B and $\gamma_{B'}$ (not shown in Fig. 1) which can be conveniently used to control the vertical and horizontal focusing of the particles. The region of stability, determined as usual by the relation $|\cos \mu_{rz}| < 1$ is found to be quite extensive, and, for example, in the case $\varphi = 40.5°$, $\varphi_1 = 84°$, $k = 0$, reaches the value $x = 0.77$. The perimeter L of the orbit is determined by the equations

$$L = L_0 + 2\pi r K; \quad L_0 = 4rx\left[1 + k\,\frac{(1+\cos\varphi_1)\sin\varphi}{2\cos(\varphi+\varphi_1)}\right];$$

$$K = 1 - \frac{2(1+\cos\varphi_1)\cos(\varphi+\varphi_1/2)\sin(\varphi_1/2)}{\pi\cos(\varphi+\varphi_1)}.$$

In the case $L_0 = 0$, which causes the relation between T, the period of revolution, and E, the total energy, to be of the form $T = E$, a constant, the region of stability is also extensive.

The use of the proposed magnetic systems with touching particle trajectories in cyclotrons will enable the replacement of the dees by a small accelerating element situated outside the magnetic field, the reduction of the size of the gap between the magnet poles, the reduction of the power required for the magnets and the radiofrequency system and the intensification of the ion beam due to improved focusing. The constancy of the period of revolution can be secured up to fairly high energies (in spite of the relativistic increase of mass) by choosing the appropriate dependence of the quantities φ, φ_1 and k on E. The number of possible resonances capable of producing betatron oscillations is smaller in the proposed magnet system than in systems of the Thomas type [1] or in the divided systems, with uniform magnetic fields in the sectors, proposed by the author jointly with M. S. Rabinovich [2, 3] and by R. S. Livingston [4].

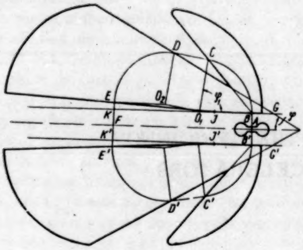

Fig. 1.

The possibility of extracting ions from any cyclotron orbit will enable the energy of the extracted beam to be changed (without altering the radiofrequency or the intensity of the magnetic field) by moving the extractor in the gap CD (or any other gap) between the sectors.

The magnet system considered here can, apparently, be also used with advantage in phasotrons (synchrocyclotrons).

The proposed magnet systems are of particular value in the case of microtrons [5, 6]. The use of the system considered will result in a reduction of the distance between the poles of the microtron magnet and will eliminate the fairly serious drawback of the microtron – lack of stability, and this will lead to a big increase of the attainable energy and electron-beam intensity.

One of the main advantages of the microtron, by comparison with other cyclic electron accelerators, is the ease with which the injection and extraction of the particles can be made because of the considerable distance between adjacent orbits. In particular, the extraction of the accelerated particles from microtrons of the type considered can be easily accomplished by means of a movable magnetic extractor of length $l \approx (r/2)(\varphi + \varphi_1 - \pi/2)$. At the same time the extraction of the particles occurs in one and the same direction, independently of the orbit from which the particles are taken.

The use of divided magnetic systems with touching stable trajectories of the accelerated particles must lead to further development of microtrons and to the extension of their use as injectors for synchrotrons, as generators of very short ($\tau < 10^{-11}$ sec), powerful electron pulses, as micro-radio-wave generators, and also generators of γ-ray pulses, efficient neutron sources, etc.

In conclusion, the author expresses his gratitude to V. I. Veksler for his interest in the present work, to M. S. Rabinovich for his interest in the work and for valuable advice and to A. A. Kolomensky for helpful discussions.

P. N. Lebedev Physical Institute of the
USSR Academy of Sciences

Received, February 20, 1957.

LITERATURE CITED

[1] L. H. Thomas, Phys. Rev. 54, 580, 588 (1938).

[2] E. M. Moroz, Doklady Akad. Nauk 108, No. 3, 436 (1956). *

[3] E. M. Moroz and M. S. Rabinovich (CERN Symposium, Proc. Geneve, 1, 1956), p. 547.

[4] R. S. Livingston, Ind. Eng. Chem. 48, (8), 1231 (1956).

[5] V. I. Veksler, Doklady Akad. Nauk 43, No. 8, 346 (1944).

[6] E M. Moroz, Doklady Akad. Nauk 106, No. 6, 986 (1956). * *

*[Soviet Physics – Doklady, p. 326].

* *[Soviet Physics – Doklady, p. 137].

ISOTOPE SEPARATION ON THE PASSAGE OF AN ATOMIC BEAM THROUGH A REGION OF IONIZATION

K. D. Sinelnikov, B. G. Safronov, G. G. Aseev and
Yu. S. Azovsky

1. Simple theoretical considerations show the possibility of isotope separation during the passage of an atomic beam, consisting of a mixture of isotopes, through a region in which it is subjected to electron bombardment. Let us assume that the atomic beam consists of particles with masses m_1 and m_2, where $m_1 < m_2$, and comes from a region of temperature T; then the mean kinetic energy of the particles will be 3/2(kT) and

$$v_1/v_2 = \sqrt{m_2/m_1},$$

where v_1 and v_2 are the root-mean-square velocities of the corresponding isotopes.

Let us assume now that such a beam is bombarded by electrons with an energy sufficient to ionize it, while the ions formed are continually removed from the beam. Then, the attenuation of the beam will be governed by the relation:

$$J(x + \Delta x) = J(x) - \frac{J(x)}{v} j\sigma\Delta x, \tag{1}$$

where J(x) and J(x + Δx) are the current densities of atoms at the points x and x + Δx; v is the mean velocity of the atoms in the beam, consequently $J(x)/v = \rho$ is the number of neutral atoms per unit volume; j is the electron-current density; σ the cross section for the ionization of atoms by electrons of a given energy.

Integrating Equation (1), we obtain:

$$J(x) = J(0)\exp\left[-\frac{j\sigma}{v}x\right], \tag{2}$$

where J(0) is the atomic-beam density before it goes through the region of ionization.

Let us denote the densities of the beams of particles with masses m_1 and m_2 by J^1 and J^2. Therefore, before their entry into the region of ionization, the ratio of the concentrations of particles with different masses is equal to $J^1(0)/J^2(0)$.

After the beam has moved a distance x into the ionized region the ratio of concentrations will be expressed as follows:

$$\frac{J^1(x)}{J^2(x)} = \frac{J^1(0)}{J^2(0)}\exp\left[-j\sigma\left(\frac{1}{v_1} - \frac{1}{v_2}\right)x\right], \tag{3}$$

in which it is assumed that the effective ionization cross sections σ_1 and σ_2 of the isotopes are approximately equal, i. e., $\sigma_1 = \sigma_2 = \sigma$. Substituting into (3) the expression for v_1 / v_2, we obtain:

$$\frac{J^1(x)}{J^2(x)} = \frac{J^1(0)}{J^2(0)} \exp\left[-\frac{j\sigma}{v_1}\left(1-\sqrt{\frac{m_2}{m_1}}\right)x\right], \tag{4}$$

or expanding $\sqrt{m_2/m_1}$ in a series and using only the first term:

$$\frac{J^1(x)}{J^2(x)} = \frac{J^1(0)}{J^2(0)} \exp\left[\frac{j\sigma}{v_1}\,\frac{\Delta m}{m_1}\,x\right]. \tag{5}$$

For the beam of mass m_1 we find from Equation (2):

$$\frac{j\sigma}{v_1} = \ln\frac{J^1(0)}{J^1(x)}. \tag{6}$$

Substituting (6) into (5), we have:

$$\frac{J^1(x)}{J^2(x)} = \frac{J^1(0)}{J^2(0)} \exp\left[\frac{\Delta m}{m_1}\ln\frac{J^1(0)}{J^1(x)}\right], \tag{7}$$

or

$$\frac{J^1(x)}{J^2(x)} = \frac{J^1(0)}{J^2(0)}\left(\frac{J^1(0)}{J^1(x)}\right)^{\Delta m/m_1} \tag{8}$$

From Equation (8) it follows that as the result of the attenuation of the beam its composition changes towards an enrichment by the light particles.

2. To discover this effect, it was necessary to use a system which would make it possible, on the one hand, to ionize the beam and, on the other, to remove and bind the ions formed. These requirements were met by the manometer triode valve LM-2.

The atomic beam, in passing through LM-2, is ionized by the electrons emitted from the cathode and accelerated by the grid potential. The region of ionization, in this case, is the space inside the grid and outside it up to a distance in which the electrons, having passed through the grid, are retarded to an energy equal to the ionization potential of the substance investigated.

The distribution of potentials in LM-2 ($V_{\text{anode-cathode}} = -25\,\text{v}$, $V_{\text{anode-grid}} = -225\,\text{v}$) is such, that the ions must be attracted towards the anode and the cathode. Ions striking the cathode will be re-emitted, while the ions striking the anode will remain on it, which will cause an attenuation of the beam and a change of its composition. This can be found by analyzing the beam with a mass-spectrometer.

Figure 1 shows the system, consisting of five LM-2 valves connected in series, which was used by us for discovering and studying the phenomenon described. Mercury, whose vapor could pass through the whole system of five valves, was used as the working substance. During the adjustment of the valves the vessel containing mercury was covered and the supply of mercury vapor to the system was stopped. During the experiment the temperature of the mercury was ~ 20° C, of the valve glass ~ 50-60° C and of the nickel leads ~ 100-120° C.

The pressure in the valves during the experiment did not exceed ~ $2 \cdot 10^{-5}$ mm Hg. The power supply to the valves came from five separate type VI-3 vacuum gages. The mercury which passed through the system was analyzed by the mass-spectrometer MS-2. The measurements were made by the single-ray method using the outer mercury isotopes (198 and 204), i. e., the ionic currents, corresponding to the isotopes 198 and 204, were measured in succession and then their ratio was calculated. The measurements were made as a series of 10 determinations of the ratio, from which the arithmetic mean was calculated. The time taken for one series of measurements was about 2 minutes.

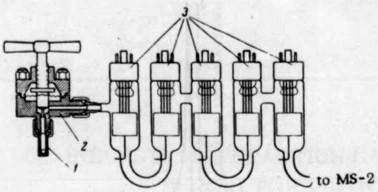

Fig. 1. 1) Vessel containing mercury; 2) valve; 3) LM-2 valves.

The reduction of the current of mercury vapor (the experiment was carried out using a current of mercury vapor and not an atomic beam) was determined from the ratio of the heights of the 198-isotope peaks before and after ionization. The measurement of the composition of the mercury-vapor current was made alternately with the valves switched off (standard composition) and switched on (altered composition). Before the experiment was begun it was shown that no operating condition of the valves, except that in which the ionization of the gas takes place, leads to a change in the isotopic composition of the mercury.

TABLE 1

Observed	Calculated
0.62±0.34	0.34±0.14
0.62±0.28	0.28±0.14
0.69±0.34	0.42±0.14
0.62±0.34	0.34±0.14
0.76±0.34	0.48±0.14
1.58±0.28	1.17±0.14

3. Table 1 gives the results of the measurements and the calculated values of Δ, the degree of enrichment of the emerging mercury current. The measurements were made for each of the five valves in turn and for all of the lamps connected in series (last row of Table 1).

$$\Delta = \frac{J^1(x)/J^2(x) - J^1(0)/J^2(0)}{J^1(0)/J^2(0)} \cdot 100\,\%.$$

The value of Δ was calculated from Equation (8) using the experimental data on the attenuation of the current.

From the comparison of the experimental and calculated results, it can be seen that they agree well within the limits of experimental error, however, it must be remarked that all the measured values are higher than the calculated. The deviation of the measured value from the calculated is particularly noticeable in the case of the valves connected simultaneously (last row of Table 1). We can only make some conjectures about the possible reasons for such a discrepancy.

First of all, it must be taken into account that in the region of ionization there is a molecular current of mercury vapor and not an atomic beam, consequently the mercury atoms can collide with the walls and electrodes and repeatedly traverse the region of ionization. Further, in the calculations, the distribution of the atomic velocities in the beam was not taken into account; however, an evaluation of the errors introduced because of this (using the normal maxwellian distribution of velocities) gave a correction smaller by a factor of 10 than the discrepancy observed.

Using the valve system (Fig. 1) measurements were carried out to determine the valve saturation time. Two curves are given in Fig. 2: the deviation of the current composition from the standard one as a function of time and the change in the 198-isotope current with time. During the periodic checks of the standard composition the upper curve shows sudden increases, which shows to what extent ionization weakens the mercury current. From the graphs it can be seen that the enrichment gradually falls, in the same way as the attenuation, although even after 20 hours' operation the current is enriched to an appreciable extent.

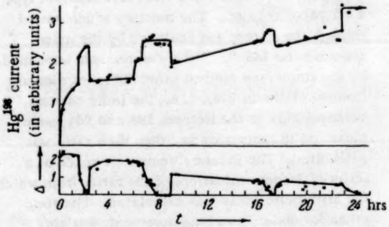

Fig. 2. The testing of five LM-2 valves by filling them with mercury vapor with a periodic check on the standard mixture.

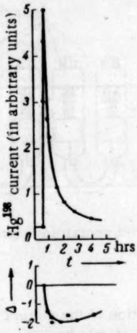

Fig. 3. The desorption of Hg from the LM-2 valve anodes.

It must be pointed out that changing the current (by altering the inflow of mercury by 1/3) during the operation of the valves did not lead to a change in its composition. This is seen from the increase in intensity of the upper curve and by the constancy of the composition, lower curve, during the period from 6 to 7 hours. (Fig. 2). The composition of the mercury desorbed from the anodes after a long operating time was also checked. The desorption of the anodes was carried out by switching the valves to "heating" in the absence of mercury vapor. As the result of the desorption a sharp increase in the intensity was observed, during which the composition of the desorbed mercury was lower than the standard, i. e., the mercury was enriched by the heavier isotope. Two graphs are given in Fig. 3: the changes of the intensity and the composition of the desorbed mercury.

It must be pointed out that the phenomenon described could be a source of serious systematic errors in accurate mass-spectrometer measurements.

Physico-technical Institute of the
Academy of Sciences Uk. SSSR

Received February 25, 1957.

INELASTIC INTERACTION CROSS SECTION OF CARBON NUCLEI FOR PROTONS ABOVE 7 Bev

K. I. Alekseeva and N. L. Grigorov

(Presented by Academician D. V. Skobeltsyn January 15, 1957)

The present paper presents measurements of the inelastic collision cross section of carbon for protons at geomagnetic latitude 31° N in the stratosphere [1], at energies for which we previously observed slight inelasticity of collisions with light nuclei [2].

The instruments for measuring the inelastic collision cross section consisted (see Figs. 1a and 2a) of a telescope (counter trays D, A, B, C) surrounded by a large number of hodoscopic counters which recorded secondary particles from interactions in graphite and lead (counters D, A, B, C also were arranged hodoscopically). Between rows B and C there was located an absorber consisting of 8 cm of lead and 0.9 cm of aluminum. Into the space between counters A and B there was inserted and removed at 3-minute intervals the absorber Σ under investigation, which consisted of pulverized graphite, of density 1.0-1.1 g/cm^3 and thickness 16.0 g/cm^2.* A detailed description of the apparatus for determining the cross section was given in [3]. We used the experimental data for altitudes above 20 km. A rough estimate shows that where determining the cross section for

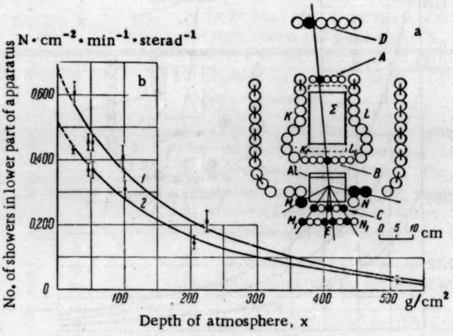

Fig. 1. 1) Number of showers produced in lead, measured without graphite absorber in telescope; 2) number of showers from lead measured with graphite absorber (16.8 g/cm^2) in telescope.

---

* The solid line shows the position of the graphite absorber inside the telescope; the dashed line shows the position of the paraffin absorber.

a flux of protons of which 80% had kinetic energy greater than 7 Bev, of which about 3/4 had the average energy ~ 12 Bev. The inelastic proton-carbon cross section was determined by two methods.

TABLE 1

Depth of atmosphere x, g/cm²		Showers in lead				Range of inelastic interaction L_p^c, g/cm²	Cross section of inelastic interaction σ_p^c, mb*
		without graphite in telescope $N^C_{\text{shower Pb}}$, cm^{-2} · min · sterad^{-1}	with graphite in telescope $N^C_{\text{showers Pb}}$, cm^{-2} min^{-1} · sterad^{-1}	$\frac{N^C_{\text{showers Pb}}}{N^b_{\text{showers Pb}}}$			
53.0	33.7	0.452±0.026	0.369±0.024	0.816±0.070	0.754±0.030	63^{+12}_{-9}	315±50
46.7		0.454±0.024	0.370±0.019	0.815±0.059			
25.0		0.609±0.029	0.431±0.012	0.709±0.039			

---

*Graphite thickness 16.8 g/cm².

1. Method of reducing the flux of the shower-producing component during passage through graphite. With the aid of hodoscopic counters we were able to study the cases in which a single charged particle (proton) passed without interaction through the upper part of the telescope (through the first three rows of counters D, A

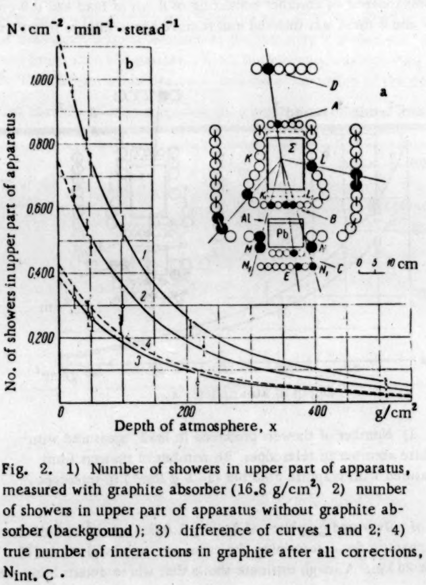

Fig. 2. 1) Number of showers in upper part of apparatus, measured with graphite absorber (16.8 g/cm²) 2) number of showers in upper part of apparatus without graphite absorber (background); 3) difference of curves 1 and 2; 4) true number of interactions in graphite after all corrections, $N_{\text{int. C}}$.

and B above the lead absorber) and underwent inelastic interactions in the lead block. We selected only those instances in which the particles produced in the lead shower entered counters C, E, M, M_1, N, N_1 in the lower part of the apparatus around the lead (the so-called showers without "reverse flux" of particles). An illustration is the shower from lead depicted in Fig. 1a (the triggered counters are denoted by filled circles). The number of such showers from lead is proportional to the flux of individual shower-producing particles entering the lead and is reduced upon insertion of the graphite into the telescope in accordance with the reduced flux of individual particles.

Figure 1b shows the counts of interactions in lead, with graphite in the telescope $N^{C}_{\text{int. Pb}}$ (Curve 2) and without the graphite $N^{b}_{\text{int. Pb}}$ (Curve 1) at different depths of the atmosphere. The curves were corrected for chance coincidences and for δ showers.* The root mean square error is indicated everywhere.**

From the data shown in Fig. 1b it is possible to determine the range L^{C}_{p} and the cross section σ^{C}_{p} of inelastic proton-carbon interactions by using a formula which takes into account the relative number of α particles in the primary cosmic radiation:

$$\frac{N^{C}_{\text{int Pb}}}{N^{b}_{\text{int Pb}}} = pe^{-16.8/L^{C}_{p}} + \alpha e^{-16.8/L^{C}_{\alpha}}; \quad \sigma^{C}_{p} = \frac{A_{C}}{N_{Av} L^{C}_{p}}.$$

Here p and α are the percentages of protons and α particles at 20-25 km; L^{C}_{α} is the range of α particle interactions in the light matter (40 g per cm²); N_{Av} is the Avogadro number. The number of primary α particles at the limit of the atmosphere was taken to be 20 percent of the total number of primary particles.

We see that this method does not require knowledge of the true flux of shower-producing particles nor of the true number of interactions in lead. The correction for α-particle interactions is 6 percent of the cross section. Also, our method of selecting showers from lead is practically free of any error due to nonlocal showers [3].

The range and cross section for inelastic proton-carbon interactions obtained by the above method at 20-25 km were:

$$L^{C}_{p} = 63^{+12}_{-9}\ \text{g/cm}^2; \qquad \sigma^{C}_{p} = 315 \pm 50\ \text{mb} \qquad \text{(see Table 1).}$$

TABLE 2

Atmos. depth x, g/cm²		Showers in upper part			Flux of shower-producing particles $I = I_0 e^{-x/150}$ with $I_0 = 2.0$	$\frac{N^{C}_{\text{showers}} - N^{b}_{\text{showers}}}{I}$		Correction for change of "reverse flux"	Correction for uncounted showers due to particles passing through gaps	$N^{C}_{\text{showers}} - N^{b}_{\text{showers}}/I$ with all corrections	Range of inelastic interaction L^{C}_{p}, g/cm²	Cross section of inelastic interaction σ^{C}_{p}, mb
		with graphite* N^{C}_{showers}, $\text{cm}^{-2}\cdot\text{min}^{-1}\,\text{sterad}^{-1}$	without graphite (background) N^{b}_{showers}	difference $N^{C}_{\text{showers}} - N^{b}_{\text{showers}}$								
53.0	33.7	0.741±0.034	0.482±0.027	0.258±0.043	1.402	0.184± ±0.030	0.190± ±0.014	+0.015	+0.010	0.215±0.014	76±7	264±24
46.7		0.815±0.028	0.542±0.026	0.274±0.038	1.467	0.186± ±0.026						
25.0		0.964±0.018	0.638±0.029	0.326±0.034	1.683	0.193± ±0.020						

*Graphite thickness 16.8 g·cm⁻².

---

*The percentage of δ showers from lead with and without graphite in the telescope was the same: 6.85 ± 0.12% of the number of registered single particles.

**In order to improve the statistical accuracy of the cross section for carbon, when plotting the curves we also used the data which we had from measurements with graphite (16.0 g/cm²) and paraffin (18.8 g/cm²) with approximate allowance for shower-production in hydrogen. The effective thickness of the graphite absorber for these combined data was 16.8 g/cm².

2. Method of indirect observation of inelastic interactions in a graphite absorber (by the number of showers from mesons produced in the graphite). The interaction range was determined from the relation

$$N_{\text{int C}} = Ip\left(1 - e^{-16{,}/8L_p^C}\right) + I\alpha\left(1 - e^{-16{,}8/L_\alpha^C}\right).$$

As we see, this method requires knowledge of the true flux I of shower-producing particles and of the true number of interactions in graphite.

Showers arising through proton-carbon interactions were recorded through triggering of the counters immediately surrounding the graphite absorber (counters K, K_1, B, L, L_1), that is, they fall into the category of showers registered in the upper part of the apparatus. Figure 2a shows an example. Figure 2b gives curves for the altitude dependence of showers recorded in the upper part of the apparatus with (1) and without (2) the graphite absorber.* Curve 3 is the difference of Curves 1 and 2. Figure 2b shows that there is a background of considerable magnitude in connection with showers in the upper part of the apparatus. This background consists of nonlocal showers, the number of which remains practically unchanged when the graphite absorber is placed in the telescope, and also of showers from lead with a "reverse flux" [3]. The introduction of a correction for the change in the number of showers with "back current" when graphite is placed in the telescope and for noncounting of two-particle showers because of particles passing through the space between counters (see Table 2) gives the true number of interactions in graphite $N_{\text{int. C}}$, which is represented by Curve 4 of Fig. 2b.

By using the above method we obtained the following values for the range and cross section of inelastic proton-carbon interactions:

$$L_p^C = 76 \pm 7\,\text{g/cm}^2; \qquad \sigma_p^C = 264 \pm 24 \text{ mb}.$$

We see that the cross section obtained by direct observation of showers in graphite is 15 percent smaller than the value obtained by reduction of the flux of individual shower-producing particles. This difference may possibly be explained by the fact that in about 10-15 percent of the cases there is an interaction without ejection of high-energy charged particles [4, 5], which are not counted by apparatus for the direct observation of showers in graphite but are registered by the first method described. A comparison with cross sections obtained by other authors [6-9] also suggest the possibility of a miscount when the proton-carbon cross section is determined by direct observation of showers in graphite.

CONCLUSIONS

Our inelastic carbon cross section for protons with about 12 Bev average energy is 315 ± 50 mb, which agrees with the geometric cross section of the carbon nucleus within the limits of error.

V. A. Sobiniakov assisted in this work.

M. V. Lomonosov Moscow State University

Received January 12, 1957.

LITERATURE CITED

[1] K. I. Alekseeva and N. L. Grigorov, J. Exptl.-Theoret. Phys. (USSR) 32, 2, 404 (1957) [Soviet Physics – JETP, p. 339].

[2] N. L. Grigorov, Uspekhi Fiz. Nauk 58, 4, 599 (1956).

---

*The curves are corrected for chance coincidences and δ showers. The correction for δ showers with graphite in the telescope was 7.0 ± 0.2 %, and without graphite 3.0 ± 0.15% of the number of registered individual particles. The mean square statistical error is shown for all points of the curves.

[3] K. I. Alekseeva, S. I. Brikker et al., Doklady Akad. Nauk SSSR 115, 1, 71 (1957) [Soviet Physics -- Doklady, p. 303].

[4] N. M. Kocharian, G. S. Saakian et al., Izv. Akad. Nauk SSSR, Ser. Fiz., 19, 515 (1955).

[5] U. Camerini, J. H. Davies et al., Phil. Mag. 42, 1241 (1951).

[6] R. R. Brown, Phys. Rev. 87, 999 (1952).

[7] W. D. Walker, S. P. Walker and K. Greisen, Phys. Rev. 80, 546 (1950).

[8] W. D. Walker, N. M. Duller and J. D. Sorrels, Phys. Rev. 86, 865 (1952).

[9] J. G. Askowith, and K. Sitte, Phys. Rev. 97 (1955).

IDENTIFICATION OF THE INTERNAL CONVERSION SPECTRUM OF THE LONG-LIVED ISOTOPES Eu^{152} AND Eu^{154}

B. V. Bobykin and K. M. Novik

(Presented by Academician A. A. Lebedev March 1, 1957)

When natural europium, which consists of the two isotopes Eu^{151} (47.77%) and Eu^{153} (52.23%), is irradiated with thermal neutrons a mixture of the radioisotopes Eu^{152} and Eu^{154} is produced. The half lives are: for Eu^{152}, 9.2 hours* and 13 years, for Eu^{154} 16 years [1]. Both isotopes are transformed by the capture of orbital electrons and by beta decay. Their radioactivities have been investigated by many workers [2-9] but there has been no satisfactory determination of the decay scheme nor of the composition of the gamma radiation. The possibility of contamination of Eu^{152,154} with other rare-earth radioisotopes and the complex character of the decay of both isotopes impedes the identification of their gamma transitions.

In our investigations a double-focusing beta spectrometer was used, with the following principal characteristics: central radius 24.3 cm, transmission 0.2%, source dimensions 1.5 · 19.5 mm^2, width of (bent) entrance slit 2 mm. In iron instruments of this type the resolving power and profile of the lines depends on the magnetic field strength and the previous magnetic history of the iron. Broadening of a line reduces the accuracy of the measurements. Conditions favorable to work in a broad range of fields (14-270 oersteds, electron energies 10-1500 kev) were produced by special preparation of the magnet. The spectrum of 10-120 kev electrons was obtained with a previously demagnetized magnet; for 100-1500 kev a "trained" magnet was used. Training was accomplished by smooth increase of the exciting current from zero to the maximum value followed by reduction to zero. The procedure was repeated until the residual magnetic field was constant (11.8 oersted). The results are illustrated in Fig. 1, where the Eu lines were taken from the corresponding sets of measurements. The 1362.5 kev electron line has a 0.32% half width. Two Geiger counters connected for coincidence served as a detector.

Beta sources were prepared by electrolysis of europium chloride dissolved in ethyl alcohol. The electrolytic tank was a vertical slit through a plexiglas disk. On the lower side of the disk the slit had the dimensions of the source. Aluminum foil on a rubber backing served both as the bottom of the tank and as cathode. The anode was a platinum wire. Electrolytic deposition proceeded for 7-10 min. The average thickness of the deposit was determined from the concentration and volume of the solution. This method is simple and economical and produces good deposits. From 1 mg of the original radioactive europium oxide we prepared about 50 sources of varying thickness and size.

The internal conversion spectrum of Eu^{152,154} was obtained from sources more than two years old. In the great majority of cases both K and L conversion lines were registered, whose energy was determined with less than 0.1% error. This permitted an unequivocal determination of the element in which the gamma transition occurred. For the purpose of eliminating electron energy losses in the active deposit and material of the backing the electron spectrum from 10 to 200 kev was taken with an average deposit thickness of 0.015-0.025 mg/cm^2 on 1.5μ aluminum foil. The harder part of the spectrum was taken with an average deposit thickness of 0.1-0.2 mg/per cm^2 on 5μ aluminum foil. The line energies were determined from the standard lines of Th(B + C + C"), Cs^{137} and Co^{60} [10]. The source holders were standardized and each source had a separate holder. The limitation on accuracy which was associated with the magnet iron was eliminated by the fact that through exchange of the sources the standard lines and some Eu lines were obtained in a single spectrum. In succeeding experiments such europium lines were used as reference lines. Interpolation was carried out by means of cubical parabolas, each of which requires four points for plotting. The cubical parabolas were distributed in such a way that different portions of the spectrum were covered by different curves.

---

* We did not investigate the short-lived isotope Eu^{152}.

We observed 73 internal conversion lines and 13 lines of Auger electrons. The identified gamma transitions are given in Table 1. In the column of references to the literature all gamma transitions observed in the decay of $Eu^{152,154}$ are shown with the corresponding values of Z in brackets. Some transitions were observed by many workers, but only the most exact values are quoted. There is a discrepancy between the energies at about 122 and 123 kev as determined in the present work and by crystal diffraction [9]. We believe that the values given in [9] are too high.*

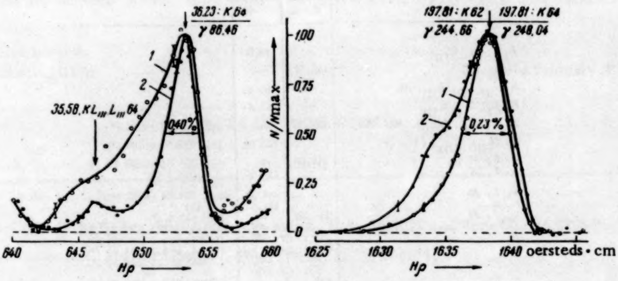

Fig. 1. Shape of lines after different methods of preparing magnet. 1) "training"; 2) demagnetization.

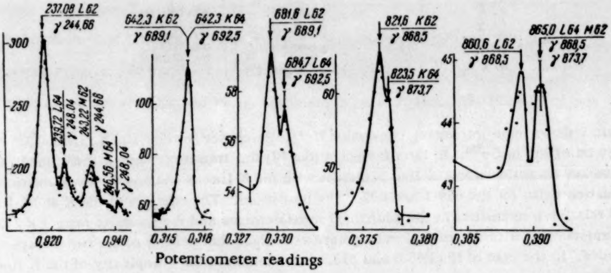

Fig. 2.

After 280 days we performed additional measurements for the purpose of observing the change in intensity of some lines which could not be assigned with certainty to $Eu^{152,154}$. It was found that transitions at 69.7

---

* V. A. Romanov has informed the authors of the energies of these transitions obtained with a prism beta spectrometer. His values of 121.75 ± 0.03 kev and 123.05 ± 0.03 kev agree with ours.

and 103.2 kev (Z = 63) accompany the decay of Gd^{153} (T = 236 days). Lines of 583.1 (586.5) and 612.1 (615.5) kev accompany the decay of radioisotopes with a lifetime approximately equal to that of $Eu^{152,154}$ (the weak 810.6 (813.9) kev line was not investigated). A 46.25 kev transition is conjectured; the L_I and L_{II} lines are possibly quenched by Auger M lines of samarium. In connection with the β^- decay of Eu^{155} with T = 1.7 years there arise Gd^{155} transitions whose energies are 18, 84 and 102 kev [12]. The observed lines of 86, 46 and 105.3 kev (18.8 kev was not investigated) showed no reduction of intensity compared with the $Eu^{152,154}$ lines. It can be assumed that these lines belong to $Eu^{152,154}$ or to Eu^{155} if the lifetime of the latter is comparable with the lifetime of $Eu^{152,154}$. We did not identify the four weak conversion lines 41.19, 43.73, 48.90 and 51.29 kev, the last two of which belong to short-lived isotopes.

TABLE 1

Identification of conversion lines	Energy of γ trans., kev		References
	Z =62	Z =64	
L_I, L_{II}, L_{III}, M	—	18.8	—
(L_{III}, M)	(46.52)	—	—
K, L_I, L_{II}, L_{III}, M	—	86.46	—
K, L_I, L_{II}, L_{III}	—	105.3	—
K, L_I, L_{II}, (L_{III}), M, (N)	121.77	—	(62) 122.31±0.04 (6)
K, (L_{II}), L_{III}, (M), N	—	123.62	(64) 123.54±0.09 (6)
K, L, M	244.66	—	(62) 244.64±0.08 (6)
K, L, M	—	248.04	(64) 247.7 (6)
—	—	—	(64) 336.4 (6)
K, L, M	—	344.32	(64) 344.34±0.23 (6)
K, L	—	411.23	(?) 410 (7)
K, L, M	444.23	—	(64) 448.4 (6)
—	—	—	(62?64) 518.5 (522.0) (6)
K	583.1 or	586.5	(62?64) 583.5 (587.0) (6)
K	612.1 or	615.5	(62?64) 608.3 (611.8) (6)
—	—	—	(62?64) 655.3 (658.8) (6)
K	676 or	679	—
K, L	689.1	—	(62?64) 687.1 (690.6) (6)
K, L	—	692.5	—
K, L	720.2	—	(62) 720 (7)
K, L	723.6	—	—
K	—	757.7	—
K, L	—	779.5	(?) 778 (7)
K	810.6 or	813.9	—
K, L	868.5	—	(62?64) 868 (871) (6)
K, L	—	873.7	—
K, L	964.8	—	(62) 964 (7)
K, L	—	996.6	—
K, L	—	1005.4	—
K, L	1086.6	—	(62) 1086 (7)
K, L	1112.7	—	(62) 1116 (7)
K, L	1272.7 or	1276.0	(?) 1280 (6)
K, L	1409.4	—	(64) 1415 (7)
K	Z =63	69.7	(63) 72±8 (11)
K, $L_I L_{II}$, M	Z=63	103.2	(63) 100±4 (11)

Figure 2 shows some interesting conversion lines. Reference [6] contains an indication of the existence of a 247.7 kev transition in Gd^{154}. In later investigations [7] this transition was not mentioned. Our data show a clear 248.04 kev transition whose K line coincides with the K line of the 244.66 kev transition (Fig. 1). A similar situation exists for the 689.1 and 692.5 kev transitions. The energies of the K and L lines, the absence of reduced relative L intensities in the additional measurements and the intensity ratio $\Sigma K / \Sigma L \simeq 7.3$ which is not in disagreement with theoretical multipolarities * show that neither of the two transitions indicated can be disregarded. In the case of the 868.5 and 873.7 kev transitions the complexity of the K line does not lead to uncertainty.

Nuclear data of 1956 [13] contains the decay scheme of long-lived Eu^{152}. The following excited levels are indicated: 122, 366, 1085, 1232, 1527, 1576, 1635 kev in $_{62}Sm^{152}$ and 344, 752, 1122, 1444, 1584 kev in

---

*In order to evaluate the K/L ratio we interpolated the data of Rose [10]: Z = 63, K/L ≅ 8.0(E1); 6.7(E2); 6.7(M1); 6.6(M2).

$_{64}\mathrm{Gd}^{152}$. The exact values of the transition energies obtained in the present work can serve as a good check of this level scheme since it contains both cascade and direct transitions. The excited states of Sm^{152} evidently exist at 121.77, 366.43, 1086.6, 1234.7, and 1531.0 kev. But we can also assume the existence of an additional combination of cascade and direct transitions: 444.23, 244.66 and 689.1 kev; 689.1, 720.2 and 1409.4 kev; 689.1, 121.77 and 810.6 kev; 689.1, 583.1 and 1272.7 kev which are not accounted for by the proposed scheme. We did not observe the 550 and 1210 kev transitions in Sm^{152} and the 1100 and 1240 kev transitions in Gd^{152} which are mentioned in [13].

Our data enables us to establish the following excited levels for $_{64}\mathrm{Gd}^{154}$: 123.02, 371.06, 996.6 and 1128 kev. We have here the cascade and direct transitions: 123.02, 873.7 and 996.6 kev; 248.04, 757.7 and 1005.4 kev.

The level schemes of $_{62}\mathrm{Sm}^{152}$ and $_{64}\mathrm{Gd}^{154}$ resemble the structure of rotational bands. A thorough study of the question is not possible because of the lack of reliable theoretical L coefficients for the given values of Z and the slight sensitivity of the multipolarity of gamma transitions to the K/L ratio.

The authors are sincerely grateful to Professor V. M. Kel'man for his interest and for valuable comments.

Physico-Technical Institute,
Academy of Sciences, USSR

Received February 27, 1957.

LITERATURE CITED

[1] D. G. Karraker, R. J. Hayden and M. G. Inghram, Phys. Rev. 87, 901 (1952).

[2] F. B. Shull, Phys. Rev. 74, 917 (1948).

[3] J. M. Cork, H. B. Keller, W. C. Rutledge and A. E. Stoddard, Phys. Rev. 77, 848 (1950).

[4] L. Ia. Shavtvalov, J. Exptl. Theoret. Phys. (USSR) 21, 1123 (1951).

[5] H. B. Keller and J. M. Cork, Phys. Rev. 84, 1079 (1951).

[6] E. L. Church and M. Goldhaber, Phys. Rev. 95, 626 (1954).

[7] R. E. Slattery, D. C. Lu and M. L. Wredenbeck, Phys. Rev. 96, 465 (1954).

[8] B. S. Dzhelepov, Zhukovskii and V. G. Nedovesov, Izv. Akad. Nauk SSSR, Ser. Fiz. 19, 296 (1955).

[9] B. Anderson, Proc. Phys. Soc. 69, No. 437 A, 415 (1956).

[10] K. Siegbahn, Beta- and Gamma-Ray Spectroscopy (Amsterdam, 1955) pp. 227, 905.

[11] S. K. Bhattacherjee and S. Raman, Nuclear Phys. 1, 486 (1956).

[12] V. C. Dubey, C. E. Mandeville and M. A. Rothman, Phys. Rev. 103, 1430 (1956).

[13] Nuclear Sci. Abstrt. 10, No. 12B, 254 (1956).

THEORY OF GAS FLOW IN A POROUS BODY NEAR THE KNUDSEN REGION. PSEUDOMOLECULAR FLOW

B. V. Deriagin and S. P. Bakanov

Two types of gas flow in porous bodies or in capillaries are known: molecular flow when α, which is the ratio of the number of intermolecular collisions to the number of collisions with pore walls is small, and viscous flow, when $\alpha \gg 1$ and a velocity profile is established in the pores. It is generally accepted that as the gas pressure p increases and α consequently also increases, the molecular type gradually passes into the viscous type so that Q, the gas flow in moles $\cdot$ cm$^{-2}\cdot$sec^{-1} increases monotonically and linearly in first approximation.

This scheme is contradicted by experiments which have revealed for round and even more so for slit-shaped capillaries that there exists a minimum of the functional relationship between Q and p. Theoretical attempts to account for this minimum have been unsuccessful because departure from Knudsen flow is accompanied by a convective component that depends on the coordinates, that is, by a velocity profile. The calculations thus become extremely complicated.

The situation is different in the case of a highly porous body, for which

$$1 - \delta \ll 1, \tag{1}$$

where δ is the porosity. In this case a porous body is characterized by two quantities which are essentially of different magnitude, the mean pore opening λ_c and the mean particle size D*, which are equal to the mean segments on a "random" straight line that result from its intersection with the walls, the segments being in the pores and the particles, respectively. It follows from a lemma which was proved in an earlier paper [1] that

$$\lambda_c = 4\frac{V}{S}, \quad D = 4\frac{V_0}{S}, \tag{2}$$

where S is the surface of the walls; V_0 is the particle volume and V is the pore volume.

It follows from (2) that

$$\lambda_c = \frac{\delta}{1-\delta} D. \tag{3}$$

It is clear that $\alpha = \frac{\lambda_c}{\lambda_g}$, where λ_g is the ordinary mean free path of gas molecules at a given pressure p.

---

*In a highly porous body it is possible to satisfy at the same time the more stringent condition $D \ll a \ll \lambda_g \ll \lambda_c$, where a is the average distance between neighboring particles.

We see that subject to condition (1) there will exist a range of gas pressures for which the following two conditions will be satisfied simultaneously:

$$\lambda_g \ll \lambda_c \quad (\alpha \gg 1), \tag{4}$$

$$D \ll \lambda_g, \tag{4'}$$

of which the first denotes the absence of Knudsen flow and the second makes the convective component independent of the coordinates.*

We shall consider gas flow in what we shall call the pseudomolecular region and in the transition region to Knudsen flow where only condition (4') is satisfied. With the exception of the limiting case of pure Knudsen flow ($\lambda_c >> \lambda_g$) the motion of the molecules is characterized by the convective component u_z, which is equal to the mean component v_z of molecular velocity. The corresponding molecular velocity distribution becomes anisotropic.

The total gas flow Q in moles/sec through 1 cm^2 of a porous body is

$$Q = Q_u + Q_D = Cu_z + Q_D, \tag{5}$$

where Q_u is the convective flow component; Q_D is the diffusive component; and C is the gas concentration per cm^3 of the volume of the porous medium.

Analogously, the resistance to the flow per unit volume of the porous body is equal to the action of the flow on unit volume of the body, given by

$$W = W_u + W_D, \tag{6}$$

where $W_u \sim u_z$, $W_D \sim$ grad p.

For a sphere of radius $R << \lambda_g$ we have the formula [2]

$$(W_u)_1 = \beta S_1 \frac{Cu_z}{8} \sqrt{2\pi MRT}, \tag{7}$$

where S_1 is the surface of the sphere, and β is a constant which depends on the law for the interaction with molecules colliding with the surface.

Assuming that in the deduction of (7) the shape of the sphere was significant only in so far as it insured an isotropic distribution in space of all parts of its surface S_1, and C takes account of the dependence of the number of collisions on the molecular concentration around the sphere, it is easy to extend (7) to the case of any convex particle shape in an isotropic distribution:

$$W_u = \beta S_0 \frac{Cu_z}{8} \sqrt{2\pi MRT}, \tag{8}$$

where S_0 is the specific surface in cm^2 per cm^3 of the porous body.

In order to derive W_D we use the formula in [3] for the velocity distribution of gas molecules with a concentration gradient:

---

*For circular cylinders D is the diameter; for spheres it is 2/3 of the diameter.

$$f^{(1)} = f^{(0)}\left(1 - \lambda_t \cos\vartheta \frac{\text{grad}\, C}{C}\right), \tag{9}$$

where $f^{(0)}$ is the Maxwell distribution function, λ_t is the molecular transport mean free path and ϑ is the polar angle of molecular velocity with respect to the direction grad C.

Equation (9), which is strictly applicable to pure Knudsen flow, will be assumed to be correct for the pressure region under consideration in a system of reference that moves with velocity u_z. Then, as previously,

$$\lambda_t = \frac{\lambda}{1 - \overline{\cos\gamma}}, \tag{10}$$

where $\overline{\cos\gamma}$ is the average cosine of the molecular scattering angle, while λ and $\overline{\cos\gamma}$ are given by

$$\frac{1}{\lambda} = \frac{1}{\lambda_c} + \frac{1}{\lambda_g}, \tag{11}$$

$$\overline{\cos\gamma} = \frac{\lambda}{\lambda_c}\overline{\cos\gamma_c} + \frac{\lambda}{\lambda_g}\overline{\cos\gamma_g}, \tag{11'}$$

where $\overline{\cos\gamma_c}$ and $\overline{\cos\gamma_g}$ refer to the scattering of a molecule in a collision with the wall and with another molecule. From (11) and (11') it follows that

$$\frac{1}{\lambda_t} = \frac{1}{(\lambda_t)_c} + \frac{1}{(\lambda_t)_g}. \tag{12}$$

Knowing $f^{(1)}$ it is easy to calculate W_D as the momentum transferred to the walls by molecules plus the recoil momentum in reflections:

$$W_D = -\left[\mu\lambda_t \frac{S_0}{4} + (1 - \delta)\right] \text{grad}\, p. \tag{13}$$

Here the second term on the right expresses the "pseudo-Archimedean" lifting force on a sphere in the field of the gradient of the pressure p, and μ is a parameter which depends on the law for interactions between molecules and the walls.

By Newton's third law, neglecting the inertial terms

$$W = -\,\text{grad p}. \tag{14}$$

Inserting (6), (8) and (13) into the left-hand side of (14) we obtain

$$Cu_z = \text{grad}\, p\left(\mu \frac{\lambda_t}{\lambda_c} - 1\right)\frac{\delta^2}{3S_0\sqrt{2\pi MRT}}. \tag{15}$$

The diffusive flow Q_D is obtained by multiplying (9) by $Cv\cos\vartheta/\delta$ and integrating over all possible velocities:

$$Q_D = -\frac{4}{3}\frac{\delta}{\sqrt{2\pi MRT}}\lambda_t\, \text{grad}\, p.$$

Thus the total gas flow Q is

$$Q = \frac{\delta^2}{S_0}\frac{\operatorname{grad} p}{\sqrt{2\pi MRT}}\left[\frac{1}{\beta}\left(\mu\frac{\lambda_t}{\lambda_c} - 1\right) - \frac{16}{3}\frac{\lambda_t}{\lambda_c}\right] = -k \operatorname{grad} p,$$

where it is also assumed, according to (2) that $\lambda_c = 4\delta/S_0$.

Hence the filtration coefficient k is

$$k = -\frac{\delta^2}{S_0}\frac{1}{\sqrt{2\pi MRT}}\left[\frac{1}{\beta}\left(\mu\frac{\lambda_t}{\lambda_c} - 1\right) - \frac{16}{3}\frac{\lambda_t}{\lambda_c}\right]. \tag{16}$$

From (10), (11) and (11') we see that

$$\frac{\lambda_t}{\lambda_c} = \frac{1}{(1 - \overline{\cos\gamma_c}) + \alpha(1 - \overline{\cos\gamma_g})}. \tag{17}$$

The Knudsen gas flow gives $u_z = 0$ and thus $Q_u = 0$, whence from (15) we have $\mu = 1 - \overline{\cos\gamma_c}$ and

$$k_{kn} = \frac{16}{3}\frac{\delta^2}{S_0}\frac{1}{\sqrt{2\pi MRT}}\frac{1}{1 - \overline{\cos\gamma_c}}. \tag{18}$$

Substituting λ_t/λ_c (17) into (16) we obtain

$$k = \frac{\delta^2}{\beta S_0}\frac{1}{\sqrt{2\pi MRT}}\frac{{}^{16}/_3\beta + \alpha(1 - \overline{\cos\gamma_g})}{\mu + \alpha(1 - \overline{\cos\gamma_g})}.$$

In pseudomolecular flow ($\alpha \to \infty$, $\lambda_t \to 0$, $W_D \to 0$, $Q_D \to 0$) we have

$$k = \frac{\delta^2}{\beta S_0}\frac{1}{\sqrt{2\pi MRT}}. \tag{19}$$

For diffusive and specular molecular reflection, respectively, with velocity conservation a calculation gives

$$\frac{1}{\beta} = \frac{27\pi}{26}; \qquad \frac{1}{\beta} = \frac{3\pi}{2}.$$

A simple calculation shows that the maximum decrease of k with increasing α is ~ 11.7%.

On the other hand, under pressures which violate the condition (4') it is possible to use a generalization of Stokes' law which was established empirically by Millikan [4] for the resistance encountered by a gas flowing around a sphere of radius a with velocity u_z:

$$W_1 = -\frac{6\pi\eta a u_z}{1 + A\frac{\lambda_g}{a} + B\frac{\lambda_g}{a}e^{-ca/\lambda_g}}. \tag{20}$$

where η is the coefficient of viscosity; A, B and c are empirical constants.

Extending (20) to the case of a porous medium and utilizing (14) we obtain (taking into account the diffusive component of the resistance (13)):

$$Cu_z = -\frac{32}{15}\frac{\delta^2 \operatorname{grad} p}{S_0 \sqrt{2\pi MRT}}\left[\frac{3(1-\delta)}{4\delta}\alpha + A + Be^{-\frac{3c(1-\delta)}{4\delta}\alpha}\right]\frac{\alpha(1-\overline{\cos\gamma_g})}{\mu+\alpha(1-\overline{\cos\gamma_g})}.$$

The total gas flow Q is

$$Q = -\frac{\delta^2 \operatorname{grad} p}{S_0 \sqrt{2\pi MRT}}\frac{16}{3}\frac{\frac{2}{5}\left(\frac{3(1-\delta)}{4\delta}\alpha + A + Be^{-\frac{3c(1-\delta)}{4\delta}\alpha}\right)(1-\overline{\cos\gamma_g})\alpha + 1}{\mu+\alpha(1-\overline{\cos\gamma_g})}.$$

Hence the filtration coefficient is

$$k = \frac{16}{3}\frac{\delta^2}{S_0 \sqrt{2\pi MRT}}\frac{0{,}4\,\{[0{,}75(1-\delta)/\delta]\,\alpha + A + Be^{-[0{,}75c(1-\delta)/\delta]\alpha}\}(1-\overline{\cos\gamma_g})\alpha + 1}{1-\overline{\cos\gamma_c}+\alpha(1-\overline{\cos\gamma_g})}.$$

Figure 1 shows the family of curves $k(\alpha/\delta)/k_{kn}$ for $\overline{\cos\gamma_c} = -4/9$, $\overline{\cos\gamma_g} = 0.406$ [1, 5], A = 1.0, B = = 0.53, c = 1.62 [4] for various values of δ. The curves reveal a clear minimum (particularly at $\delta = 0.9$). At high pressures the flow is directly proportional to the pressure. This is evidently analogous to the physical cause of the minimum on the flow-pressure curve found experimentally by Knudsen [7], Gaede [8] and others. We note that the mutual diffusion coefficient of the two gases also decreases as the pressure rises [5].

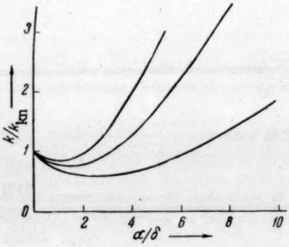

Fig. 1. Upper curve for $\delta = 0.7$; middle curve for $\delta = 0.8$; lower curve for $\delta =$ = 0.09.

We note in conclusion that the deduction of W_D and Q_D presupposed the correctness of (9) and that λ_t is independent of molecular velocity. These assumptions are apparently close to reality because, as we have shown [6], a more rigorous calculation leads to a similar relation with somewhat different coefficients. Since in the deduction of (19) it was assumed that $W_D = 0$ and $Q_D = 0$ the accuracy of (19), the character of the pseudomolecular flow and the deduction of the depth of the flow curve minimum are independent of the accuracy of (9).

The similarity of the filtration coefficients for Knudsen and pseudomolecular flow, despite the essentially different mechanisms, is a very much unexpected and important result.

Institute of Physical Chemistry
Academy of Sciences, USSR

Received March 1, 1957.

LITERATURE CITED

[1] B. V. Deriagin, Doklady Akad. Nauk SSSR 53, 627 (1946).

[2] P. Epstein, Phys. Rev. 23, 710 (1924).

[3] S. P. Bakanov, J. Tech. Phys. (USSR) 27, No. 7 (1957).*

---

* As in original — Publisher's note.

[4] R. Millikan, Phys. Rev. 22, 1 (1923).

[5] S. Chapman and J. G. Cowling, The Mathematical Theory of Non-Uniform Gases (Cambridge, 1939).

[6] B. V. Deriagin and S. P. Bakanov, J. Tech. Phys. 27, No. 9 (1957) [see Soviet Physics – Technical Physics, p. 1904].

[7] M. Knudsen, Ann. Physik. 28, 75 (1909).

[8] W. Gaede, Ann. Physik. 41, 289 (1913).

SOUND DIFFRACTION BY A THIN BOUNDED ELASTIC CYLINDRICAL SHELL

L. M. Liamshev

(Presented by Academician N. N. Andreev February 28, 1957)

1. We shall study the diffraction of a plane sound wave

$$p_i = \exp\left[ik\cos\theta\cos\varphi r + ik\sin\theta z\right]$$

where θ is the angle of incidence, by a thin* bounded cylindrical shell of circular cross section using an integro-differential equation [1, 2] based on more general assumptions than in recently published papers [3, 4], which considered only the special case of perpendicular incidence of a plane wave on an unbounded shell. It is assumed that the shell, whose axis coincides with the z axis of the cylindrical system of coordinates r, φ, z, forms a joint at the points $z = 0$, d on a perfectly rigid cylindrical fixed screen and that the vibrations of the shell can be described by the equations given in reference [5].

2. Using Green's theorem [6], the radiation condition [7] and the equality of the normal velocity components at the boundary between the shell and the surrounding medium, the solution of the wave equation $(\Delta + k^2)\,p = 0$ can be represented as

$$\begin{aligned} p(r, \varphi, z) &= p_i(r, \varphi, z) + p_r(r, \varphi, z) - \\ &- i\omega\rho\int_s G(r, a, \varphi - \varphi', z - z')\, w(\varphi', z')\, ds'. \end{aligned} \tag{1}$$

Here s is the shell surface; $p_r(r, \varphi, z)$ is the part of the solution which describes the scattered field from a completely rigid unbounded cylinder [8] and $G(r, a, \varphi - \varphi', z - z')$, $r > r' = a$ is Green's function which is the solution of

$$(\Delta + k^2)\, G(r, r', \varphi - \varphi', z - z') = -\frac{\delta(r - r')}{r}\,\delta(\varphi - \varphi')\,\delta(z - z')$$

with $\operatorname{Im} k > 0$ and is bounded everywhere except at the point r', φ', z' and which satisfies the condition $\frac{\partial G}{\partial n} = 0$; on the surface of the cylinder:

---

* It is assumed that the thickness of the shell is much smaller than the wavelength of a longitudinal wave in the material of the shell.

$$G(r,\ a,\ \varphi-\varphi',\ z-z') = \frac{1}{4\pi^2 a}\int_{-\infty}^{+\infty}\sum_{m=0}^{\infty}\varepsilon_m \frac{H_m^{(1)}(r\sqrt{k^2-\xi^2})}{\sqrt{k^2-\xi^2}H_m'^{(1)}(a\sqrt{k^2-\xi^2})}\times \tag{2}$$

$$\times\cos m(\varphi-\varphi')\exp[i\xi(z-z')]\,d\xi;\quad r>a.$$

When (1) is inserted into the equations of [5] the problem is reduced to the solution of a set of integro-differential equations for $w(\varphi, z)$:

$$\omega^2\rho_1 u + E_1\left[\frac{\partial^2 u}{\partial z^2} + \frac{1}{2a}(1-\nu)\frac{\partial^2 u}{\partial\varphi^2} + \frac{1}{2a}(1+\nu)\frac{\partial^2 v}{\partial\varphi\,\partial z} + \frac{\nu}{a}\frac{\partial w}{\partial z}\right] = \tag{3}$$

$$= \frac{i\omega}{2}\frac{\nu}{1-\nu}\frac{\partial p(a,\ \varphi,\ z)}{\partial z};$$

$$\omega^2\rho_1 v + E_1\left[\frac{1}{a^2}\frac{\partial^2 v}{\partial\varphi^2} + \frac{1}{2}(1-\nu)\frac{\partial^2 v}{\partial z^2} + \frac{1}{2a}(1+\nu)\frac{\partial^2 u}{\partial\varphi\,\partial z} + \frac{1}{a^3}\frac{\partial w}{\partial\varphi}\right] + \tag{4}$$

$$+\frac{1}{8}h^2E_1\frac{\nu}{1-\nu}\left(\frac{1}{a^4}\frac{\partial^3 w}{\partial\varphi^3} + \frac{1}{a^4}\frac{\partial w}{\partial\varphi}\right) = \frac{i\omega}{2a}\frac{\nu}{1-\nu}\frac{\partial p(a,\ \varphi,\ z)}{\partial\varphi};$$

$$\omega^2\rho_1 w - E_1\left(\frac{\nu}{a}\frac{\partial u}{\partial z} + \frac{1}{a^2}\frac{\partial v}{\partial\varphi} + \frac{w}{a^2}\right) -$$

$$-\frac{h^2}{24}\frac{E_1}{1-\nu}\left[2(1-\nu)\left(\frac{\partial^4 w}{\partial z^4} + \frac{2}{a^2}\frac{\partial^4 w}{\partial z^2\,\partial\varphi^2} + \frac{1}{a^4}\frac{\partial^4 w}{\partial\varphi^4}\right) + \right. \tag{5}$$

$$\left. + (4-\nu)\frac{1}{a^4}\frac{\partial^2 w}{\partial\varphi^2} + (2+\nu)\frac{w}{a^4}\right] = i\omega\left[\frac{1}{h} + \frac{1-2\nu}{2(1-\nu)a}\right]p(a,\ \varphi,\ z),$$

where

$$p(a,\ \varphi,\ z) = p_i(a,\ \varphi,\ z) + p_r(a,\ \varphi,\ z) -$$

$$-\frac{i\omega\rho}{4\pi^2}\int_0^{2\pi}\int_0^{d}\int_{-\infty}^{+\infty}\sum_{m=0}^{\infty}\varepsilon_m w(\varphi',\ z')\frac{H_m^{(1)}(a\sqrt{k^2-\xi^2})}{\sqrt{k^2-\xi^2}\,H_m'^{(1)}(a\sqrt{k^2-\xi^2})}\times \tag{5a}$$

$$\times\cos m(\varphi-\varphi')\exp[i\xi(z-z')]\,d\varphi'dz'd\xi.$$

After determining $w(\varphi, z)$ from Equations (3), (4) and (5) and substituting $w(\varphi, z)$ in (1) we obtain the desired solution $p(r, \varphi, z)$. In (1) - (5) $\underline{p}$ is the sound pressure; $\underline{c}$ is the velocity of sound in the medium; ρ is the density of the medium; $\underline{a}$ is the radius; $\underline{h}$ is the thickness of the shell; $E_1 = (E/1 - \nu^2)$ is Young's modulus; ν is the Poisson coefficient; ρ_1 is the density of the material of the shell; $\underline{n}$ is the inside normal to the shell surface; $\underline{u}$, $\underline{v}$, $\underline{w}$ are the velocities of displacement of the shell surface in the axial, peripheral and radial directions; $H_m^{(1)}(\alpha)$ is a Hankel function of the first kind. A prime denotes differentiation with respect to the argument; $\epsilon_0 = 1$, $\epsilon_m = 2$ with $m = 1, 2, 3, \ldots$

3. The solution of the integro-differential Equations (3), (4) and (5) can be reduced to the solution of linear algebraic equations if the displacement velocities $u(\varphi, z)$, $v(\varphi, z)$, $w(\varphi, z)$ and the pressure $p_i(a, \varphi, z) + p_r(a, \varphi, z)$ are expanded in series of eigenfunctions that satisfy the homogeneous differential equation of the shell and the boundary conditions at the points $z = 0, d$ [9]. In particular,

$$w(\varphi,\ z) = \sum_{m=0}^{\infty}\sum_{n=0}^{\infty}a_{mn}\cos m\varphi\sin\frac{\pi nz}{d}. \tag{6}$$

Approximately determining* the coefficients a_{mn} from the solution of the algebraic equations, substituting the values of a_{mn} into (6) and then in (1) and using the method of steepest descent for the integration, we obtain finally

$$p(r,\ \varphi,\ z) \simeq p_i(r,\ \varphi,\ z) + p_r(r,\ \varphi,\ z) + \frac{\rho c^2 d}{2\pi^2 \omega a \cos\theta \cos\theta'} \frac{\exp[ikR]}{R} \times$$
$$\times \sum_{m=0}^{\infty} \sum_{n=1}^{\infty} \varepsilon_m^2 \exp\left[-i\frac{m-3}{4}\pi\right] \frac{\cos m\varphi}{H_m^{'(1)}(ka\cos\theta)\, H_m^{'(1)}(ka\cos\theta')\,(Z_{mn} + Z_{mnmn})} \times$$
$$\times \left[\frac{\exp[i(k\sin\theta d + \pi n)] - 1}{k\sin\theta d + \pi n} - \frac{\exp[i(k\sin\theta d - \pi n)] - 1}{k\sin\theta d - \pi n}\right]\left[\frac{\exp[i(k\sin\theta' d + \pi n) - 1}{k\sin\theta' d + \pi n} - \right.$$
$$\left. - \frac{\exp[i(k\sin\theta' d - \pi n)] - 1}{k\sin\theta' d - \pi n}\right]. \tag{7}$$

Here $R = \sqrt{r^2 + z^2}$; θ' is the scattering angle:

$$Z_{mnmn} = \frac{j\omega\rho}{2\pi d} \int_0^d \int_0^d \int_{-\infty}^{+\infty} \varepsilon_m \frac{H_m^{(1)}(a\sqrt{k^2 - \xi^2})}{\sqrt{k^2 - \xi^2}\, H_m^{'(1)}(a\sqrt{k^2 - \xi^2})} \sin\frac{\pi n z}{d} \times \tag{8}$$
$$\times \sin\frac{\pi n z'}{d} \exp[i\xi(z - z')]\, dz\, dz'\, d\xi;$$

$$Z_{mn} = +i\frac{E_1 h}{\omega a^2} \frac{D}{D_1}; \tag{9}$$

$$D_1 = \begin{vmatrix} -\frac{\pi n h}{2d}\frac{\nu}{1-\nu}; & \frac{1+\nu}{2} m \frac{\pi n a}{d}; & \frac{\rho_1 \omega^2 a^2}{E^1} - \frac{\pi^2 n^2 a^2}{d^2} - \frac{1-\nu}{2} m^2 \\ \frac{mh}{2a}\frac{\nu}{1-\nu}; & \frac{\rho_1 \omega^2 a^2}{E_1} - m^2 + \frac{1-\nu}{2}\frac{\pi^2 n^2 a^2}{d^2}; & \frac{1+\nu}{2} m \frac{\pi n a}{d} \\ -\left[1 + \frac{1-2\nu}{2(1-\nu)}\frac{h}{a}\right] & -m; & \nu\frac{\pi n a}{d} \end{vmatrix}; \tag{10}$$

$$D = \begin{vmatrix} \nu\frac{\pi n}{d} a; & \frac{1+\nu}{2} m\pi n \frac{a}{d}; & \frac{\rho_1 \omega^2 a^2}{E_1} - \frac{\pi^2 n^2 a^2}{d^2} - \frac{1-\nu}{2} m^2; \\ -m + \frac{1}{8}\frac{h^2}{a^2}\frac{\nu}{1-\nu} m(m^2 - 1); & \frac{\rho_1 \omega^2 a^2}{E_1} - m^2 + \frac{1-\nu}{2}\frac{\pi^2 n^2 a^2}{d^2}; & \frac{1+\nu}{2} m \frac{\pi n a}{d}; \\ \frac{\rho_1 \omega^2 a^2}{E_1} - 1 - \frac{h^2 a^2}{24}\frac{1}{1-\nu}[2(1 -- \nu) \times \times \left(\frac{\pi^4 n^4}{d^4} + 2\frac{m^2}{d^2}\frac{\pi^2 n^2}{a^2} + \frac{m^4}{a^4}\right) - (4-\nu)\frac{m^2}{a^4} + \frac{2+\nu}{a^4}\Big]; & -m; & \nu\frac{\pi n a}{d} \end{vmatrix}. \tag{11}$$

---

* The approximation is essentially based on the assumption that the system of orthogonal eigenfunctions which satisfy the homogeneous differential equations of the shell and the given boundary conditions, also satisfy the inhomogeneous differential (integro-differential) equations of the shell.

Calculations show that in a number of important cases this assumption is justified and confirmed experimentally. Details will be found in references [1, 2, 10], for example.

Z_{mnmn} and Z_{mn} are, respectively, the radiation impedance and the mechanical impedance of the mn normal mode of vibration of the shell. If the frequency of the incident wave coincides with one of the natural frequencies of the shell $Z_{mn} + \mathrm{Im}\, Z_{mnmn} = 0$, and if $|\pi n| = |k \sin \theta d| = |k \sin \theta' d|$ considerable scattering is observed not only in the direction of specular reflection but also in the direction opposite to that of the incident wave (non-specular reflection) [1, 11]. It can be shown that non-specular reflection is observed whenever the phase velocity of the incident wave along a shell coincides with the velocity of one of the normal free waves in the shell propagated along its axis [11].

Acoustics Institute,
Academy of Sciences, USSR

Received February 27, 1957.

LITERATURE CITED

[1] L. M. Liamshev, Sound Reflection by Thin Plates and Shells in a Liquid [In Russian] (Izd AN SSSR, 1955).

[2] L. M. Liamshev, Acta Phys. Hungarica 6, 33 (1956).

[3] M. Junger, J. Acoust. Soc. Am. 24, 366 (1952).

[4] M. Junger, J. Acoust. Soc. Am. 24, 899 (1953).

[5] E. Kennard, J. Appl. Mech. 20, 33 (1953).

[6] R. Courant and D. Hilbert, Methoden der Mathematischen Physik II (Julius Springer, Berlin, 1937) [Russian translation, 1951, p. 421].

[7] A. Sommerfeld, The Partial Differential Equations of Physics (Russian translation, 1950) p. 270.

[8] P. Morse, Vibration and Sound (Mc Graw-Hill, New York, 1948) [Russian translation, 1949, p. 379].

[9] S. Timoshenko, Theory of Plates and Shells (Mc Graw-Hill, New York, 1940).

[10] M. Lax, J. Acoust. Soc. Am. 16, 5 (1944).

[11] L. M. Liamshev, Acoustics J. 2, 188 (1956) [Soviet Physics – Acoustics, p. 145].

ON THE THEORY OF CONCENTRATION QUENCHING OF FLUORESCENCE IN SOLUTIONS

B. Ia. Sveshnikov

(Presented by Academician A. N. Terenin March 13, 1957)

Forster [2] has shown that the fluctuations in the distribution of molecules of a fluorescent substance in a solution* must produce the result that the concentration quenching of fluorescence for individual excited molecules will take place with different probabilities. A further consequence must be the non-exponential fluorescence damping of a quenched solution and nonproportionality between changes of yield and changes of fluorescence persistence with concentration quenching – the yield must be reduced with rising concentration more rapidly than the persistence which is in accordance with experimental findings.

In attempting to provide a mathematical formulation of his hypothesis Forster derived formulas for the damping, yield and persistence of fluorescence in quenched solutions with a fluctuating distribution of dissolved molecules. We have shown [1] that his treatment of the problem is not entirely unobjectionable. It would be difficult to obtain a rigorous solution of the problem, but it is relatively easy to calculate the quenching of fluorescence from an excited molecule by its nearest unexcited neighbor while taking account of the fluctuating distribution of the molecules. The effect due to more distant quenching molecules will only reduce the fluctuation effects, that is, reduce the distortions of the damping law and reduce the difference between the changes of peristence and changes of yield which are obtained when we confine ourselves to a consideration of quenching by nearest-neighbor molecules alone. It must also be noted that in the case of concentration quenching, (it is assumed that the probability of quenching is inversely proportional to the 6th power of the separation between excited and quenching molecules) it will be determined mainly by the action of the nearest unexcited molecule of a given substance.

In order to derive formulas for the fluorescence damping, yield and persistence of quenched solutions by taking account of the action of nearest unexcited molecules one must know the distribution of nearest neighbors. This problem was first studied by P. Hertz [3]. We shall reproduce his deductions as applied to our case.

Let W(R) dR be the probability that a molecule which is the nearest neighbor of an individual molecule of the same substance is located in the layer between R and R + dR. It is evident that the probability in question is given by the product of two probabilities: the probability that some molecule is between R and R + dR and the probability that in the volume from 0 to R there is no molecule except the given individual molecule; that is,

$$W(R)\,dR = \left[1 - \int_0 W(R)\,dR\right] 4\pi R^2 c\,dR \tag{1}$$

(where c is the number of molecules per unit volume). Hence

---

* All of Forster's arguments as well as our own refer to viscous solutions where it is possible to neglect the Brownian motion of the molecules while they are in an excited state.

$$W(R) = e^{-{}^4/_3\pi R^3 c} 4\pi R^2 c. \tag{2}$$

Knowing the distribution of nearest neighbors and assuming in accordance with the foregoing that the probability of quenching by the nearest neighbor in the time t to t + dt is given by $\frac{p\,dt}{R^6}\rho(t)$ (where p is a constant and R is the distance from the excited molecule to its nearest neighbor while t is the time from the instant when the molecule was excited) we can write for the change with time of the probability $\rho(t)$ of retention of excitation energy in the given molecule

$$-\frac{d\rho(t)}{dt} = \left(\frac{1}{\tau_0} + \frac{p}{R^6}\right)\rho(t). \tag{3}$$

From (3) it can be seen that $\rho(t)$ varies exponentially.

Since we are limiting ourselves to quenching only by the nearest neighbor the same law will govern fluorescence damping of the entire group of excited molecules for which the separation from nearest neighbors lies in the range from R to R + dR. The number of excited molecules in this group will evidently be determined by the distribution of nearest neighbors W(R) dR. Hence for the damping law of the entire ensemble of excited molecules n(t) we have

$$n(t) = n_0 \int\limits_0^\infty \exp\left(-\left[\frac{1}{\tau_0} + \frac{p}{R^6}\right)t\right] \exp[-{}^4/_3 R^3 c]\, 4\pi R^2 c\, dR, \tag{4}$$

where n_0 is the number of excited molecules at t = 0.

Assuming $R^3 = x$ and ${}^4/_3 \pi c = a$ we obtain

$$n(t) = a n_0 \int\limits_0^\infty \exp\left[-\left(\frac{1}{\tau_0} + \frac{p}{x^2}\right)t\right] \exp[-ax]\, dx. \tag{5}$$

Knowing the fluorescence damping law we can easily write expressions for the relative yield and persistence of fluorescence * in quenched solutions. We have

$$\frac{B}{B_0} = \frac{a}{\tau_0} \int\limits_0^\infty \int\limits_0^\infty \exp\left[-\left(\frac{1}{\tau_0} + \frac{p}{x^2}\right)t\right] \exp[-ax]\, dx\, dt; \tag{6}$$

$$\tau = \frac{a}{\tau_0 B} \int\limits_0^\infty \int\limits_0^\infty t \exp\left[-\left(\frac{1}{\tau_0} + \frac{p}{x^2}\right)t\right] \exp[-ax]\, dx\, dt, \tag{7}$$

where B, B_0 are the yields, and τ and τ_0 are the persistences, respectively, in quenched and unquenched solutions.

It is easily shown that the double integrals on the right-hand side of (9) amd (10) are easily converted to expressions containing tabular integrals [5]:

---

* Fluorescence persistence for nonexponential damping was determined in reference [4].

$$\frac{B}{B_0} = a\int_0^\infty e^{-ax}\,dx - ab^2\int_0^\infty \frac{e^{-ax}}{x^2+b^2}\,dx = \tag{8*}$$
$$= 1 - q\,\{\mathrm{ci}\,(q)\sin(p) - \mathrm{si}\,(q)\cos(q)\}\ ^*,$$

where

$$b = \sqrt{p\tau_0},\ q = ab = \frac{4}{3}\,\pi c\sqrt{p\tau_0}\,; \tag{9}$$

$$\frac{\tau}{\tau_0} = \frac{1 - \frac{3}{2}q\,\{\mathrm{ci}\,(q)\sin(q) - \mathrm{si}\,(q)\cos(q)\} - \frac{q^2}{2}\{\mathrm{ci}\,(q)\cos(q) + \mathrm{si}\,(q)\sin(q)\}}{1 - q\,\{\mathrm{ci}\,(q)\sin(q) - \mathrm{si}\,(q)\cos(q)\}}\,. \tag{10}$$

Equations (8) and (10) give the dependence of fluorescence yield and persistence on a single variable q which, according to (9) depends on the concentration of the dissolved substance and two constants, the quenching probability p and the fluorescence persistence of the unquenched solution τ_0.

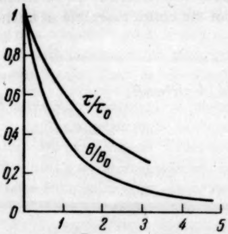

Fig. 1.

Figure 1 contains curves of the values of B/B_0 and τ/τ_0 for different values of q. The figure shows that, in accordance with experiment, fluorescence persistence varies with increased concentration of the fluorescing substance considerably more slowly than the yield.

It is of interest to note that for very small concentrations, i. e., with $q \ll 1$,

$$\frac{B}{B_0} = 1 - Q, \quad \frac{\tau}{\tau_0} \approx 1 - {}^1\!/_2 Q, \tag{11}$$

where $Q = q\,\{\mathrm{ci}(q)\sin(q) - \mathrm{si}(q)\cos(q)\}$.

The Formulas in (11) resemble those derived by Forster and Galanin [6] with the single difference that Q is a different function of c, τ_0 and p.

It must be mentioned in conclusion that we have not only taken more distant molecules into account but it have assumed a completely random distribution of all molecules. This cannot be correct for extremely small separations of the molecules, because the separation cannot be smaller than a certain critical value. The interaction between very close molecules is also probably quite different from the form of the interaction which is assumed above.

Received March 6, 1957.

LITERATURE CITED

[1] B. Ia. Sveshnikov, Doklady Akad. Nauk SSSR 111, 78 (1956) [Soviet Physics – Doklady, p. 633].

[2] T. H. Forster, Zs. Naturforsch. 4a, 321 (1949).

---

* $\mathrm{si}\,(p) = \int_p^\infty \frac{\sin t}{t}\,dt,\ \mathrm{ci}\,(p) = \int_p^\infty \frac{\cos t}{t}\,dt.$

[3] P. Hertz, Math. Ann. 67, 387 (1909).

[4] L. A. Kuznetsova, B. Ia. Sveshnikov and V. I. Shirokov, Optika i Spectroskopiia (USSR, 1957, No. 5).

[5] I. M. Ryzhik and I. S. Gradshtein, Tables of Integrals, Sums, Series and Products (in Russian) (1951).

[6] M. D. Galanin, J. Exptl. Theoret. Phys. (USSR) 28, 485 (1955) [Soviet Physics – JETP, p. 317].

ON THE THEORY OF THE DECAY OF A QUASI-STATIONARY STATE

L. A. Khalfin

(Presented by Academician V. A. Fok January 20, 1957)

We shall here consider some aspects of the theory of decay of an almost stationary state. This theory is very important for the investigation of alpha decay, the passage of particles through a potential barrier, the distribution of nuclear energy levels etc., [1, 2].

1. Let $\psi_0 = \psi(x, 0)$ be the wave function which describes the state of a physical system at time $t = 0$*. The probability that after the time t the system will still be in the initial state, ψ_0, is given by the formula

$$L(t) = |p(t)|^2, \tag{1}$$

where

$$p(t) = \int e^{-\frac{i}{\hbar}Et}\,\omega(E)\,dE; \tag{2}$$

$\omega(E)$ is the energy density distribution in the initial state and thus also at the time t. This theorem concerning the relation between the decay law of an almost stationary state and the energy distribution function in the state was derived by V. A. Fok and N. S. Krylov in an investigation of the time-energy indeterminancy relation [1]. They there showed that in connection with the emission of a particle from a potential well through a potential energy barrier the distribution density $\omega(E)$ is a meromorphic function of the complex variable E. Taking into account only the pair of poles of $\omega(E)$ nearest to the real axis:

$$E = E_0 \pm \Gamma; \quad E_0 > 0; \quad \Gamma > 0, \tag{3}$$

for sufficiently large t we obtain [1]

$$L(t) = e^{-\frac{2\Gamma}{\hbar}t} \tag{4}$$

which expresses the usual exponential decay law of a quasi-stationary state. In this case $\omega(E)$ is given by

$$\omega(E) = \frac{1}{\pi}\,\frac{\Gamma}{(E - E_0)^2 + \Gamma^2}, \tag{5}$$

---

* We have retained the notation in [1].

which is the usual dispersion formula for the energy distribution.

2. For our further investigation we shall refine some of the basic equations. In all formulas intergration with respect to the energy is carried out over the continuous spectrum E ϵ (0, ∞), so that

$$p(t) = \int_{\infty}^{\infty} e^{-\frac{i}{\hbar}Et} \overline{\omega}(E)\, dE, \tag{6}$$

where the function $\overline{\omega}$ (E) is semi-finite:

$$\overline{\omega}(E) = \begin{cases} \omega(E), & E > 0; \\ 0, & E \leqslant 0. \end{cases} \tag{7}$$

From (6) we obviously obtain

$$\overline{\omega}(E) = \frac{1}{2\pi\hbar} \int_{-\infty}^{\infty} e^{\frac{i}{\hbar}Et} p(t)\, dt\,, \tag{8}$$

so that a knowledge of p(t) in (8) provides an analytic function for the distribution $\overline{\omega}$(E).

The limitation in (7) on the distribution functions $\overline{\omega}$(E) imposes definite restrictions on p(t). Introducing

$$p_1(t) \equiv p(-t) = \int_{-\infty}^{\infty} e^{\frac{i}{\hbar}Et} \overline{\omega}(E)\, dE, \tag{9}$$

it can be shown that (9) determines $p_1(t)$ as an analytic function in the upper half plane Im t > 0. Using the Cauchy formula

$$\frac{1}{i\pi} P \int_{-\infty}^{\infty} \frac{p_1(t')}{t'-t}\, dt' = p_1(t) + \sum_i \frac{1}{t_i - t} \operatorname{Res} p_1(t_i), \tag{10}$$

we obtain the desired "dispersion" relations, with the real and imaginary parts separated in (10). Assuming that $p_1(t)$ has no poles on the real axis and making use of the equations which result from the reality of $\overline{\omega}$(E) we obtain the following "dispersion" relations:[*]

$$\operatorname{Re} p(t) = -\frac{2}{\pi} P \int_{0}^{\infty} \frac{t' \operatorname{Im} p(t') - t \operatorname{Im} p(t)}{t'^2 - t^2}\, dt',$$

$$\operatorname{Im} p(t) = \frac{2t}{\pi} P \int_{0}^{\infty} \frac{\operatorname{Re} p(t') - \operatorname{Re} p(t)}{t'^2 - t^2}\, dt'. \tag{11}$$

Thus the fact that $\overline{\omega}$(E) is semi-finite has the result that the real and imaginary parts of p(t) are related by integral "dispersion" relations.

---

[*] In deducing (10) and, consequently, (11) it was assumed that $p_1(t)$ decreases very rapidly for $|t| \to \infty$.

Introducing the modulus M(t) and the phase N(t) of p(t):

$$p(t) = M(t)\exp(iN(t));$$
$$\operatorname{Re} p(t) = M(t)\cos N(t); \quad \operatorname{Im} p(t) = M(t)\sin N(t), \tag{12}$$

we easily obtain the following "dispersion" relations:

$$\operatorname{Re} p(t) = M(t)\cos N(t) = -\frac{2}{\pi} P \int_0^{\infty} \frac{t'M(t')\sin N(t') - tM(t)\sin N(t)}{t'^2 - t^2}\, dt',$$
$$\operatorname{Im} p(t) = M(t)\sin N(t) = \frac{2t}{\pi} P \int_0^{\infty} \frac{M(t')\cos N(t') - M(t)\cos N(t)}{t'^2 - t^2}\, dt', \tag{13}$$

which relate the modulus M(t) (the square of which is a physically measurable quantity L(t)) and the phase N(t) of p(t).

Analogous "dispersion" relations can be derived in the more general case when $\bar{\omega}(E)$ is semi-finite in the sense

$$\bar{\omega}(E) = \begin{cases} \omega(E), & E > E_1; \\ 0 & E \leqslant E_1. \end{cases} \tag{14}$$

3. Another consequence of the semi-finiteness of $\bar{\omega}(E)$ is a criterion which must be satisfied by the modulus M(t) of p(t), which criterion has immediate physical meaning. The problem is stated as follows: Let the non-negative function M(t) be given; can we find a real function N(t) such that the function $\omega(E)$ whose Fourier transform in p(t) will be semi-finite in the sense of (14).

We find that M(t) cannot be arbitrary. The limitations on M(t) follow from the fundamental Paily-Wiener theorem [3]. In the theory of the decay of a quasi-stationary state this theorem can be stated as follows:

In order that L(t) be the probability of decay of a quasi-stationary state ψ_0 the following criterion must be satisfied:

$$\int_{-\infty}^{\infty} \frac{|\log M(t)|}{1+t^2}\, dt < \infty, \tag{15}$$

where $L(t) = M^2(t)$.

This criterion which must be satisfied by the modulus M(t) of p(t) will be called the criterion of finiteness or physical realizability [4] in the theory of the decay of a quasi-stationary state. It must be noted that whereas the "dispersion" relations depend essentially on the limit of semi-finitness E_1 the criterion of finiteness or physical realizability is entirely independent of E_1 so long as it is finite. Since the integral in (15) is absolutely convergent if at all convergent it is subject to the Cauchy test for convergence [5].

The criterion (15) enables us to assert the following with respect to the function M(t):

a) M(t) cannot vanish in any interval of t, and we cannot have

$$L(t) = 0 \text{ when } t \geq T_0; \tag{16}$$

b) When $|t| \to \infty$ the convergence of (15) is ensured by the inequality

$$\frac{|\log M(t)|}{1+t^2} < \frac{A}{t^l}, \tag{17}$$

where $A > 0$, $l > 1$.

c) Convergence at the points t_0: where $M(t_0) = 0$ and $M(t_0) = \infty$ is insured by the inequality

$$\frac{|\log M(t)|}{1+t^2} < \frac{A_1}{(t-t_0)^{l_1}}, \tag{18}$$

where $A_1 > 0$, $l < 1$.

The inequalities (17) and (18) are of fundamental significance in the theory of the decay of a quasi-stationary state, especially (17). Indeed (17) denotes that when $|t| \to \infty$ we have in any case

$$L(t) \geqslant Ae^{-\gamma|t|^q}, \tag{19}$$

where $A > 0$, $\gamma > 0$, $q < 1$, that is, in principle there can be no exponential decay law for all $t \in (0, \infty)$. In [1] the exponential decay law was obtained by an approximate calculation. Considering that $\omega(E)$ in (5) for $E \leq 0$ is zero we obtain

$$p(t) = \frac{1}{\pi}\int_0^\infty e^{-\frac{i}{\hbar}Et}\frac{\Gamma}{(E-E_0)^2+\Gamma^2}dE \simeq e^{-\frac{i}{\hbar}E_0t-\frac{\Gamma}{\hbar}t} - \frac{i}{\pi}\frac{\Gamma\hbar}{(E_0^2+\Gamma^2)\,t} \tag{20}$$

for $\frac{t}{\hbar}\sqrt{E_0^2+\Gamma^2} > 1$. The presence of the second non-exponential term in (20) confirms the criterion of physical realizability (15). It follows from (20) that the exponential decay law is valid in only a finite region of values of $\Gamma t/\hbar$:

$$\frac{\Gamma t}{\hbar}e^{-\Gamma t/\hbar} \geqslant \left(\frac{\Gamma}{E_0}\right)^2. \tag{21}$$

Similar results can be obtained in the more general case when $\overline{\omega}(E)$ differs from (5) by the factor $\sqrt{E}$.

4. When $p_1(t)$ has no zeros in the half-plane $\operatorname{Im} t > 0$ it is possible to obtain a direct relation between $M(t)$ and $N(t)$:

$$N(t) = \frac{2t}{\pi}P\int_0^\infty \frac{\log M('') - \log M(t)}{t'^2-t^2}dt', \tag{22}$$

so that knowing $M(t')$ from an experimental determination of the decay law of $L(t')$ it is possible on the basis of (22) to determine $N(t)$ uniquely, and consequently $\overline{\omega}(E)$ also on the basis of (8).

If $p_1(t)$ in the half-plane $\operatorname{Im} t > 0$ has, for example, a zero at $t_n = \alpha_n + i\beta_n$, $\beta_n > 0$ then (22) determines $N(t)$ to within

$$\tan^{-1}\frac{2(t-\alpha_n)\beta_n}{(t-\alpha_n)^2-\beta_n^2}. \qquad (23)$$

In conclusion I wish to thank Academician V. A. Fok for discussions and valuable comments and also the members of the theoretical physics seminar of the Leningrad State University.

All-Union Research Institute of
Exploratory Geophysics

Received January 23, 1957.

LITERATURE CITED

[1] N. S. Krylov and V. A. Fok, J. Exptl. Theoret. Phys. (USSR) 17, 93 (1947).

[2] J. Blatt and V. Weisskopf, Theoretical Nuclear Physics (John Wiley and Sons, New York, 1952).

[3] R. E. A. C. Paily and N. Wiener, Am. Math. Soc. Colloquium Publ., 19 (1934).

[4] L. A. Khalfin, Doklady Akad. Nauk SSSR 111, 2, 345 (1956) [Soviet Physics – Doklady, p. 671].

[5] G. M. Fikhtengol'ts, Course of Differential and Integral Calculus, [in Russian] (1948).

ON THE MODES OF PLASMA OSCILLATIONS IN A MAGNETIC FIELD

S. I. Braginskii

(Presented by Academician M. A. Leontovich January 18, 1957)

1. Fundamental Equations. The small oscillations of a homogeneous plasma in a magnetic field have often been studied both in the hydrodynamic approximation [1-12] and by means of the kinetic equation (see [13] for example). However, it will be useful to consider the oscillations in a unified manner over the entire range of frequencies for an arbitrary direction of propagation and arbitrary wavelength, using the model of two ideal charged gases, electronic and ionic. This will permit a classification of the different types of vibrations and some new results. We shall start with a set of linearized hydrodynamic equations for electrons and ions:

$$\begin{gathered}\dot{\rho}_\alpha + \rho^0_\alpha \operatorname{div} \mathbf{v}_\alpha = 0,\\ \rho^0_\alpha \dot{\mathbf{v}}_\alpha = e_\alpha n^0_\alpha \left(\mathbf{E} + \frac{1}{c}\left[\mathbf{v}_\alpha \mathbf{H}_0\right]\right) - \nabla p_\alpha.\end{gathered} \tag{1}$$

The subscript α denotes the kind of particle: α = e for electrons and α = i for ions. Undisturbed densities, particle concentrations and external magnetic field are denoted by the subscript zero. The fluctuating quantities, which are the densities ρ_α, the velocities $\mathbf{v}_\alpha$, the pressures p_α and the fields **E** and **H** are assumed to be small. The undisturbed plasma is neutral. We assume as the basic crude assumption of our theory, that the perturbation of the pressure is a scalar which is related to the density perturbation by the usual ideal gas expression

$$p_\alpha = c^2_\alpha \rho_\alpha, \tag{2}$$

where $c^2_\alpha = \partial p_\alpha/\partial \rho_\alpha = \gamma_\alpha T^0_\alpha/m_\alpha$; T^0_α is the temperature; m_α is the mass of particles α; and γ_α is a coefficient of the order of unity with the sense of an effective adiabatic exponent. The equations of (1) must be solved simultaneously with the Maxwell equations.

Let us consider a plane monochromatic wave. Here all quantities are proportional to $e^{i(\mathbf{kr} - \omega t)}$, so that we can replace $\partial / \partial t$ by $-i\omega$ and ∇ by $i\mathbf{k}$. Using the Maxwell time independant equations to eliminate two quantities [such as (**kE**) and (**kH**)], we obtain for the remaining 12 quantities (ρ_i, ρ_e, $\mathbf{v}_i$, $\mathbf{v}_e$, [**kE**], [**kH**]) a set of homogeneous equations of the form $i\omega f = \ldots$, where the right-hand sides do not contain the frequency. Setting the determinant of the system equal to zero we obtain the dispersion equation. This equation is of the 12th degree in ω, but since we are not considering any dissipative processes the equations are reversible so that the dispersion equation contains directly not ω but ω^2. Thus we obtain in general 6 branches of the function $\omega^\alpha(\mathbf{k})$. In practice it is more convenient to arrange the calculations somewhat differently. Instead of the velocities of ions and electrons we introduce the velocity **v** of a particle and the relative velocity $\mathbf{u} = \mathbf{v}_i - \mathbf{v}_e$. All quantities are easily expressed in terms of **u** and (**kv**), for which we obtain the equations

$$(\omega^2 - \omega_0^2 - c_e^2 k^2)\, \mathbf{u}_\parallel + \frac{\omega^2 (\omega^2 - \omega_0^2 - c^2 k^2)}{\omega^2 - c^2 k^2}\, \mathbf{u}_\perp - i\omega\Omega_e\, [\mathbf{hu}] + \tag{3}$$

$$+\, i\omega\Omega_e\, [\mathbf{hv}_\parallel] + \mu\Omega_e^2\, [\mathbf{h}\, [\mathbf{hu}]_\perp] + c_e^2 k^2 \mathbf{v}_\parallel = 0;$$

$$(\omega^2 - c_0^2 k^2)\, \mathbf{v}_\parallel + \mu i\omega\Omega_e\, [\mathbf{hu}]_\parallel + \mu c_e^2 k^2 \mathbf{u}_\parallel = 0. \tag{4}$$

Here $\mathbf{h} = \mathbf{H}_0/H_0$. The symbol $\perp$ denotes vector components perpendicular to $\mathbf{k}$; the symbol $\parallel$ denotes parallel components. We use the notation

$$\omega_0^2 = 4\pi e^2 n_e / m_e; \quad \Omega_e = eH_0/m_e c; \quad c_0^2 = c_e^2 \rho_e^0 + c_i^2 \rho_i^0; \quad \mu = \rho_e^0/\rho_i^0. \tag{5}$$

In the coefficients of the equations we have neglected terms of the order μ compared with unity. The coordinate axes are such that the vector $\mathbf{k}$ is in the direction of the $\underline{x}$ axis and that $h_y = 0$.

2. High frequencies. In order to simplify further calculations we shall assume that the Larmor electron frequency is small compared with the Langmuir frequency:

$$\Omega_e \ll \omega_0. \tag{6}$$

This assumption is valid if the magnetic energy is not too much greater than the particle energy:

$$\Omega_e^2/\omega_0^2 = (H_0^2/4\pi\rho_e c_e^2)\,(c_e^2/c^2) \ll 1.$$

It results from (6) that three of the six roots of the dispersion equation are of a greater order of magnitude than the others. For high-frequency oscillations the motion of the ions can be neglected and we obtain a solution from Equation (3) by setting $\mu = 0$, $\check{v} = 0$. The dispersion equation becomes

$$(\omega^2 - \omega_e^2)(\omega^2 - \omega_c^2)^2 - \Omega_e^2\, [h_x^2 \omega^{-2} (\omega^2 - \omega_e^2)(\omega^2 - c^2 k^2)^2 + \tag{7}$$

$$+\, h_z^2 (\omega^2 - \omega_c^2)(\omega^2 - c^2 k^2)] = 0,$$

where

$$\omega_e^2 = \omega_0^2 + c_e^2 k^2; \tag{8}$$

$$\omega_c^2 = \omega_0^2 + c^2 k^2. \tag{9}$$

Equation (7) is of the fourth degree in ω^2 but determines only three roots correctly. The fourth root is small ($\sim \Omega_e^2$) and is not always correctly given by means of (7); we shall consider it below. In order to obtain simple explicit expressions for the three "large" roots we shall consider the limiting cases of small and large wavelengths with a characteristic length given by

$$a = (c^2/\omega_0 \Omega_e)^{1/2}. \tag{10}$$

A. Short waves. When $a^2 k^2 \gg 1$ Equation (7) has the roots

$$\omega^2 = \omega_e^2 + \Omega_e^2 h_z^2 (1 - \omega_e^2/c^2 k^2); \tag{11}$$

$$\omega^2 = \omega_c^2 \pm \omega_0 \Omega_e h_x (1 + c^2k^2/\omega_0^2)^{-1/2}. \tag{12}$$

Root (11) corresponds to longitudinal electron plasma waves. Their energy is concentrated mainly in the electric field, in the kinetic energy of the electrons and in their pressure. Electromagnetic waves such as light waves in the plasma possess the dispersion given by (12). One of the roots of (12) corresponds to vibrations with right-handed circular polarization; the other root corresponds to left-handed circular polarization. The energy of the oscillations is contained in the electromagnetic field and in the kinetic energy of the electrons.

B. Long waves. When $a^2 k^2 << 1$ the roots of (7) are

$$\omega^2 = \omega_e^2 + h_z^2 c^2 k^2; \tag{13}$$

$$\omega^2 = \omega_c^2 \pm \omega_0 \Omega_e. \tag{14}$$

In the oscillations at the frequency given by (13) the electrons move principally along the magnetic lines of force, while in the oscillations (14) they move in a plane perpendicular to the magnetic lines of force, and in this plane one of the oscillations of (14) is polarized clockwise while the other is polarized counterclockwise. The energy in all three cases is concentrated principally in the electric field and in the kinetic energy of the electrons.

3. Low frequencies. We find the low-frequency branches by making the assumption (which is confirmed by the result) that $\omega^2 << \omega_0^2$, $\omega^2 << c^2k^2$. Projecting (3) on the x axis, we easily see that u_x is small. The low-frequency oscillations are thus quasi-neutral and can be studied with sufficient accuracy while neglecting space charge and the displacement current. We denote

$$\varkappa = \omega_c^2/c^2k^2 = 1 + \omega_0^2/c^2k^2; \tag{15}$$

$$\Omega_0^2 = \mu \Omega_e^2/\varkappa. \tag{16}$$

The dispersion equation is

$$(\omega^2 - \Omega_0^2 h_x^2) [\omega^4 - \omega^2 (\Omega_0^2 + c_0^2k^2) + \Omega_0^2 h_x^2 c_0^2 k^2] - \mu\varkappa)^{-1} \Omega_0^2 h_x^3 \omega^2 (\omega^2 - c_0^2 k^2) = 0. \tag{17}$$

Exact simple expressions for the roots of (17) are obtained when $h_x = 1$ or $h_x = 0$.

For the propagation of a wave along the magnetic field ($h_x = 1$) we have

$$\omega^2 = c_0^2 k^2; \quad \omega^2 = \frac{\Omega_e^2}{\varkappa^3} (\mu\varkappa + 1/2 \pm \sqrt{\mu\varkappa + 1/4}) \tag{18}$$

For propagation transverse to the magnetic field ($h_x = 0$) we have

$$\omega^2 = c_0^2 k^2 + \Omega_0^2; \quad \omega^2 = 0; \quad \omega^2 = 0. \tag{19}$$

In order to obtain the frequencies for any direction of propagation we consider two limiting cases.

A. Long waves. Let $\mu\kappa \gg 1$. In this case $\omega_0^2/c^2k^2 \gg 1$, so that this condition is equivalent to $b^2k^2 \ll 1$, where

$$b^2 = \rho_i\, c^2/4\pi e^2 n_e^2. \tag{20}$$

The roots of the dispersion Equation (17) are approximately

$$\omega^2 = \Omega_0^2 h_x^2 \simeq c_A^2 (\mathrm{hk})^2, \text{ where } c_A^2 = H_0^2/4\pi\rho_0; \tag{21}$$

$$\omega^2 = {}^1/_2 \left[c_A^2 + c_0^2 \pm \sqrt{c_A^4 + c_0^4 + 2c_A^2 c_0^2 (1 - 2h_x^2)}\right] k^2. \tag{22}$$

The first of these roots corresponds to Alfven's waves; the other two roots correspond to the magneto-acoustic waves which were investigated in [5-8].

B. Short waves. Let $\mu\kappa \ll 1$; we can then have $\omega_0^2/c^2k^2 \gtrless 1$. In this case the roots of the dispersion equation are approximately

$$\omega^2 = \mu\kappa\Omega_0^2 h_x^2 = \Omega_i^2\, h_x^2, \quad \text{где } \Omega_i = e_i H_0 / m_i c; \tag{23}$$

$$\omega^2 = {}^1/_2 \left[\Omega_0^2 h_x^2 / \mu\kappa + \Omega_0^2 + c_0^2 k^2 \pm \sqrt{(\Omega_0^2 h_x^2 / \mu\kappa + \Omega_0^2 + c_0^2 k^2)^2 - 4c_0^2 k^2 \Omega_0^2 h_x^2 / \mu\kappa}\right]. \tag{24}$$

The frequency in (23) corresponds to waves which can be called gyromagnetic ionic waves. The energy of these waves is concentrated in planes perpendicular to the wave vector (not to the magnetic field), so that the condition for a quasi-neutral plasma is satisfied. In a weak magnetic field ($\Omega_e \ll \kappa^2 c_0^2 k^2$) one of the roots of (24) corresponds to waves which are near sonic frequencies $\omega^2 \approx c_0^2 k^2$ (Equation (24) does not give a correction to $c_0^2 k^2$). The other root, $\omega^2 = \Omega_e^2 h_x^2/\kappa^2$, corresponds to oscillations in which the vectors **H** and **u** are parallel and circularly polarized. The energy of these oscillations at $\omega_0^2/c^2k^2 \gg 1$ is concentrated principally in the magnetic field; for $\omega_0^2/c^2k^2 \lesssim 1$ it is concentrated in the magnetic field and in the kinetic energy of the electrons, so that these can be called magneto-electronic oscillations. In a strong field ($\Omega_e^2 \gg \kappa^2 c_0^2 k^2$) with $h_x^2 \gg \mu\kappa$ one of the roots $\omega^2 \approx c_0^2 k^2$ also corresponds to sonic oscillations and the other $\omega^2 \approx \Omega_e^2 h_x^2/\kappa^2$ to magneto-electronic oscillations. When the direction of propagation is very close to the direction of the magnetic field ($h_x^2 \ll \mu\kappa \ll 1$) the first root approaches zero and the second approaches $\Omega_0^2 + c_0^2 k^2$. Both oscillations become complicated because of the essential participation of both ions and electrons.

Short magnetohydrodynamic waves are considerably different from the long waves. This shows that tha usual equations of magnetohydrodynamics which lead (for infinite conductivity) to the picture of "frozen-in" magnetic lines of force and to Equations (21) and (22) are invalid for lengths smaller than b.

It is of interest to compare b with the mean free path of the particles. Setting $l = 1/n_0\sigma$, we obtain $l/b = (4\pi e^2/\rho_i c^2\sigma^2)^{1/2}$. If we take $\sigma \sim 10^{-14}$ cm as the cross section for Coulomb collisions at a temperature of a few electron volts, for a hydrogen plasma this gives $l/b \sim (10^{13}/n_0)^{1/2}$. Thus two cases can exist: in a dense plasma $l < b$ and in a rarefied plasma $l > b$.

Let us compare the possible modes of oscillations in the presence and in the absence of an external magnetic field. When $H_0 = 0$ we can have longitudinal electronic waves ($\omega = \omega_e$), transverse electromagnetic waves with two independent directions of polarization (the frequency $\omega = \omega_c$ is doubly degenerate) and sound waves ($\omega = c_0 k$). It is also possible to have stationary shears in directions perpendicular to the wave vector ($\omega = 0$). The frequency $\omega = 0$ is quadruply degenerate since there are two kinds of particles and two independent shear directions. In a magnetic field such shears are possible only for $\mathbf{k} \perp \mathbf{H}$; for other directions of **k** they are "twisted" by the magnetic field and give two additional modes of vibration (two branches of ω^2). The first four branches are also distorted, and the degeneracy of the frequency ω_c is removed.

The author thanks A. Kazantsev for a valuable discussion.

Received December 20, 1956.

LITERATURE CITED

[1] V. L. Ginsburg, The Theory of Radio Propagation in the Ionosphere [in Russian] (1949).

[2] H. Alfven, Cosmical Electrodynamics (Oxford Univ. Press, 1950) [Russian translation, IL, 1952].

[3] E. Astrom, Nature 165, 1019 (1950); Ark. f. Fysik 2, No. 42, 443 (1950).

[4] H. Herlofson, Nature 165, 1020 (1950).

[5] H. C. Van de Holst, Coll. Problems of Cosmical Aerodynamics (Central Air Documents Office, Dayton 1951) [Russian translation, (IL, 1953), p. 58].

[6] V. L. Ginsburg, J. Exptl.-Theoret. Phys. (USSR) 21, 788 (1951).

[7] A. Shliuter, Coll. Plasma Dynamics [Russian translation] (IL, 1956), p. 80..

[8] A. Baños, Phys. Rev. 97, 1435 (1955); Proc. Roy. Soc. A 233, 350 (1955).

[9] V. C. Ferraro, Proc. Roy. Soc. A 233, 310 (1955).

[10] L. Spitzer, Physics of Fully Ionized Gases (N. Y., 1956).

[11] B. N. Gershman, J. Exptl.-Theoret. Phys. (USSR) 31, 707 (1956) [Soviet Physics – JETP, p. 572].

[12] J. H. Piddington and M. N. Roy, Astr. Soc. 114, 638 (1954).

[13] B. H. Gershman, J. Exptl.-Theoret. Phys. (USSR) 24, 453 (1953).

AN X-RAY STUDY OF THE EFFECT OF MECHANICAL STRESS ON THE STRUCTURE OF POLYCRYSTALLINE BARIUM TITANATE

I. G. Ismailzade

(Presented by Academician N. V. Belov March 12, 1957)

The dielectric constant of barium titanate is considerably affected by various physical factors including pressure. The influence of hydrostatic pressure on the dielectric properties of barium titanate was first investigated by B. M. Vul and L. F. Vereshchagin [1], who showed that at room temperature the dielectric constant increases with pressure. The effect of hydrostatic pressure on the Curie point of a barium titanate single crystal was studied by Merz [2], who observed a linear shift of the Curie point towards lower temperatures at the rate of $5.8 \cdot 10^{-3}$ deg per atm.

The effect of mechanical stress perpendicular to the surface of electrodes made of ceramic $BaTiO_3$ has been studied by Takagi, Sawaguchi and Akioka [3], who showed that the specific inductive capacitance is reduced with increasing pressure. Shirane and Sato [4] have investigated the effect of hydrostatic and mechanical pressures on the dielectric properties of ceramic $BaTiO_3$ and solid solutions of $BaTiO_3$ and $SrTiO_3$. It has been established that under mechanical pressures up to 600 kg/cm^2 directed parallel or perpendicular to the surfaces of electrodes, unlike the case for hydrostatic pressure, with increasing pressure the dielectric constant is reduced below the Curie point while above the Curie point it is increased. It was also observed that with increasing mechanical pressure the Curie temperature increases at the rate $dT/dp = 4.0 \cdot 10^{-3}$ $deg \cdot cm^2/kg$. The dependence of ferroelectric dielectric properties on mechanical pressure was subsequently investigated by E. V. Siniakov and I. A. Izhak [5], who obtained similar results.

The present paper is devoted to an investigation of ferroelectrics under pressure. Mechanical pressures of the order of 600-1000 kg/cm^2 have only a small effect on the structure of barium titanate, so that ordinary x-ray photographic analysis is inadequate. For this reason we have used an ionization method in employing URS-50-I x-ray equipment. We designed a simple x-ray gonimeter head so that samples could be subjected to pressure in the direction of the axis of the head. Pressure was applied by a lever system with a 1 : 10 arm ratio. Pressures were measured to within 3-5%. The head permits movement of the specimen in two mutually perpendicular directions.

The barium titanate specimen was a polished rectangular plate of 2 mm^2 cross sectional area. The plate was measured with a measuring microscope.

All of the x-ray photographs were obtained with filtered copper radiation under absolutely identical conditions, which were a stabilized anode current of 6 ma and an accelerating potential of 36 kv at room temperature.

For the purpose of attaining high accuracy several points were used for each diffraction maximum. At certain reflection angles θ the number of pulses was counted in 15 and 32 seconds. At each angle 5 to 10 counts were obtained and the diffraction maxima were plotted from the arithmetical means of the pulse counts in 15 seconds (for (110) reflection) and 32 seconds.

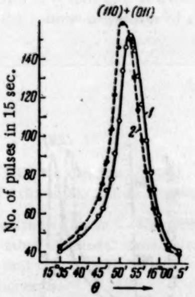

Fig. 1. Diffraction maximum of $BaTiO_3$ from (110) + (011) without pressure (1) and under 1000 kg/cm² (2).

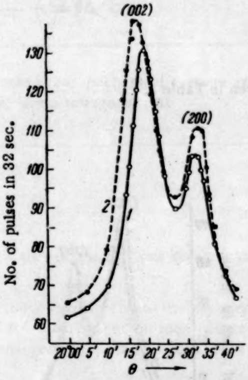

Fig. 2. Diffraction maxima of $BaTiO_3$ from (002) and (200) without pressure (1) and under 1000 kg/cm² (2).

All maxima were obtained four times in the following order: without pressure, under pressure, without pressure, under pressure. Identical results were obtained under identical conditions.

This was the method of plotting the diffraction maximum from the planes (110) + (011), (200), (002), (103), (301) and (224) without pressure and under mechanical pressure of 700 kg/cm², and for the planes (110) + + (011) as well as (200) and (002) using 1000 kg/cm² (Figs. 1-4). The curves are compared in Table 1.

TABLE 1

Increase of the angle θ (in minutes)

Pressure	(110) + (011)	(200)	(002)	(301)	(103)	(224)
700 kg/cm²	−1.0	+1.0	−1.5	+1.5	−2.5	−4.0
1000 kg/cm²	−2.0	+1.5	−2.5	—	—	—

The table shows that:

1. In reflections from the planes (200) and (301) under pressure the diffraction maxima are shifted toward larger angles, while the (002), (103) and (224) maxima are shifted toward smaller angles θ.

2. With greater pressure the absolute values of the shifts are increased.

The shift of the diffraction maxima from (200) and (301) towards larger angles θ indicates that under mechanical pressure the parameter a of the barium titanate lattice is somewhat shortened. The shift of the (002) and (103) maxima toward smaller angles, on the other hand, is due to an increase of the parameter c. The increments

Δa and Δc were calculated from the expression

$$\Delta\theta = -\frac{\lambda^2}{4\sin\theta\cos\theta}\left[\frac{h^2+k^2}{a^3}\Delta a + \frac{l^2}{c^3}\Delta c\right] \tag{1}$$

and are given in Table 2.

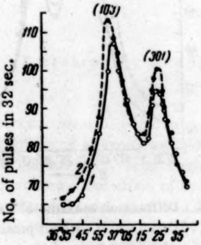

Fig. 3. Diffraction maxima of $BaTiO_3$ from (103) and (301) without pressure (1) and under 700 kg per cm² (2).

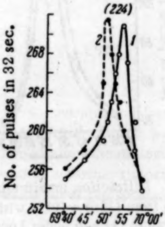

Fig. 4. Diffraction maximum of $BaTiO_3$ from (224) without pressure (1) and under 700 kg/cm² (2).

TABLE 2

Pressure kg/cm²	$\Delta a - \Delta b$, Å		a, Å	Δc, Å		c, Å	c/a
	from (200)	from (301) and (103)		from (002)	from (301) and (103)		
	—	—	3,9935	—	—	4,0325	1,0098
700	—0,0026	—0,002	3,9915	+0,0042	+0,004	4,0365	1,0113
1000	—0,004	—	3,9895	+0,006	—	4,0385	1,0123

Thus in the $BaTiO_3$ lattice under mechanical pressure the parameters a and b are shortened while c is lengthened. This results in increased tetragonality c/a.

The effect of mechanical pressure on the structure of barium titanate can be explained on the basis of the expression for the free energy of the system. We know that the differential of the free energy is

$$dF = -p\,dv - S\,dT. \tag{2}$$

For the isothermal process which occurs in our case we have

$$p = -\left(\frac{dF}{dv}\right)_T, \quad \left(\frac{dp}{dv}\right)_T = -\left(\frac{d^2F}{av^2}\right)_T, \quad \left(\frac{dp}{dv}\right)_T < 0. \qquad (3)$$

Since $dp > 0$ it follows that $dv < 0$, that is, in the general case under mechanical pressure at constant temperature the volume increment of a unit cell will be negative. For a tetragonal cell

$$\Delta v = 2ac\ \Delta a + a^2\ \Delta c \leqslant 0 \text{ or}$$
$$|\Delta a| \geqslant \frac{a\Delta c}{2c}. \qquad (4)$$

For $BaTiO_3$ we can assume that $a \approx c$; then $|\Delta a| \geq \Delta c/2$, that is, the smallest absolute value of the increment of a(b) is $\Delta c/2$, which corresponds to $\Delta v = 0$.

Our data show (Table 2) that within the limits of error the above case applies to our experiment. It can thus be stated that under mechanical pressure of the order of 700-1000 kg/cm^2 at room temperature the volume of a unit cell of polycrystalline $BaTiO_3$ is practically unchanged while the tetragonality c/a of the lattice increases.

The shift of the Curie point toward higher temperatures under mechanical pressure [4, 5] results from increased tetragonality c/a of the barium titanate lattice. Indeed, the increase of c and the reduction of a and b impedes the transition to a cubic lattice, that is, under mechanical pressure a higher temperature is required for the phase transition from a tetragonal to a cubic lattice.

The author is grateful to Professor L. S. Maiants for a discussion of the results and for valuable suggestions.

Petroleum Institute, Academy of Sciences,
Azerbaydzhan SSSR

Received July 6, 1957.

LITERATURE CITED

[1] B. M. Vul and L. F. Vereshchagin, Doklady Akad. Nauk SSSR 48, 9, 662 (1945).

[2] W. J. Merz, Phys. Rev. 78, 52 (1950).

[3] Y. Takagi, E. Sawaguchi and T. Akioka, J. Phys. Soc. Japan 3, 270 (1948).

[4] G. Shirane and K. Sato, J. Phys. Soc. Japan 6, 20 (1950).

[5] E. V. Siniakov and I. A. Izhak, Doklady Akad. Nauk SSSR 100, 2, 243 (1955).

COLORATION OF $BaTiO_3$ SINGLE CRYSTALS

M. S. Kosman and E. V. Bursian

(Presented by Academician A. F. Ioffee February 18, 1957)

It is well known that the growing of single crystals of barium metatitanate yields crystals varying from bright yellow to dark brown and almost black shadings. We have observed that the character of the coloring of these crystals is similar to that of alkali halide crystals and silver halide salts. The darkening of polycrystalline specimens under various influences has already been noted in the literature [1]. This darkening is associated with partial reduction and precipitation of the metal, which naturally increases the conductivity and produces changes of other electrical properties. The coloration which we have observed is a different and purely physical process which is associated with the movement of current carriers.

The samples were prepared by the method of Matthias, but the relative amounts of the components were varied [2]. Crystals were grown in the form of flat triangles, rectangular parallelepipeds or cubes. The exterior form, color and appearance of the crystals was strongly dependent on the composition of the mixture and on the conditions of growth. The crystals showed the ferroelectric properties which are described in the literature. For optical measurements we chose plates with plane-parallel faces and with as few internal defects as possible which could induce scattering. Absorption was measured with an SF-4 spectrometer.

In Figure 1 Curve A gives the absorption spectrum of single crystals which became brown during growth. The crystal was then heated in hydrogen at 1000° or simply in the reducing portion of an alcohol lamp flame, as a result of which it became almost transparent with a light yellow tint; the absorption spectrum was then represented by Curve B. In this case our data almost agree with those in reference [3]. After heating in air or in oxygen the crystals again acquire a reddish-brown coloring (Curve C). In analogy with alkali-halide crystals this coloration can be called additive.

Field coloration such as is known in the case of alkali-halide crystals is also observed in $BaTiO_3$. When a single crystal about 1.5 mm thick is bleached, placed in a furnace mounted on the stage of a microscope and subjected to a voltage (different electrodes being tried, such as annealed silver, copper and platinum plates, and aquadag), at 300° and 500 v it is possible to observe the slow progress from the anode (at about 1 mm per minute) of heavy reddish-brown coloration possessing a very even front (Fig. 2, I). Sometimes this is preceded by a relatively rapid spreading from the cathode of irregular blue coloring (Fig. 2, II), which is soon terminated. The brownish coloration proceeds not only from the electrode but also from all cracks and other macrodefects. At the contact between the brownish and blue coloring the progress of the brown front is halted and something like color annihilation occurs. Thereupon the blue coloring is obliterated by the brown and the entire crystal becomes uniformly reddish brown; this is represented by Curve D of Fig. 1. Curve E represents the absorption band which arises from coloration by oxygen; Curve F is the absorption band for field coloration.

If at the instant depicted in Fig. 2 the sign of the field is reversed the brown coloring leaves, although not completely, and the coloring advancing from the other side may overtake the previous coloration. It is thus possible to produce coloring with an alternating field. Such simultaneous coloration proceeding from both electrodes is easily observed experimentally at 50 cycles. The progress of the brownish coloration is strongly dependent on temperature. At room temperature the speed is about 1 mm per day in a field E = 10 kv per cm.

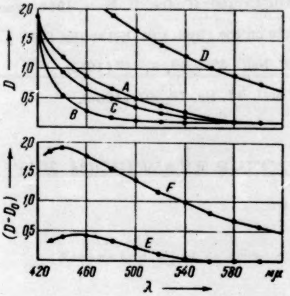

Fig. 1. Changes in the absorption curve following coloration. D is the optical density of the crystal; D_0 is the optical density of the decolorized crystal.

Field coloration and oxygen coloration are probably due to the same color centers. It must be noted that the curves in Figure 1 were obtained from only two specimens because good optical crystals are rare; therefore the exact shape of the curves cannot be regarded as established. However, the fact of reddish-brown coloration has been established for a large number of specimens including some which were kindly made available to us by I. E. Myl'nikova. Blue coloration is unstable and seldom encountered. Weak reddish coloration can also be detected in ceramic specimens, but observations in this case are very difficult because of the impossibility of using transmitted light.

The coloration of $BaTiO_3$ is also of interest because it is always associated with ionic conduction [4], whereas some investigators report that $BaTiO_3$ possesses only electronic conductivity [5].

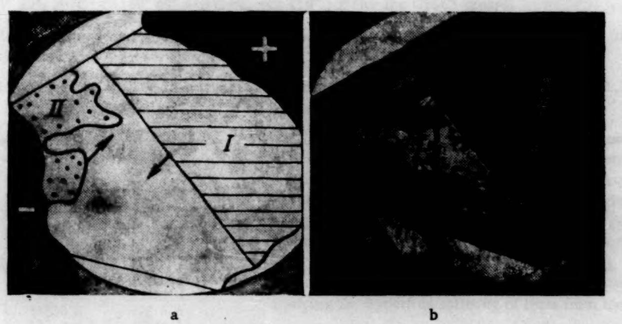

a b

Fig. 2. Photograph of a crystal partially colored by a field (b) and the explanation (a).

It follows from the foregoing measurements that the coloration of single crystals changes their electric characteristics, although this investigation is still in progress. Since coloration also takes place at room temperature it is possible that a comparison of the properties of colored and uncolored specimens will clarify the question of the aging of barium titanate condensers [6, 7].

A. M. Herzen Leningrad State Pedagogical Institute

Received February 7, 1957.

LITERATURE CITED

[1] N. S. Novosil'tsev, A. L. Khodakov and M. S. Shul'man, Doklady Akad. Nauk SSSR 83, 6, 829 (1952).

[2] S. Safrata, V. Bednarova and J. Benes, Czechoslov. J. Phys. 6, No. 2, 185 (1956).

[3] T. Horie, K. Kawabe and S. Sawada, J. Phys. Soc. Japan 9, No. 5, 823 (1954).

[4] N. F. Mott and R. W. Gurney, Electronic Processes in Ionic Crystals (Oxford U. Press, 1950), 2nd edition.

[5] M. D. Mashkovich, Abstracts of the All-Union Conference on the Physics of Dielectrics (1956).

[6] N. P. Bogoroditskii and T. N. Verbitskaia, Doklady Akad. Nauk SSSR 89, 3, 447 (1953).

[7] M. C. McQuarrie and W. R. Buessem, Am. Ceram. Soc. Bull. 34, No. 12, 402 (1955).

THE MICROWAVE SPECTRUM OF 1,2-FLUOROCHLOROETHANE

I. A. Mukhtarov

(Presented by Academician V. N. Kondrat'ev February 27, 1957)

This paper concerns an investigation of the microwave spectrum of molecules of 1,2-fluorochloroethane. The study of such molecules is of special intesest because they can be found in several different isomeric states.

Using the approximation of a rigid asymmetric top the rotational spectrum was calculated for various values of the angle between the projections of the C−F and C−Cl bonds on a plane perpendicular to the C−C bond. The following structural data was used in the calculations: interatomic distances C−C 1.54 A; C−H 1.10 A; C−F 1.375 A and C−Cl 1.78 A; C−C−F, H−C−C and H−C−H angles 109° 28' (for the CH_2F group); H−C−H 110° 20', H−C−C 109° 49' and C−C−Cl 110° 30' (for the CH_2Cl group).

Calculations showed that a large number of different rotational absorption lines are to be found in the frequency interval from 10,000 to 30,000 megacycles.

A radiospectroscope with Stark modulation was used to study the microwave spectrum of 1,2-fluorochloroethane from 10,000 to 20,000 Mc and a large number of absorption lines were discovered.

TABLE 1

Transitions $J_{K_{-1},K_1}-J_{K'_{-1},K'_{-1}}$	Frequency in Mc	
	calculations	experiment
$1_{01}-1_{10}$	—	10729.7
$2_{02}-2_{11}$	—	11155.0
$3_{03}-3_{12}$	11815.5	11815.4
$4_{04}-4_{13}$	12737.6	12736.4
$5_{05}-5_{14}$	13954.8	13952.1

It was found that the overall scheme of observed lines is in good agreement with the calculated scheme for $\alpha = 70°$. According to the calculations for $\alpha = 70°$ the 10,000 to 20,000 Mc region should reveal groups of lines belonging with the Q branch $\Delta K_{-1} = -1$ and $\Delta K_1 = 1$ from J = 1 to J = 8. We observed and identified absorption lines corresponding to the transitions $1_{01}-1_{10}$; $2_{02}-2_{11}$; $3_{03}-3_{12}$; $4_{04}-4_{13}$ and $5_{05}-5_{14}$ of the $FH_2C-CH_2Cl^{35}$ molecule. Identification was performed by studying the hyperfine splitting of lines from these transitions.

Table 1 shows the experimental and theoretical frequencies of the lines. In the calculations it was assumed that A−C = = 10729.6 Mc and $\kappa = -0.923$, which we determined from the measured frequencies for the transitions $1_{01}-1_{10}$ and $2_{02}-2_{11}$. An analysis of the hyperfine structure of the lines yielded values of the quadrupole bond constants in the directions of the principal axes of inertia of the $FH_2C-CH_2Cl^{35}$ molecule: $\chi_a = -23.5$ Mc and $\chi_b = -8.8$ Mc.

The discrepancy between the experimental and theoretical values of the frequencies in Table 1 increases with J; this is evidently associated with a centrifugal perturbation resulting from "non-rigidity" of the molecule, which was not taken into account in the calculations.

Thus, from an analysis of the spectrum of 1,2-fluorochloroethane it was established that this molecule possesses a stable configuration with $\alpha = 70°$ (a so-called "twisted" isomer). From considerations of symmetry we would expect $\alpha = 60°$ for a twisted isomer. The 10° difference in the angle α is evidently associated with the strong repulsion between the fluorine and chlorine atoms.

The author is indebted to Academician I. L. Knunianets for providing the 1,2-fluorochloroethane and to Doctor of Physico-Mathematical Sciences A. M. Prokhorov for valuable suggestions while the work was in progress.

P. N. Lebedev Physics Institute,
Academy of Sciences, USSR

Received February 21, 1957.

THE NATURAL SHAPE OF ENERGY LEVELS

Academician* B. I. Stepanov and P. A. Apanasevich

In quantum mechanics broadening of spectral lines is associated with broadening of the energy levels. The uncertainty principle enables us to determine the average level breadth. The question of the shape of levels corresponding to the naturally broadened shape of spectral lines has not been considered. The usual quantum electrodynamical methods [1-3] based on a solution of the time-dependent Schrodinger equation give a correct expression for the shape of a spectral line but do not include the broadening of the energy levels. In some instances it is assumed that the shape of a line completely reproduces the shape of an excited energy level [2], without clarification of the meaning of the assumption. The present paper gives the derivation of an expression which can be regarded as the natural shape of energy levels.

Let us consider an isolated system consisting of two interacting subsystems, an atom and an electromagnetic field. The Schrodinger equation for the stationary states of this system is

$$(H_a + H_f + U)\Psi = E\Psi. \tag{1}$$

Here H_a and H_f are the Hamiltonians of the independent atom and electromagnetic field, respectively. The interaction operator is [1]

$$U = -\frac{e}{mc}\mathbf{pA}, \tag{2}$$

where **p** is the momentum operator of the optical electron of the atom, and **A** is the vector potential of the electromagnetic field:

$$\mathbf{A} = \sum_{\mathbf{k},\,l}(q_{\mathbf{k}l}e^{i\mathbf{kr}} + q_{\mathbf{k}l}^{+}e^{-i\mathbf{kr}})\,e_{\mathbf{k}l}. \tag{3}$$

In (3) the summation is performed over the two values of the polarization l and over all values of the wave vector **k** as determined by the size V of the periodic cube. The summation over l and **k** will hereinafter be denoted by a single index.

The matrix elements of the operators q_κ and q_κ^+ are

$$(q_\varkappa)_{m_\varkappa,\,n_\varkappa} = \sqrt{\frac{2\pi c^2 h}{V\omega_\varkappa}}\sqrt{n_\varkappa}\,\delta_{n_\varkappa-1,\,m_\varkappa};\quad (q_\varkappa^{+})_{m_\varkappa,\,n_\varkappa} = \sqrt{\frac{2\pi c^2 h}{V\omega_\varkappa}}\sqrt{n_\varkappa+1}\,\delta_{n_\varkappa+1,\,m_\varkappa}. \tag{4}$$

Here n_κ and m_κ are the quantum numbers of the states of the κ-th oscillator; ω_κ is the frequency; e_κ is the polarization vector.

---

*Academy of Sciences, Byelorussian SSR.

The solution of (1) will be obtained in the form

$$\Psi = \sum_{i\,,\,(n_\varkappa)} C_{i\,(n_\varkappa)} \psi_{i\,(n_\varkappa)}, \tag{5}$$

where $\psi_{i(n_\kappa)}$ is the product of the eigenfunction of the free atom in the i-th state and the eigenfunction of the field in the state (n_κ). The symbol (n_κ) denotes the set of all the numbers $n_1, n_2, \ldots, n_\kappa, \ldots$ denoting the states of all the field operators. Substituting (2) and (5) in (1) and performing some well-known transformations, we obtain a set of equations for the determination of $C_{i(n_\kappa)}$:

$$(E_{i\,(n_\varkappa)} - E)\, C_{i\,(n_\varkappa)} - \sum_{j,\,\varkappa'} (p_{ij})_{\varkappa'} \sqrt{n_{\varkappa'}+1}\; C_{j\,(n_\varkappa+\delta_{\varkappa\varkappa'})} - \sum_{j,\,\varkappa'} (p_{ij})_{\varkappa} \sqrt{n_{\varkappa'}}\; C_{j\,(n_\varkappa-\delta_{\varkappa\varkappa'})} = 0, \tag{6}$$

where

$$E_{i\,(n_\varkappa)} = E_i + \sum_\varkappa h\omega_\varkappa (n_\varkappa + {}^1/_2), \tag{7}$$

$$(p_{ij})_\varkappa = -\, ie \sqrt{\frac{2\pi h}{V\omega_{\varkappa'}}}\; \omega_{ij}\, (\mathbf{r}\mathbf{e}_{\varkappa'})_{ij}. \tag{8}$$

In (6) and (8) it is assumed that within the atom $kr \ll 1$ [4]. The notation has been borrowed from [5], with the following meaning: $(n_\kappa + \delta_{\kappa\kappa'})$ differs from (n_κ) only in that the oscillator κ' is in the state $n_{\kappa'} + 1$ instead of $n_{\kappa'}$. For simplicity we assume that the atom has only two energy levels: $E_1 = 0$ and E_2.

The equations of (6) can be solved by successive approximations. The zeroth approximation will be the state in which the atom is excited while the field contains no photons, that is, only $C_{2(0)}(E)$ differs from zero. Equation (6) in first approximation becomes

$$\begin{gathered}(E_2 - E)\, C_{2\,(0)} - \sum_{\varkappa'} (p_{21})_{\varkappa'}\, C_{1\,(\delta_{\varkappa\varkappa'})} = 0,\\ (h\omega_{\varkappa'} - E)\, C_{1\,(\delta_{\varkappa\varkappa'})} - (p_{12})_{\varkappa'}\, C_{2\,(0)} = 0.\end{gathered} \tag{9}$$

Equation (9) describes the interaction of the excited atomic level with the practically continuous spectrum of possible field states. A similar set of equations has been solved by Rice [6] and Stepanov [7] in the theory of predissociation. In distinction from (9) these writers assumed that the matrix elements do not depend on energy and that the energy spectrum is uniform. In our case these conditions are not fulfilled, since the matrix elements $(p_{12})_{\kappa'}$ and the density of energy levels of the electromagnetic field

$$\rho_\omega = \frac{\omega^2}{\pi^2 c^3} V \tag{10}$$

depend on ω. Nevertheless, the solution obtained in [6, 7] can be applied to the present problem. Indeed, from the form of (9) it follows that the interaction of the two subsystems is of resonant character; the values of $C_{2(0)}(E)|$ are large only for the energies E of the system that are close to E_2, and at $E \sim E_2$ the change of the matrix elements and of the energy level density is small and can be neglected. Therefore, according to [7] $|C_{2(0)}(E)|^2$, that is, the probability of finding the atom on the second level when the energy of the entire system is E (close to E_2), is given by

$$|C_{2(0)}(E)|^2 = \frac{\overline{|p_{21}|^2_{\varkappa'}}}{\dfrac{\pi^2(\overline{|p_{21}|^2_{\varkappa'}})^2}{\varepsilon^2} + (E_2 - E)^2}, \tag{11}$$

where ϵ is the separation of adjacent energy levels of the field and is given by $h/\rho\,\omega_{21}$, and a bar over a matrix element denotes averaging over all directions of $e_{\kappa'}$:

$$\overline{|p_{21}|^2} = \frac{2\pi h\omega_{21}e^2}{V}\frac{1}{4\pi}\int_0^{2\pi} d\varphi \int_0^{\pi} \sin\vartheta\, d\vartheta\, |(\mathbf{r}e_{\varkappa'})_{21}|^2 = \frac{2}{3}\frac{\pi h\omega_{21}}{V}|r_{21}|^2. \tag{12}$$

Introducing the notation

$$\beta = \frac{\pi\,\overline{|p_{21}|^2_{\varkappa'}}}{\varepsilon} = \frac{2}{3}\frac{e^2\omega_{21}^3}{c^3}|r_{21}|^2, \tag{13}$$

we can write (11) as

$$|C_{2(0)}(E)|^2 = \frac{\beta\varepsilon}{\pi}\frac{1}{\beta^2 + (E_2 - E)^2}. \tag{14}$$

Equation (14) gives the probability for a single field level. In order to obtain the probability density, that is, the probability per unit energy interval, (14) must be multiplied by the number of levels in unit energy interval ($1/\epsilon$). The result is

$$|C_{2(0)}(E)|^2_E = \frac{\beta}{\pi}\frac{1}{\beta^2 + (E_2 - E)^2}. \tag{15}$$

Solving the transition problem, quantum electrodynamics [1, 3] yields the following expression for the shape of a spectral line:

$$I(\omega) = I_0\frac{\gamma}{\pi}\frac{1}{\gamma^2 + (\omega_{21} - \omega)^2}, \tag{16}$$

where γ is the half-width of the line:

$$\gamma = \frac{2}{3}\frac{e^2\omega_{21}^3}{c^3h}|r_{21}|^2 = \frac{\beta}{h}. \tag{17}$$

It can thus be seen that the parameter β agrees with the halfwidth of a spectral line on the energy scale. The similarity of (15) and (16) suggests that (15) can be regarded as the shape of an atomic energy level resulting from the interaction with the zero-point electromagnetic field.

No absolutely isolated atom exists in nature. The simplest real system is not an isolated atom but an atom in a zero-point electromagnetic field which can not be eliminated in principle. Therefore the simplest atomic system is described by the Hamiltonian $H_a + U$, where U is the operator of the interaction with the field. This system possesses a practically continuous spectrum of energy E and eigenfunctions $\Psi(E)$. The physical meaning of $|C_{2(0)}(E)|_E^2$ is the probability of the existence of certain atomic properties in the total state $\Psi(E)$, that is, the probability of the state ψ_2. Different energy levels E of the total system correspond in accordance with (15) to different degrees of probability of the atomic properties. The dependence of $|C_{2(0)}(E)|_E^2$ on E gives the natural shape of atomic energy levels which appears under the most varied experimental conditions and, specifically, in the shape of absorption and emission lines.

Institute of Physics and Mathematics,
Academy of Sciences, Byelorussian SSR

Received March 4, 1957.

LITERATURE CITED

[1] W. Heitler, Quantum Theory of Radiation (Oxford University Press, London, 1936).

[2] V. Weisskopf and E. Wigner, Z. Physik. 63, 54 (1930).

[3] V. Weisskopf, Ann. Physik. 9, 23 (1931).

[4] A. Sokolov and D. Ivanenko, Quantum Theory of Fields [in Russian] (1952).

[5] L. Landau, Z. Physik. 45, 430 (1927).

[6] O. K. Rice, Phys. Rev., 33, 748 (1929); 35, 1551 (1930).

[7] B. I. Stepanov, J. Exptl. Theoret. Phys. (USSR) 15, 435 (1945).

CONCENTRATION DEPENDENCE OF THE SIGN OF BIREFRINGENCE IN A STREAMING POLYMER SOLUTION

E. V. Frisman and E. N. Arkhipova

(Presented by Academician A. A. Lebedev March 16, 1957)

Birefringence in a streaming polymer solution is determined by the difference of the principal polarizabilities of the macromolecules in the solution. Numerous experiments [1-3] provide a basis for regarding a macromolecule in a solution as an ellipsoidal particle saturated with the solvent, whose refractive index differs from that of the polymer.

On this basis an expression has been obtained [4] for the difference between the polarizabilities of a macromolecule, which combines the results of statistical theory [5, 6] and the laws of colloidal optics [7-9]:

$$\gamma_1 - \gamma_2 = \left(\frac{n_s^2+2}{3}\right)^2 \frac{3}{5}(\alpha_1 - \alpha_2)\frac{\overline{h^2}}{\overline{h_0^2}} + \left(\frac{n_k^2 - n_s^2}{4\pi\rho n_s N_A}\right)^2 \frac{M^2}{v}(L_2 - L_1). \quad (1)$$

Here $\alpha_1 - \alpha_2$ is the difference of the polarizabilities of a statistical segment in a vacuum; n_s and n_k are the refractive indices of the solvent and polymer, respectively; $\overline{h_0^2}$ and $\overline{h^2}$ are the mean square end-to-end distance of a molecular chain in an undisturbed and disturbed state, respectively; ρ is the density of the polymer; M is the molecular weight of the polymer; V is the volume of the molecular ellipsoid; N_A is Avogadro's number; $L_2 - L_1$ is a factor which depends on the ratio of the semiaxes of the ellipsoid. The first term in (1) is determined by the intrinsic anisotropy of the macromolecule; the second term depends on the form anisotropy and plays a part only when $n_k \neq n_s$. Depending on the structure of the molecule the intrinsic anisotropy can be positive or negative while the form anisotropy is always positive.

Thus for a macromolecule with negative anisotropy the sign of the resulting difference of the polarizabilities depends on the contributions of the separate terms of Equation (1).

It is easily seen that during laminar flow in a solution the separate terms depend differently on the hydrodynamic force which acts on the macromolecule and therefore on the gradient of the velocity, g. Indeed, the first term of (1) increases proportionally to $\overline{h^2}/\overline{h_0^2}$ while the second term is proportional to $\sqrt{\overline{h^2}/\overline{h_0^2}}$, because it can be shown that $L_2 - L_1 \sim \sqrt{\overline{h^2}/\overline{h_0^2}}$ when constancy of volume is assumed. Thus a change of g can lead to a change of the sign of $\gamma_1 - \gamma_2$ when M^2/v and $(n_k - n_s)$ are given.

When the hydrodynamic force is small ($g \to 0$) it can be assumed that $\overline{h^2}/\overline{h_0^2} \approx 1$ and $L_2 - L_1$ is constant. Then the sign of $\gamma_1 - \gamma_2$ depends only on M^2/v and $(n_k - n_s)$.

It follows that when $g \to 0$ we can expect a change of sign of the optical anisotropy with a change of molecular weight in the same solvent ($n_k \neq n_s$).

This effect was detected [10] in an investigation of the solutions of two fractions ($M = 3 \cdot 10^5$ and $M = 100 \cdot 10^5$) of polystyrene in dioxane. Solutions of the low molecular fraction possess negative birefringence over a broad range of concentrations and velocity gradients. Solutions of the high molecular fraction possessed positive birefringence Δn, but only for small velocity gradients g. With increasing g the positive birefringence is reduced, passes through the zero point and acquires a large positive value. This results from the fact that with increasing velocity gradient the first term of (1) increases more rapidly than the second.

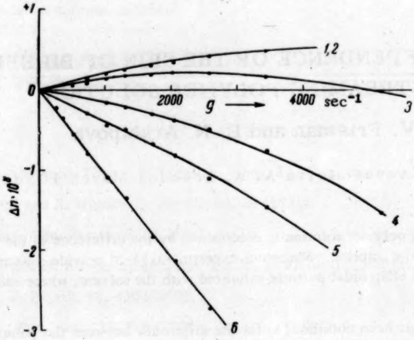

Fig. 1. The relation Δn = f(g) for solutions of polystyrene (M = 1.5·10⁶) in dioxane. 1, 2) C = 0.1 g/100 cm³ (the curves coincide on the scale used here); 3) C = 0.3 g per 100 cm³; 4) C = 0.5 g/100 cm³; 5) C = 0.6 g/100 cm³; 6) C = 0.8 g/100 cm³.

We must assume that the value of g at which Δn = 0 corresponds to $\gamma_1 - \gamma_2 = 0$, that is, there is identical importance of the two terms in (1) (which is valid for a singly dispersed system); this enables us to calculate the dilatation of the molecule under such conditions.

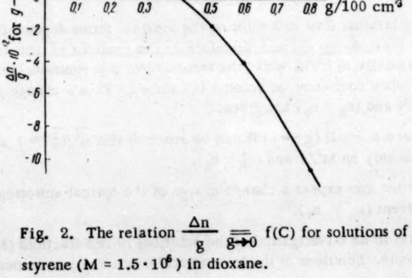

Fig. 2. The relation $\frac{\Delta n}{g} \underset{g \to 0}{=} f(C)$ for solutions of polystyrene (M = 1.5·10⁶) in dioxane.

The experiment which has been mentioned enables us to show the dependence of g on the magnitude of Δn due to intrinsic anisotropy and on Δn due to form [13]. We note that the value of g at which Δn changes sign is reduced with increasing concentration [10]. This enables us to understand the new phenomenon discussed in the present paper, which was discovered during the investigation of solutions of a polystyrene fraction ($M = 1.5 \cdot 10^6$) in dioxane.

The magnitude and orientation of the birefringence were measured in a device with an external rotor [2, 10-12] of effective length $l = 10$ cm and gap $\Delta r = 0.085$ cm. Our optical arrangement was described in previous papers [2, 3, 11].

The relation between the magnitude of the birefringence Δn and the velocity gradient g for solutions of different concentration is shown in Fig. 1. In agreement with previous results [10] for large values of g the sign of Δn is reversed; this occurs for the solution with C = 0.3 g per 100 cm^3 when g is close to 5000. For smaller concentrations the positive sign of Δn is retained in the investigated region of velocity gradients, while higher concentrations (C = 0.5 g per 100 cm^3 and higher) reveal negative birefringence beginning with the smallest values of g.

Figure 2 shows that for C = 0.4 g per 100 cm^3 we have $\Delta n = 0$.

In view of the fact that the hydrodynamic force in the flow depends on the viscosity of the solution we could expect that with increased concentration the deformation birefringence would increase, as a result of which Δn would become negative. However, since in a number of the solutions Δn is negative when $g \to 0$ the observed effect cannot be explained by this fact alone.

We can assume that the optical behavior of a solution here shows dependence on the concentration. In a dilute solution, where each macromolecule is surrounded by molecules of the solvent, the refractive index of the region which contains the macromolecule differs from the refractive index of the surrounding medium. With increasing concentration the macromolecules come into contact. Further increase of concentration produces interpenetration of parts of the macromolecules; the medium thus becomes more homogeneous optically and the form birefringence is diminished. An evaluation of h^3 from viscosity (by the method of Flory) and from the volume (by the method of Kuhn) shows that in the solution with C = 0.5 g per 100 cm^3 for the given M interlocking of the macromolecules has already taken place, thus reducing the positive component of Δn.

We imagine that in sufficiently high concentrations, where the macromolecules are highly entangled, birefringence should be determined only by the intrinsic anisotropy.

The observed reversal of the sign of Δn with increasing concentration is also associated with a change of the hydrodynamic behavior of a macromolecule in a solution with changing concentration [14, 15]. However, a quantitative interpretation of this will require more extensive experimental data and further development of the theory. In any event, it can be stated that experiment confirms our point of view, according to which form birefringence is determined by the geometrically asymmetric macromolecular ellipsoid.

We are indebted to Professor V. N. Tsvetkov for valuable discussions.

A. A. Zhdanov Leningrad State University Received March 12, 1957.

LITERATURE CITED

[1] V. N. Tsvetkov and E. V. Frisman, J. Exptl.-Theoret. Phys. (USSR) 15, 276, 351 (1945).

[2] E. V. Frisman and V. N. Tsvetkov, J. Tech. Phys. (USSR) 25, 3, 447 (1955)

[3] V. N. Tsvetkov, E. V. Frisman and L. S. Mukhina, J. Exptl.-Theoret. Phys. (USSR) 30, 649 (1956) [see Soviet Physics – JETP, p. 492].

[4] V. N. Tsvetkov and E. V. Frisman, Doklady Akad. Nauk SSSR 97, 647 (1954).

[5] W. Kuhn and F. Grun, Kolloid Z. 101, 248 (1942).

[6] W. Kuhn and H. Kuhn, Helv. Chim. Acta 26, 1394 (1943).

[7] A. Peterlin and H. A. Stuart, Z. Physik. 112, 129 (1939).

[8] J. C. Maxwell, Treatise on Electricity and Magnetism (1873).

[9] R. Gans. Ann. Physik 37, 881 (1912).

[10] E. V. Frisman and V. N. Tsvetkov, Doklady Akad. Nauk SSSR 106, 1, 42 (1956) [see Soviet Physics – Doklady, p. 12].

[11] E. V. Frisman and V. N. Tsvetkov, J. Exptl.-Theoret. Phys. (USSR) 23, 690 (1952).

[12] V. N. Tsvetkov and S. M. Savvon, J. Tech. Phys. (USSR) 24, 348 (1954).

[13] M. Copic, J. Polymer Sci. 20, 593 (1956).

[14] A. Peterlin, R. Signer, Helv. Chim. Acta 36, 1575 (1953).

[15] A. Peterlin, J. Polymer Sci. 12, 45 (1954).

THE INTERACTION BETWEEN LEAD NUCLEI AND COSMIC RAY PROTONS AT ABOUT 10^{10} ev

L. T. Baradzei V. I. Rubtsov, Iu. A. Smorodin, M. V. Solov'ev,
B. V. Tolchakev and Z. I. Tulinova

(Presented by Academician D. V. Skobel'tsyn March 5, 1957)

The investigation of the interactions between cosmic ray protons and lead was conducted at an altitude of 9000 meters with a Wilson cloud chamber in a field of 9200 oersteds. The experimental arrangement is shown in Fig. 1. Expansion of the chamber resulted from the passage of not less than one penetrating charged particle through counter trays $C_1C_2C_3C_4C_5$ and not less than two charged particles through the telescopes B.

In order to exclude interactions induced by pions we considered mixed (electron-nuclear) showers generated in a lead plate by a single charged particle. Thirty-eight instances were selected; typical photographs of the showers are shown in Fig. 2. The photographs were used to measure the spatial arrangement of the tracks, the momenta of charged particles and their ionizing power. The maximum momentum was 3 Bev/c for tracks of 6 cm average length. The directions of the particles were measured within 2°. The ionizing power was determined visually.

TABLE 1

n	1	2	3	4	5	6	7	8	9
No. of showers	2	7	9	5	8	1	4	1	1

Table 1 gives the distribution of showers according to the number of particles *n* per shower. The first line of the table represents the sum of the charged pions produced in a shower and the protons whose ionizing power was not distinguished from the minimum in the chamber (proton momentum above 600 Mev/c).

The small number of recorded showers with few particles resulted from the selective control of the cloud chamber. The average number *n* of particles per interaction was 3.9 ± 0.3.

The experimental data furnish certain information concerning the principal components of mixed showers. Electrons could be distinguished from mesons and heavier particles as follows. For momenta below 100 Mev/c they posses the minimum ionizing power. Particles with momenta greater than 100 Mev/c were assigned to the electron component when they emerged from the plate as electron-positron pairs or were accompanied by an electron cascade.

Figure 3a shows the energy distribution of the electrons. If this spectrum is described by a power law of the form $dN/dE \sim E^{-\gamma}$ the exponent γ is variable, changing from the value 1 at low energies to 2.5 at about 1 Bev.

For momenta smaller than 600 Mev/c mesons could be distinguished from protons and heavier particles by their momentum and ionizing power. In this range the ratio of positive to negative mesons was 1.2 ± 0.4. Above 600 Mev/c all negatively charged particles except electrons were considered to be π^- mesons and the number of π^+ mesons was taken to be $N_{\pi^+} = 1.2 \cdot N_{\pi^-}$.

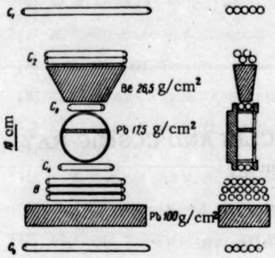

Fig. 1. Experimental arrangement.

Figure 3b gives the meson energy distribution. The solid curve represents the distribution of pions produced in a photographic emulsion exposed in the atmosphere [1]. The spectra were normalized according to the total number of particles. The two distrubutions agree within the limits of error. If the distribution is described by a power law, from 200 to 2000 Mev the experimental results are best satisfied by $\gamma = 1.6$. The average number of charged mesons with energy < 2 Bev is 2.8 ± 0.3 per interaction.

Figure 3c represents the energy distribution of protons and heavier particles, which will hereinafter be called δ particles. The solid curve is compared with the distribution of protons, deuterons and tritons from emulsion data [1] (normalized by the total number of particles). The distributions do not differ within the limits of experimental error. From 900 to 1300 Mev the distribution obtained here can be described by a power law with $\gamma = 1.5$. The number of particles in this energy interval is 2 ± 0.2 per interaction.

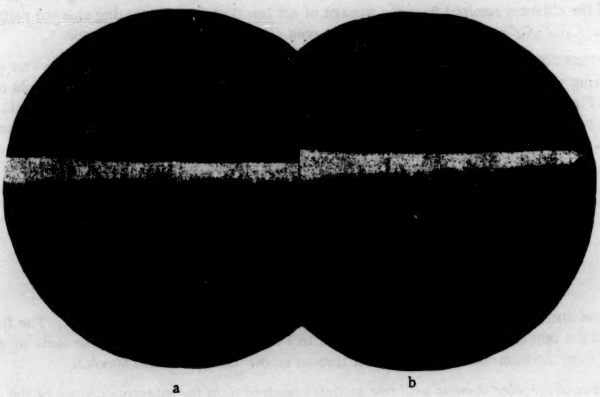

a b

Fig. 2. Examples of nuclear interactions in lead.

We shall now consider the energy distribution between the different shower components.

Charged mesons with energies < 2 Bev carry away an average of 1150 ± 130 Mev per interaction. The pion spectrum in Fig. 3b can be extrapolated to the energy region > 2 Bev by a power law with the exponent $\gamma = 2.5$, which agrees with the value of γ in the energy spectrum of pions produced in photographic plates [1] as well as with the spectrum of pions produced in the atmosphere [2, 3]. By this extrapolation the number of mesons with energy > 2 Bev is 0.14 per interaction, carrying away about 800 Mev of energy. Thus all charged mesons carry away an average of 2 Bev per interaction.

The energy of π^0 mesons can be determined from the energy of the electron-photon cascades produced by photons arising from the decay of π^0 mesons. The energy of the electrons whose distribution is given in Fig. 3a is 270 ± 70 Mev.

Photons resulting from the decay of π^0 mesons traversed an average path equal to 2 radiation units in the lead plate. For the photon energy interval from 50 to 1000 Mev this is close to the path in which maximum cascade development occurs. For small electron energies the observed electron energy spectrum is close to the spectrum at the maximum of a cascade from 330-Mev photons, which was calculated in [5]. For large energies, according to calculations in [4, 5] the exponent of the electron spectrum coincides with the exponent of the π^0 meson energy spectrum. The observed electron spectrum satisfies this condition.

Extrapolating the electron spectrum in the high energy region according to the law $dN/dE \sim E^{-2.5}$, we find that electrons with energy > 2 Bev carry about 160 Mev per interaction. The photographs revealed one electron with > 2 Bev paired with a 1.4 Bev positron. Thus the combined electron energy is 430 Mev per interaction.

In the equilibrium spectrum the ratio of photon energy to electron energy is 1.3. The energy of the π^0 mesons, which is equal to the total energy of the electron-photon cascade, is thus about 1 Bev per shower. The ratio of π^0 meson energy to $\pi^{\pm}$ meson energy is 1/2. The total energy of both charged and neutral pions is about 3 Bev per interaction

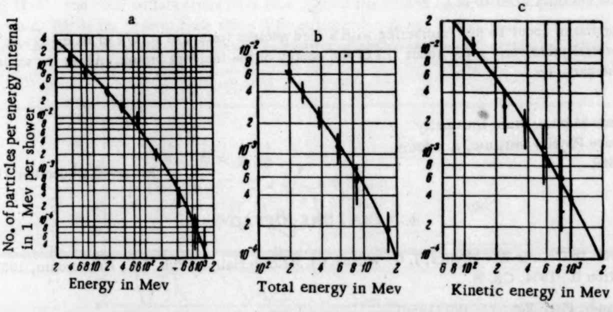

Fig. 3. Energy distribution of particles ejected as a result of nuclear interactions in lead: a) electrons; b) $\pi^{\pm}$ mesons; c) δ particles.

Charged δ particles from 90 to 1300 Mev carry away 700 ± 120 Mev per interaction. In the energy range > 1300 Mev the distribution of δ particles in Fig. 3c can be extrapolated according to $dN/dE \sim E^{-3}$, which corresponds to emulsion data in [1]. The number of δ particles in this energy range is 0.13 per interaction, carrying away about 300 Mev. Taking into account the δ particles with energies in the interval 25-90 Mev, the number of which was extrapolated from the data in Fig. 3c, the energy carried by charged δ particles is 1.1 Bev.

The energy of neutral δ particles can be obtained on the assumption that the ratio of the numbers of neutrons and protons is 1.5, which is the ratio in the lead nucleus. The total energy of δ particles thus increases to 2.4 Bev per shower.

The experiments which have beeb described give no information concerning particles with energies < 25 Mev, which produce the so-called "black" tracks. When a 10-Bev proton interacts with an emulsion nucleus the energy carried away by these particles is 280 Mev. For a lead nucleus this energy can increase in proportion to the linear dimensions of the nucleus and amounts to about 400 Mev.

In the interactions under consideration high-energy particles are ejected which have not yet been taken into account. The average number of particles with momentum > 2 Bev/c is 0.81 ± 0.14 per interaction.

Extrapolations give the number of $\pi^{\pm}$ mesons and δ nucleons in this momentum range as 0.27.

The extra high-energy particles cannot be regarded as charged pions because the energy of the electron-photon component resulting from the decay of the corresponding π^0 mesons would then be about 2 Bev per interaction. It was possible experimentally to observe an increase of the energy of the electron-photon component exceeding 20% of the indicated value.

Therefore the extra high-energy particles, amounting to 0.5 particles per interaction, must be regarded as protons. It should be noted that in 16 of the 38 recorded showers a single particle with energy above 2 Bev is observed. It is reasonable to assume that high-energy neutrons are produced to the same extent as protons.

The minimum combined energy of the particles following an interaction is thus about 8 Bev.

If it is assumed that the emitted high-energy nucleons possess a power-law spectrum with the exponent $\gamma = 2.5$, which coincides with the spectrum of incident protons, the average energy of such high-energy nucleons is $\frac{\gamma - 1}{\gamma - 2} E_l = 4$ Bev, where the average interaction energy is 11 Bev.

Methods of estimating the average energy from the flux of shower-producing particles, comprising 0.046 particles $\mathrm{cm}^{-2} \cdot \mathrm{min}^{-1} \cdot \mathrm{sterad}^{-1}$, the average multiplicity and the angular distribution of shower particles yield primary particle energies from 10 to 13 Bev.

Thus a proton of about 10 Bev interacting with a lead nucleus loses 2/3 to 1/2 of its energy on the average. Charged and neutral pions carry away about 1/3 of the energy of the incident proton. About the same energy is carried by the particles.

M. V. Lomonosov Moscow State University
and P. N. Lebedev Physics Institute, Academy
of Sciences, USSR

Received December 21, 1956.

LITERATURE CITED

[1] Progress in Cosmic Ray Physics, J. G. Wilson, ed., (North Holland Pub. Co., Amsterdam, 1952) [Russian translation IL, 1954, Ch. I].

[2] M. Sands, Phys. Rev. 77, 180 (1950).

[3] G. M. Garibian and I. I. Gol'dman, J. Exptl.-Theoret. Phys. (USSR) 26, 257 (1954).

[4] A. G. Carlson, I. E. Hooper and D. T. King, Phil. Mag. 41, 701 (1950).

[5] I. P. Ivanenko, Dissertation (Moscow State University, 1956).

THE INTERACTION OF MOLECULAR AND LATTICE VIBRATIONS IN CRYSTALS AND THE INGRA-RED SPECTRUM

Associate Academician E. F. Gross and A. A. Shultin

The study of the excitation of vibrations and of energy redistribution in crystal lattices, which has been of increasing interest during the past ten years, depends primarily on spectroscopic methods. A. S. Davydov [1-3] has done some interesting work on the theory of light absorption by molecular crystals. R. Halford [4, 10], D. Hornig [11-17] and their collaborators have investigated the vibrational spectra of molecules and complex ions in crystals. But at the present time there is no quantitative theory of the influence of the crystalline field and of temperature on the width, location and intensities of absorption bands in crystal spectra.

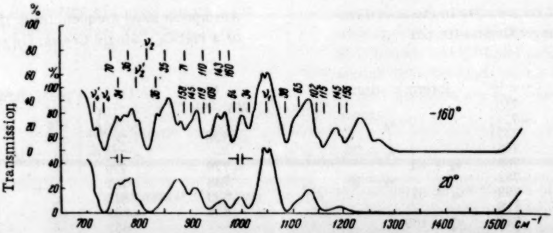

Fig. 1. Infrared transmission spectrum of a single crystal of $Ba(NO_3)_2$.

It is known that in a crystal lattice the molecules possess a fixed equilibrium position and orientation. Oscillations of the particles about their equilibrium positions and orientations, that is, the lattice vibrations, possess energy which is 10 to 100 times less than the energy of internal vibrations and can thus be excited at relatively low temperatures.

According to theory [1, 2] the excitation of lattice vibrations will increase the probability of transitions in which light excites internal vibrations together with lattice vibrations. Also, at higher temperatures there is increasing probability that light will excite molecules on already excited lattice levels. Both of these processes should be observed in the absorption spectra of molecular crystals in the form of satellites of molecular bands.

This question has been treated only incidentally thus far in investigations of molecular vibrations in crystals and efforts have not been made to obtain clearer results; the literature contains isolated instances in which some absorption bands can be interpreted in the manner described above.

Since the interaction of phonons and molecular vibrations is of great interest we have investigated the infrared absorption spectra of single crystals of $Ba(NO_3)_2$ and $Pb(NO_3)_2$. Our purpose was to determine the existence and characteristics of such "combined" transitions, whose intensity should depend appreciably on temperature and whose separation from the centers of bands of intra-ionic excitation must be of the order of magnitude of lattice vibration frequencies. The probability of such transitions must also depend on the form of the intra-ionic excitation and the kind of lattice vibrations, while the width of the corresponding bands will be determined by the combined frequency density distributions of both zones or branches of excited states.

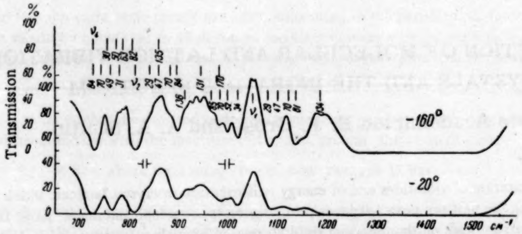

Fig. 2. Infrared transmission spectrum of a single crystal of $Pb(NO_3)_2$.

TABLE 1

Absorption Band Frequencies in the Spectrum of a $Ba(NO_3)_2$ Single Crystal (in cm^{-1}).

$t = 20°$	$t = -160°$	Interpretation	
717	716		
—	~724	ν_4	
730	732		
—	748		$\nu_2 - 70$
764	766	$\nu_4 + 34$	
~778	782		$\nu_2 - 36$
~797	799	$\nu_4 + 67$	
~821	818		ν_2
—	841	$\nu_4 + 109$	
—	~853		$\nu_2 + 35$
—	877	$\nu_4 + 143$	
896	889	$\nu_1 - 158$;	$\nu_2 + 71$
—	~902	$\nu_1 - 145$	
935	928	$\nu_1 - 119$;	$\nu_2 + 110$
—	938	$\nu_1 - 109$	
952	961		$\nu_2 + 143$
975	983	$\nu_1 - 64$;	$\nu_2 + 160$
1013	1013	$\nu_1 - 34$	
—	~1028	$\nu_1 - 19$	
—	~1038	$\nu_1 - 9$	
1047	1047	ν_1	
1085	1085	$\nu_1 + 38$	
~1111	~1112	$\nu_1 + 65$	
—	~1149	$\nu_1 + 102$	
1158	1162	$\nu_1 + 115$	
—	~1192	$\nu_1 + 145$	
—	1202	$\nu_1 + 155$	
—	1258		
1190—1550	1300—1550	ν_3, $2\nu_4$	

TABLE 2

Absorption Band Frequencies in the Spectrum of a $Pb(NO_3)_2$ Single Crystal (in cm^{-1})

$t = 20°$	$t = -160°$	Interpretation	
714—734	~715	ν_4	
	~724		
758	761		$\nu_2 - 49$
—	~774	$\nu_4 + 50$	
~779	779		$\nu_2 - 31$
788	787	$\nu_4 + 63$	
809	810	ν_2	
~835	~839		$\nu_2 + 29$
—	857		$\nu_2 + 47$
~876	~879		$\nu_2 + 70$
891	894		$\nu_2 + 84$
—	~914	$\nu_1 - 136$	
920	926		
—	941		
—	965	$\nu_1 - 85$	
979	980	$\nu_1 - 70$	
997	998	$\nu_1 - 52$	
1014	1016	$\nu_1 - 34$	
—	1050	ν_1	
1079	1079	$\nu_1 + 29$	
—	1097	$\nu_1 + 47$	
~1131	1131	$\nu_1 + 81$	
—	~1150		
—	~1184	$\nu_1 + 134$	
1185—1540	1250—1500	ν_3, $2\nu_4$	

In the crystals under investigation the structural units which possess internal vibrational degrees of freedom are the NO_3^- ions, which are plane equilateral triangles with oxygen atoms at their vertices and a nitrogen atom at the center. This system possesses six normal modes of vibration with frequencies from 700 to 1500 cm^{-1}. The lead nitrate specimen was a 0.30 × 10 × 20 mm plate; the barium nitrate specimen was a 0.56 × 10 × 20 mm plate. The spectra are represented in Figs. 1 and 2, with the upper curve corresponding to a temperature of

– 160° and the lower curve to 20°. A group-theoretical analysis of the selection rules for these crystals, which belong to the T_h^6 space group, yields the result that all fundamental internal vibrations of the NO_3^- ions must be involved in the absorption, as is actually observed. But in addition to these transitions the spectra reveal an additional large number of weak absorption bands beyond those mentioned in the literature [10, 18]. The key to their interpretation may be the prominent absorption peaks that are located symmetrically on both sides of absorption peak ν_1 (at 1050 cm^{-1}). When the temperature is reduced to – 160° the intensity of the "red" satellites is considerably diminished. Considering the separation of these bands from the fundamental transition ν_1 and their temperature dependence, it should also be possible to detect such bands around ν_2 and ν_4. Since there is no possibility of explaining these additional absorption peaks on the basis of pure intra-ionic vibrational transitions, the characteristics which have been mentioned suggest that these satellites result from combined transitions in which there is a simultaneous change of the quantum numbers of intra-ionic and lattice levels. In other words, in these transitions when a light quantum is absorbed an exciton is created with the simultaneous creation (or annihilation) of a phonon. A more careful study of the spectrum of $Ba(NO_3)_2$ shows that with respect to the ν_1 vibrational band the satellites are separated symmetrically by 109, 119, 145 and 158 cm^{-1} on the red side and by 102, 115, 145 and 155 cm^{-1} on the violet side of the fundamental frequency 1047 cm^{-1}. Some of these frequencies are very close to the lattice frequencies of barium nitrate, which are known from the Raman spectra [19].

TABLE 3

Separation Between the Centers of the Fundamental Bands of Intra-Ionic Excitation and the Absorption Bands Which are Interpreted as Combinations With the Lattice, for Various Internal Vibrations in the Spectrum of $Ba(NO_3)_2$ (in cm^{-1})

~(155)	~(160)	(155)	on the shorter wavelength side
143	143	145	
(109)	~(110)	115	
—	—	102	
(67)	71	65	
(34)	35	38	
ν_4	ν_2	ν_1	fundamental vibrations
. . .	36	34	on the longer wavelength side
. . .	~(70)	64	
. . .	. . .	109	
. . .	. . .	119	
. . .	. . .	145	
. . .	. . .	158	

Note: Here and in Table 4 the numbers in parentheses refer to transitions whose occurrence is not definitely established. The dotted lines indicate possible transitions beyond the limits of the spectrum under investigation here.

It is reasonable to assume that the character of the interaction between molecular vibrations and lattice vibrations depends on the nature of the intramolecular excitation. Differences here must affect the combination absorption bands with respect to their peak intensities, intensity distributions and different numbers of satellites around different fundamental absorption bands. These statements are fully confirmed by experiment.

TABLE 4

Separations Between the Centers of Fundamental Bands of Intra-Ionic Excitation and Absorption Bands Which are Interpreted as Combinations with the Lattice, for Various Internal Vibrations in the Spectrum of $Pb(NO_3)_2$ (in cm^{-1})

—	131	134	on the shorter wavelength side
~(82)	—	81	
63	~(70)	~(70)	
50	47	47	
~(30)	29	29	
ν_4	ν_2	ν_1	fundamental vibrations
. . .	31	34	on the longer wavelength side
. . .	49	52	
. . .	(70)	70	
. . .	(84)	85	
. . .	. . .	136	

We believe that the most probable interpretation of the observed transitions is given in the third column of Tables 1 and 2 as well as directly in the spectra (Figs. 1 and 2).

It can be seen from a comparison of the results that despite the overall complexity of the absorption spectra the majority of the bands fit into the scheme outlined above. The similarity of the structures surrounding the individual intra-ionic vibrational transitions in the infrared spectra of barium nitrate and lead nitrate single crystals is very clearly seen from Tables 3 and 4.

In some portions of the spectra of these crystals there is some overlapping of the compound structures of different vibrational bands. In some instances this considerably hinders the clear interpretation of the absorption peaks.

It can be noted in conclusion that the closest satellites in these absorption bands correspond to lattice vibrations of the order of 30-35 cm^{-1}, whereas in the Raman spectrum the lines of lowest frequency are separated from the exciting frequency by 80-90 cm^{-1}. It is evident that these satellites in the infrared spectrum result from the participation of lattice vibrations which do not affect the polarization of the molecules.

A. A. Zhdanov Leningrad State University Received March 23, 1957.

LITERATURE CITED

[1] A. S. Davydov, Trans. Inst. Fiz., Akad. Nauk Ukr. SSR, Vol. 1 (1951).

[2] A. S. Davydov, Trans. Inst. Fiz., Akad. Nauk Ukr. SSR, Vol. 3, 36 (1952).

[3] A. S. Davydov, and S. I. Vavilov, Com. Volume (Izd. AN SSSR, 1952), p. 211.

[4] R. S. Halford, J. Chem. Phys. 14, 8 (1946).

[5] R. S. Halford and O. A. Schaeffer, J. Chem. Phys. 14, 141 (1946).

[6] R. S. Halford and G. B. Carpenter, J. Chem. Phys. 15, 99 (1947).

[7] W. E. Keller and R. S. Halford, J. Chem. Phys. 17, 26 (1949).

[8] H. Winston and R. S. Halford, J. Chem. Phys. 17, 607 (1949).

[9] R. Karplus and R. S. Halford, J. Chem. Phys. 18, 910 (1950).

[10] R. Newman and R. S. Halford, J. Chem. Phys. 18, 1276 (1950).

[11] D. F. Hornig, J. Chem. Phys. 16, 1063 (1948).

[12] R. D. Mair and D. F. Hornig, J. Chem. Phys. 17, 1236 (1949).

[13] E. L. Wagner and D. F. Hornig, J. Chem. Phys. 18, 296, 305 (1950).

[14] F. P. Reding and D. F. Hornig, J. Chem. Phys. 19, 594 (1951).

[15] W. E. Osberg and D. F. Hornig, J. Chem. Phys. 20, 1345 (1952).

[16] F. P. Reding and D. F. Hornig, J. Chem. Phys. 22, 1926 (1954).

[17] D. F. Hornig and W. E. Osberg, J. Chem. Phys. 23, 662 (1955).

[18] F. A. Miller and C. H. Wilkins, Anal. Chem. 24, 1253 (1952).

[19] L. Couture and J. P. Mathieu, Ann. Physik. 12, 3, 521 (1948).

NEAR-ELECTRODE EFFECTS IN ALKALI-HALIDE CRYSTALS AT HIGH TEMPERATURES

M. S. Kosman and V. F. Pisarenko

(Presented by Academician A. N. Terenin December 17, 1956)

The existence of a potential barrier at the contact between a dielectric and a metal [1] results in the formation of space charge near the electrodes when a current passes through the dielectric [1]. These space charges produce a number of special effects [3-10].

The accumulation of near-electrode space charge is noticed in the electrolysis of alkali-halide crystals [11-13]. It is of interest to investigate the optical properties of the near-electrode regions of crystals subjected to electrolysis.

We investigated specimens of NaCl, KCl, KBr and KI single crystals. The largest faces of the specimens, in the shape of $12 \times 15 \times 5$ mm^3 parallelepipeds, were polished and tightly clamped to electrodes made of 10 μ aluminum foil in a special spring holder. These specimens were heated at a constant temperature between 450 and 600° and subjected to a direct voltage of 50-400 v/cm during a period ranging from a few minutes to 1 hour. The following quantities were measured: the forward current; the back current, for which every 1-3 minutes a reverse field was applied for 10 seconds; the potential drop of the unshorted specimen, for which the field was turned off periodically during 10 seconds and the PD was measured with a Compton electrometer.

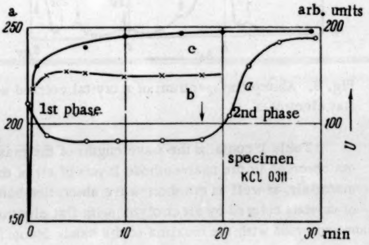

Fig. 1. Variation of current through a specimen at 15 v and 525°. a) Current through specimen; b) back current; c) Pd of unshorted specimen without external field.

For all of the investigated materials in the indicated temperature and voltage ranges the current varied with time as shown in Fig. 1. The processes can be divided into two phases: during the first phase the current at first diminishes and then becomes constant, while the back current and the PD at the ends of the unshorted specimen attain their highest value and then remain constant; during the second phase the current usually increases and the specimen is colored by F-centers. The duration of the first phase depends a) on the quality of the cathode-crystal contact, reducing to a certain minimum value with improvement of the contact, and b) on the applied voltage, diminishing as the voltage increases.

Before and after electrolysis an SF-4 spectrophotometer was used to study the absorption spectrum of the specimens at room temperature; light was sent through the specimens in the same direction as the applied field.

In the absorption spectrum of a thin near-cathode layer (< 0.05 mm) for all of the investigated materials, after the first phase of electrolysis 2 or 3 weak absorption bands appear. The maxima of these bands coincide with the maxima of the V_{2-4}-, V_3- and V_7-bands (Fig. 2). If the specimen was colored, in addition to the familiar F-, M- and U-bands the absorption spectrum also contained the indicated bands (Fig. 3).

TABLE 1

Material	Location of absorption centers	λ_{max}, millimicrons				
		U	V_2	V_3	V_4	V_7 (?)
KBr	Near-cathode layer	228±2	223±3	267±3		300 (?)
	Body of specimen colored with flat electrodes					
KCl	Near-cathode layer	228±2	223±3	267±3		300 (?)
	Body of specimen colored with flat electrodes	214±2	210±2	227±3	245±6	
KI	Near-cathode layer	214±2	210±2	228±3	246±6	
	Body of specimen colored with flat electrodes		278±3	310		
NaCl	Near-cathode layer		280±3	310		
	Body of specimen colored with flat electrodes		210±2	230±3		270±10
			210±2	230±4		290±10

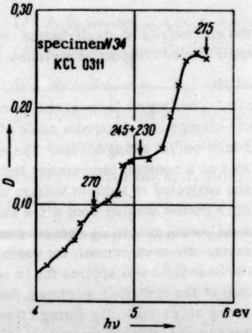

Fig. 2. Absorption spectrum of a near-cathode layer.

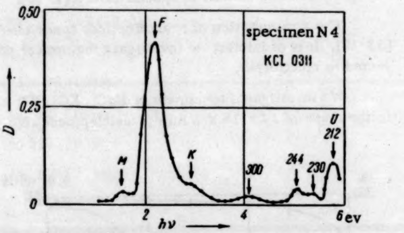

Fig. 3. Absorption spectrum of a crystal colored with flat electrodes.

Table 1 contains the wavelengths of the maxima observed in the near-cathode layers of all of the materials, as well as the short-wave absorption bands of crystals colored by electrolysis, with flat electrodes. Within the limits of error the maxima of the observed bands coincide with the maxima of the bands denoted in the columns of the table.

The observations fit into the following picture of the passage of current through the dielectrics. Under the influence of the external field space charge accumulates in the near-electrode regions as a result of the electrons and holes produced in the thermal ionization zones of impurity centers. In the given temperature region for alkali-halide crystals the space charge at the cathode presumably creates a stronger field which enables ions of the alkali metal to pass the boundary barrier and "evaporate" into the cathode, where they are neutralized. The cation vacancies which are created in the crystal will partly neutralize the space charge by combining with holes and thus forming V-centers. The current is maintained by holes from the anode, where their entrance is aided by the electronic space charge. The alkali metal precipitated at the cathode reduces the potential barrier for the entrance of electrons into the crystal. The electrons entering the crystal create a layer of higher conductivity which acts essentially as a fore-electrode, so that at the boundary between the colored and uncolored portions of the crystal the processes which occur are similar to those at the electrode, so that a small concentration of V-centers is formed also in the body of the crystal.

LITERATURE CITED

[1] N. F. Mott and R.W. Gurney, Electronic Processes in Ionic Crystals (Clarendon Press, Oxford, 1950), 2nd edition [Russian translation, IL, 1950, 1st edition, pp. 193-199].

[2] A. F. Ioffee, Semiconductors in Modern Physics (Leningrad, 1953), pp. 28-30 (In Russian).

[3] M. Karev, J. Exptl. Theoret. Phys. (USSR) 7, 1018 (1937).

[4] M. Karev, J. Exptl. Theoret. Phys. (USSR) 7, 1185 (1937).

[5] M. S. Kosman and N. A. Sozina, J. Exptl. Theoret. Phys. (USSR) 17, 340 (1947).

[6] M. S. Kosman and A. N. Sozina, J. Exptl. Theoret. Phys. (USSR) 17, 472 (1947).

[7] Ia. N. Pershits, J. Exptl. Theoret. Phys. (USSR) 24, 3 (1953).

[8] Ia. N. Pershits, J. Exptl. Theoret. Phys. (USSR) 29, 362 (1955).

[9] Ia. A. Porfianovich, J. Exptl. Theoret. Phys. (USSR) 9, 163 (1939).

[10] M. Dolov, Author's Abstract of Dissertation, Leningrad, 1953.

[11] V. Kuznetsov and K. I. Ambroz, J. Russ. Phys.-Chem. Soc. 59, 407 (1927).

[12] M. S. Kosman and S. L. Rappoport, J. Exptl. Theoret. Phys. (USSR) 17, 460 (1947).

[13] M. S. Kosman and N. A. Petrova, Reports of the Conference on Dielectric Physics, Dnepropetrovsk, 1956 (In Russian).

Received November 19, 1956

A. I. Herzen Leningrad State Pedagogical Institute

LOWEST EXCITED LEVELS OF AXIALLY SYMMETRIC EVEN-EVEN NUCLEI

G. F. Filippov

(Presented by Academician I.E. Tamm, March 13, 1957)

In accordance with the collective model [1] the Schrödinger equation for heavy nuclei is

$$(\hat{H}_s + \hat{H}_p + \hat{H}_{int}) = E\psi, \tag{1}$$

where $\hat{H}_s$ is the Hamiltonian of the core; $\hat{H}_p$ is the Hamiltonian of the "extracore" nucleons; $\hat{H}_{int}$ is the interaction operator between the core and the "extra" nucleons. The motion of the core is characterized by the three Euler angles and the variables β and γ, with β taking account of the change of nuclear surface area with the departure from spherical form and γ showing the degree of destruction of axial symmetry.

Equation (1) has been solved in the approximations of strong and weak coupling [2-4]. The present paper is an attempt to consider the rotation-vibrational spectrum of axially symmetric nuclei in the strong-coupling approximation. The assumption of conservation of axial symmetry is apparently correct for the lowest excited levels.

The collective model gives the following Hamiltonian for the free vibrations of the nuclear core [1]:

$$H' = \frac{1}{2} B(\dot{\beta}^2 + \beta^2\dot{\gamma}^2) + \frac{1}{2}\sum_{\chi=1}^{3}\frac{M_\chi^2}{T_\chi} + \frac{1}{2}C\beta^2,$$

where $T_\chi = 4B\beta^2\sin^2(\gamma - \chi\frac{2\pi}{3})$.

When $\gamma \equiv 0$, * this expression is greatly simplified:

$$H = \frac{1}{2}B\dot{\beta}^2 + \frac{M^2}{6B\beta^2} + \frac{1}{2}C\beta^2.$$

Hence, according to the Pauli principle, the Schrödinger equation can be written as

$$-\frac{\hbar^2}{2B}\left\{\frac{1}{\beta^2}\frac{\partial}{\partial\beta}\beta^2\frac{\partial}{\partial\beta} + \frac{1}{3\beta^2}\left[\frac{1}{\sin\theta}\frac{\partial}{\partial\theta}\sin\theta\frac{\partial}{\partial\theta} + \frac{1}{\sin^2\theta}\frac{\partial^2}{\partial\varphi^2}\right]\right\}\Psi + \frac{1}{2}C\beta^2\Psi = E\Psi. \tag{2}$$

The presence of an even number of extracore neutrons and protons changes the expression for the potential energy; the "extra" nucleons deform the core and the equilibrium position becomes $\beta = \beta_0$. A doubly magic nucleus corresponds to $\beta_0 = 0$.

Thus, for a deformed nucleus we have instead of (2):

$$-\frac{\hbar^2}{2B}\left\{\frac{1}{\beta^2}\frac{\partial}{\partial\beta}\beta^2\frac{\partial}{\partial\beta} + \frac{1}{3\beta^2}\left[\frac{1}{\sin\theta}\frac{\partial}{\partial\theta}\sin\theta\frac{\partial}{\partial\theta} + \frac{1}{\sin^2\theta}\frac{\partial^2}{\partial\varphi^2}\right]\right\}\Psi + \\ + \frac{1}{2}C(\beta - \beta_0)^2\Psi = E\Psi. \tag{3}$$

Equation (3) was used by Wilets and Jean [5].

The wave function Ψ will be obtained in the form

$$\Psi(\beta, \theta, \varphi) = \frac{u(\beta)}{\beta} Y_l^m(\theta, \varphi).$$

The wave function must not depend on the orientation of the axis of symmetry of the system; therefore l takes only even values. For $u(\beta)$ we have

$$-\frac{h^2}{2B}\left[\frac{d^2u}{d\beta^2} - \frac{l(l+1)}{3\beta^2}u\right] + \frac{1}{2}C(\beta-\beta_0)^2 u = Eu. \tag{4}$$

For $l = 0$ this equation can be solved exactly. When $l \neq 0$ the spectrum can be found approximately by expanding in powers of β the expression

$$\frac{h^2}{2B}\frac{l(l+1)}{3\beta^2} + \frac{1}{2}C(\beta-\beta_0)^2 \tag{5}$$

(expanding around the point where (5) is a minimum) and by limiting ourselves to the second power of β. Then (4) becomes the equation for Hermite functions.

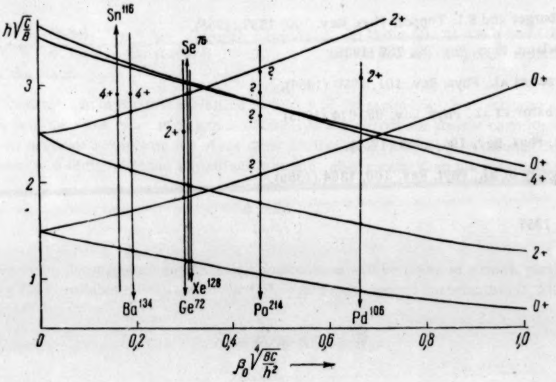

Fig. 1.

The energy spectrum which is obtained from Equation (4) is shown in Figure 1. The horizontal axis gives values of $\beta_0\sqrt[4]{BC/h^2}$; the vertical axis gives the energy in units of $h\sqrt{C/B}$.

The collective model still does not provide correct absolute values of the separations of nuclear energy levels, because the hydrodynamic assumptions used in calculating the parameters B and M are far removed from reality. Therefore it is possible to compare with experiment only the ratios of level separations and the spins of the levels. In order to locate a nucleus on the diagram the ratio E_2/E_1 was computed, where E_1 and E_2 are the energies of the first and second excited levels with respect to the ground state. Then the abscissa was found which corresponds to a given value of E_2/E_1 and the spins of these levels which were determined experimentally. A question mark indicates that the level spin has not been determined experimentally.

We have considered all heavy and semi-heavy nuclei (A > 70) with a known spectrum of lowest excited levels. In a large group of nuclei the first two excited levels are approximately equidistant and with positive parity have spin 2. The theoretical 0+ level which lies next to the low 2+ level is not observed. This conflict with experiment can possibly be attributed to insufficient experimental accuracy, as the 0 − 0 transition which takes place with the assistance of conversion electrons is weak compared with the 2 − 0 transition of similar energy.

We note that the proposed scheme does not include nuclei with a small degree of deformation (Pb^{206}, Sr^{88}, Ge^{140} and Po^{210}). The experimental data were taken from References [6-13].

In conclusion the author wishes to thank Academician I.E. Tamm and A.S. Davydov for valuable comments and V.M. Strutinskii for his interest.

LITERATURE CITED

[1] A. Bohr, Problems of Modern Physics (USSR) 9, 1 (1955) [Russian translation].

[2] A. Bohr and B. Mottelson, Problems of Modern Physics (USSR) 1, 2 (1956) [Russian translation].

[3] K. Ford, Problems of Modern Physics (USSR) 1, 3 (1956) [Russian translation].

[4] A. Bohr, Problems of Modern Physics (USSR) 1, 1 (1956) [Russian translation].

[5] L. Wilets and M. Jean, Phys. Rev. 102, 788 (1956).

[6] R.P. Scharenberg et al., Phys. Rev. 101, 689 (1956).

[7] J.J. Kraushaar et al., Phys. Rev. 101, 139 (1956).

[8] D.E. Alburger and B.J. Toppel, Phys. Rev. 100, 1357 (1955).

[9] R.E. Rowland, Phys. Rev. 99, 757 (1955).

[10] N. Benezer et al., Phys. Rev. 101, 1030 (1956).

[11] J.D. Kurbatov et al., Phys. Rev. 98, 674 (1955).

[12] H. Motz, Phys. Rev. 104, 1353 (1954).

[13] L.J. Baggerly et al., Phys. Rev. 100, 1364 (1955).

Received March 2, 1957

CALCULATION OF THE MAGNETIZATION OF A UNIAXIAL FERRITE AT LOW TEMPERATURES

I. N. Iakovlev

(Presented by Academician N.N. Bogoliubov, April 5, 1957)

The energy of a uniaxial ferrite, which consists of two ferromagnetic sublattices [1], can be represented as follows [2]:

$$\widetilde{H} = -\frac{1}{2}\sum_{h_1h_2} I(h_1h_2)(\mathrm{S}_{h_1}\mathrm{S}_{h_2}) - \frac{1}{2}\sum_{h_1h_2} \Delta(h_1h_2)\, S^z_{h_1}S^z_{h_2}, \tag{1}$$

where $\Delta(h_1h_2) = I_{ZZ}(h_1h_2) - I_{XX}(h_1h_2)$, $I_{XX}(h_1h_2) = I_{yy}(h_1h_2)$; S_h is the spin at site $\underline{h}$ and OZ is the axis of easy magnetization. $\underline{h}$ goes through the values f_i $(i = 1, \ldots\ldots, N_1)$ for one ferromagnetic sublattice and g_i $(i = 1, \ldots\ldots, N_2)$ for the other.

Let the resultant spin of the first sublattice be S_1 and of the second S_2. We shall also assume that the difference $S_1 - S_2$ is of the same order as S_1 and S_2. Since two sublattices are present each ion of one sublattice has as its nearest neighbor a magnetic ion of the other lattice. It is reasonable to assume that the exchange interaction between ions of the different sublattices is considerably greater than the magnetic interaction, that is,

$$\left|\frac{\Delta(h_1h_2)}{I(h_1h_2)}\right| \ll 1. \tag{2}$$

The Ratio (2) between the magnetic and exchange interactions will be taken as a small parameter. At low temperatures, using the Bogoliubov-Tiablikov method of approximate second quantization [2, 3], the Hamiltonian can be represented by

$$\widetilde{H} = E_0 + \Delta E_0 + \widetilde{H}_2. \tag{3}$$

The meaning of E_0, ΔE_0 and $\widetilde{H}_2$ appears when the spin operators, in accordance with this method, are represented in the form [3]

$$S^{\alpha}_h = \sigma^{\alpha}_h\left(1 - \frac{2n_h}{\sigma_h}\right) + A^{\alpha}_h b_n + A^{\alpha}_h b^{+}_h \quad (\alpha = x,\ y,\ z); \tag{4}$$

n_h is the departure of a spin from its orientation at absolute zero; b_h and b^+_h are Bose statistical operators with $b^+_h b_h = n_h$. The vector $\vec{\sigma}_h$ is determined by the requirement that E_0 be a minimum when $|S_h| = |\vec{\sigma}_h|$. A^{α}_h and $\mathring{A}^{\alpha}_h$ are coefficients in which any existing field is involved.

The first two terms, E_0 and ΔE_0, of the Hamiltonian do not contain the operators b_h, b^+_h; $\widetilde{H}_2$ is quadratic in b_h and b^+_h. In the first approximation with respect to the anisotropy parameter (2) at absolute zero the energy $E_0 + \Delta E_0$ of the system is a minimum when the spins of the two sublattices are strictly antiparallel.

In a magnetic field the spins are rotated, remaining antiparallel. The angle φ formed with the axis of easy magnetization is obtained from the equation

$$\mu H_x - \frac{\sin\varphi}{\varkappa} = \operatorname{tg}\varphi \cdot \mu H_z, \tag{5}$$

where

$$I_{11} = \sum_{f_1} I(f_1 f_2);\; I_{12} = \sum_g I(f, g);\; \Delta_{12} = \sum_g \Delta(f, g) \text{ etc.}$$

$$\varkappa = \frac{(S_1 - S_2) N_1 N_2}{\Delta_{11} S_1^2 N_2^2 + \Delta_{22} S_2^2 N_1^2 - 2 S_1 S_2 \Delta_{12} N_1}. \tag{6}$$

This holds true for fields of the order of the anisotropy fields $\mu H \sim |\Delta_{12}|$. For fields of the order of the exchange fields the antiparallel orientation is destroyed, as was shown in [3]. In the case of a field oriented perpendicular (or parallel) to the anisotropy axis the direction of the magnetization can be determined exactly:

$$\sin\varphi_1 = -\frac{n_1\xi_2 - n_2(1-\omega)}{\omega(2-\omega)}.\ \sin\varphi_2 = -\frac{n_2\xi_1 - n_1(1-\omega)}{\omega(2-\omega)}\ (\Delta_{11} = \Delta_{22} = 0). \tag{7}$$

where φ_1 and φ_2 are the angles between the anisotropy axis and the directions of magnetization of the first and second sublattices. ξ_1, ξ_2, ω, n_1, n_2 are defined by

$$\xi_1^2 = \frac{\omega(2-\omega) + n_1^2}{\omega(2-\omega) + n_2^2}:\quad \xi_2^2 = \frac{\omega(2-\omega) + n_2^2}{\omega(2-\omega) + n_1^2}:$$

$$\omega = \frac{\Delta_{12}}{I_{12} + \Delta_{12}}:\quad n_1 = \frac{\mu H_x a_1}{\sigma_2(I_{12} + \Delta_{12})}:\quad n_2 = \frac{\mu H_x a_2}{\sigma_1(I_{21} + \Delta_{21})} \tag{8}$$

Limiting ourselves to first order terms we have

$$\sin\varphi_1 = \mu\varkappa H_x + \frac{\mu H_x a_1}{2\sigma_1 |I_{21}|}:\quad \sin\varphi_2 = -\mu\varkappa H_x + \frac{\mu H_x a_2}{\sigma 2_2 |I_{12}|}. \tag{9}$$

$$a_1 = \frac{(S_1 + S_2)(S_1\cos 2\varphi_0 - S_2)}{2S_2(S_1 - S_2)}.$$

The intensity of magnetization of the ferrite is then

$$M_0 = \mu^2\varkappa H_x(S_1 - S_2) + \mu^2 H_x \frac{N_2}{|I_{12}|}\frac{1}{2}(a_1 + a_2). \tag{10}$$

For fields parallel to the anisotropy axis it can be shown that the spins are antiparallel along the axis up to the order of exchange fields. If, without changing the orientation of the field, its magnitude is reduced past zero, hysteresis is observed, that is, the system of antiparallel spins does not immediately change its direction, but only after the field reaches the value given by $\mu H' = -1/\kappa$. The intensity of magnetization in this case changes abruptly from $M_0 = \mu(S_1 - S_2)$ to $M_0 = -\mu(S_1 - S_2)$.

For the magnetization in the temperature interval $|\Delta_{12}| \ll \vartheta \ll \vartheta_C \sim |\bar{I}_{12}|$, with the field directed perpendicular to the anisotropy axis, we have

$$\frac{M}{V} = \frac{M_0}{V}(1 + c_1 T^{3/2});\quad \mu H \leqslant 1/\varkappa \sim |\Delta_{12}| \quad (M_0 \text{ of } (10));$$

$$\frac{M}{V} = \frac{M_0}{V}(1 - c' T^{3/2});\quad |\Delta_{12}| \ll \mu H \ll \mu H_1 = \frac{\sqrt{\bar{I}_{12}\bar{I}_{21}}}{\sqrt{N_1 N_2}}:\quad M_0 = \mu(S_1 - S_2); \tag{11}$$

$$\frac{M}{V} = \frac{M_0}{V}(1 + c'' T^{3/2}) \quad \mu H \leqslant \mu H_1;\quad M_0 = \mu(S_1 - S_2),$$

where the coefficients c are given by

$$c_1 = c' \sin\varphi = \frac{\mu V \cdot 0{,}12}{M_0 (\alpha'/k)^{3/2}}; \quad c'' = \frac{\mu V \cdot 0{,}12}{M_0 (\alpha''/k)}; \tag{12}$$

V is the volume; $\alpha', \alpha'' \sim |I_{12}|$.

In the case of fields which are parallel to the anisotropy axis the intensity of magnetization diminishes for small fields according to

$$M = M_0 (1 - cT^{3/2}), \tag{12'}$$

where $c = c'$; for large fields with $\mu H \lesssim \mu H_1$ it increases according to

$$M = M_0 (1 + cT^{3/2}), \tag{12''}$$

where $c = c''$.

The increase of the intensity of magnetization with temperature in some fields can also be understood physically. Thus, the increased intensity of magnetization in small fields which are perpendicular to the anisotropy axis results from the fact that an inclination of a magnetic moment in the direction of the field is energetically more favorable than in the opposite direction. Therefore, during heating, when the moments depart from their original orientations, the "amplitude" of the deviation is greater in the direction of the field than opposed to it.

Increased intensity of magnetization in a ferrite can also result from the fact that the number of inverted spins of one sublattice may not be equal to the number of inverted spins of the other sublattice. This occurs, for example, in large fields $\mu H \lesssim \mu H_1$ [3]. Then it is more favorable to rotate the spin of the sublattice which is opposed to the field than to change the direction of spin of the sublattice which is oriented in the direction of the field.

The magnetization curve agrees qualitatively with that obtained in [4] for uniaxial crystals of magnetite.

We have considered above the most probable case of a strong exchange interaction between nearest neighbors in different sublattices. But it is possible to also consider the case in which the ferrite consists of two ferromagnetic sublattices which are weakly coupled to each other. The intensity of magnetization is then the slightly corrected sum of the intensities for the two separate sublattices. In this case also the magnetization agrees qualitatively with experiment [4]. However, the height of the hysteresis loop for weak coupling must be greater than that of the loop for strong coupling and will be equal to $\mu(S_1 + S_2)$ in order of magnitude. This evidently makes it possible to determine the kind of coupling which is present in any case.

In conclusion the author takes this opportunity to thank S.V. Tiablikov for discussions and a number of valuable comments.

LITERATURE CITED

[1] L. Neel, Ann. Physik 3, 137 (1948).

[2] N.N. Bogoliubov, Lectures on Quantum Statistics (Kiev, 1949) (In Ukrainian).

[3] S.V. Tiablikov, Physics of Metals and Metallography (USSR) 3, 3 (1956).

[4] L.R. Bickford, Rev. Mod. Phys. 25, 75 (1953); E.I. Kondorskii, A.S. Pakhomov and T. Shiklosh, Doklady Akad. Nauk SSSR 109, 5, 931 (1956). [Soviet Physics – Doklady, p. 501].

Received June 3, 1957

V.A. Steklov Mathematical Institute
Academy of Sciences, USSR

DISPERSION RELATIONS FOR WEAK INTERACTIONS

Academician N. N. Bogoliubov, S. M. Bilen'kii and A. A. Logunov

Dispersion relations are of great interest at the present time in connection with the experimental possibility of establishing the existence of an elementary length. It is of interest to analyze these relations in the case of weak interactions. As an example, let us consider the reaction

$$\mu + p \rightarrow n + \nu, \tag{1}$$

in which, in addition to the weak interaction, there is a strong interaction of the nucleon and meson fields.

In the theory of dispersion relations the amplitude of the process is divided into parts which are Hermitian and anti-Hermitian in some sense. In the coordinate system in which the sum of the nucleon momenta before and after the reaction is zero the "Hermitian part" D is equal to some integral of the "anti-Hermitian part" A plus an arbitrary polynomial $P_n(E)$ in the energy E of the incident particle. The anti-Hermitian part of the amplitude can be expressed by the product of the "meson" and "neutrino" currents. Because of the smallness of the coupling constant C in weak interactions we can consider terms containing the coupling constant only to the first power. The product of the currents mentioned possesses smallness of not less than the second order, so that in this approximation the anti-Hermitian part is zero.* Consequently, the dispersion relations assume the very simple form

$$D(E) = P_n(E). \tag{2}$$

We know that the principal difficulties which are encountered in the proof of dispersion relations proceed from the necessity of analyzing the analytic properties of A. Since in the present case A is identically zero the proof becomes especially simple and can be obtained either from general principles or from the ordinary theory.

We shall write the matrix element of Process (1) in the form

$$S(p, q; p', q') = (2\pi)^3 \langle \dot{\Phi}_{p's'} a_\nu^{(-)}(q') S a_\mu^{(+)}(q) \Phi_{ps} \rangle, \tag{3}$$

where Φ_{ps} is the state vector of the original nucleon; $a_\mu^{(+)}$ is the μ^- meson creation operator; and $a_\nu^{(-)}$ is the neutrino annihilation operator.

Transposing the creation operator in (3) to the extreme left-hand position and the annihilation operator to the extreme right-hand position, we obtain

$$S(p, q; p', q') = \bar{u}_\nu(q') \int e^{i(q'x - qy)} \left\langle p's' \left| \frac{\delta^2 S}{\delta \bar{\psi}_\nu(x) \, \delta \psi_\mu(y)} S^+ \right| ps \right\rangle dx \; dy \, u_\mu(q), \tag{4}$$

where ψ_μ is the μ-meson field and ψ_ν is the neutrino field.

---

*The case of electromagnetic interactions requires special examination, because the matrix elements in first approximation can then be proportional to either e or e^2.

We introduce the "meson" and "neutrino" current operators:

$$j_\mu(y) = -i\frac{\delta S}{\delta\bar{\psi}_\mu(y)} S^+; \quad j_\nu(x) = -i\frac{\delta S}{\delta\bar{\psi}_\nu(x)} S^+. \tag{5}$$

We then have

$$\frac{\delta^2 S}{\delta\bar{\psi}_\nu(x)\,\delta\psi_\mu(y)} S^+ = \begin{cases} -i\dfrac{\delta\bar{j}_\mu(y)}{\delta\bar{\psi}_\nu(x)} - \bar{j}_\mu(y)\, j_\nu(x), \\ -i\dfrac{\delta j_\nu(x)}{\delta\psi_\mu(y)} + j_\nu(x)\,\bar{j}_\mu(y). \end{cases} \tag{6}$$

But, by the causality principle [2],

$$\frac{\delta j_\nu(x)}{\delta\psi_\mu(y)} = 0, \quad y \leqslant x; \qquad \frac{\delta\bar{j}_\mu(y)}{\delta\bar{\psi}_\nu(x)} = 0, \quad x \leqslant y. \tag{7}$$

Therefore, taking the first term of the expansion in the weak interaction constant C, we obtain

$$\left\{\frac{\delta^2 S}{\delta\bar{\psi}_\nu(x)\,\delta\psi_\mu(y)} S^+\right\}_C = 0 \quad \text{for} \quad x \neq y. \tag{8}$$

This means that the expression is a quasilocalizable operator which contains $\delta(x-y)$ and possibly its derivatives. If we make the usual assumption that the interaction Lagrangian does not contain derivatives of the meson and neutrino fields, we have

$$\left\{\frac{\delta^2 S}{\delta\bar{\psi}_\nu(x)\,\delta\psi_\mu(y)} S^+\right\}_C = \delta(x-y)\,\Lambda(x). \tag{9}$$

Taking (8) into account we obtain

$$\begin{aligned} \int e^{i(q'x-qy)} \left\langle p's' \left| \frac{\delta^2 S}{\delta\bar{\psi}_\nu(x)\,\delta\psi_\mu(y)} S^+ \right| ps \right\rangle dx\,dy &= \\ = \int e^{i(q'-q)x} \langle p's' \,|\, \Lambda(x) \,|\, ps\rangle\, dx &= \\ = (2\pi)^4 \delta(p'+q'-p-q) \langle p's' \,|\, \Lambda(0) \,|\, ps\rangle. \end{aligned} \tag{10}$$

Equation (10) depends on the momenta p and q' − q but is independent of the momentum q + q'. If we use the reference system in which p + p' = 0 this means that (10) is a function of **p** and is independent of E.

Thus, the unknown amplitude functions which are determined by strong interactions depend only on the transfer of momentum to the nucleon.

Substituting (10) in (4) and considering relativistic invariance, we obtain

$$S(p, q; p', q') = \sum_{\alpha,\beta} (\bar{u}_\nu(q')\, O^\alpha u_\mu(q))\, (\bar{u}_n(p')\, \Omega^\beta_\alpha u_p(p))\, F_{\alpha\beta}(|p-p'|). \tag{11}$$

The fact established above that the functions $F_{\alpha\beta}$ are independent of the momentum q + q' can also be derived from the ordinary theory by means of the graph technique. The most general form of the diagrams which contribute to (1) is shown in Figure 1.

Since the meson and neutrino lines in the diagrams converge to a single point (which in this case reflects localizability), we see that the portion of the graph which contains the strong interactions depends only on p and p − p' and is independent of the momentum q + q', that is, we again arrive at (11). It is easily noticed that if

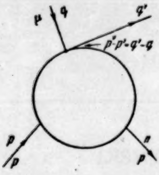

Fig. 1.

causality is violated and a form factor is inserted between the appropriate lines in Figure 1, the investigated amplitude also becomes essentially dependent on q + q'.

We see from (11) that for a given transfer of momentum to the nucleon the energy dependence of the differential cross section (1) is determined by familiar matrix elements and constants $F_{\alpha\beta}$. The experimental determination of this dependence can serve as a direct verification of causality in (1).

A study of the dependence of $F_{\alpha\beta}$ on the transfer of momentum to the nucleon could also make it possible to determine the "meson-neutrino" structure of the nucleon.

By comparing the diagram of Figure 1 with the diagrams for electron scattering by a nucleon we are enabled to conclude that the effective magnitude of the "meson-neutrino" structure of the nucleon is of the same order as the "electromagnetic" structure.

It must be emphasized that the foregoing results are entirely applicable to β-decay and to those decays of hyperons and K-mesons in which μ, $\underline{e}$ and ν particles participate in addition to strongly interacting particles.*

It is of special interest for the verification of causality to study the angular and energy distributions of electrons and μ-mesons in hyperon and K-meson decays, because in these processes μ and $\underline{e}$ particles can have relatively high energies.

LITERATURE CITED

[1] N.N. Bogoliubov, B.V. Medvedev and M.K. Polivanov, Dispersion Relations [in Russian] (Moscow, 1957).

[2] N.N. Bogoliubov, Izv. Akad. Nauk SSSR, ser. fiz. 19, 237 (1955).

Received May 22, 1957

Joint Institute for Nuclear Studies

---

*We note among other things that the reaction $\mu^- \to e^- + \nu + \tilde{\nu}$ is a special situation. Since only weakly interacting particles are involved here the condition of localizability is equivalent to the application of the first approximation in ordinary perturbation theory.

ON THE THEORY OF THE POLARIZATION OF FLUORESCENCE OF SOLUTIONS

P. I. Kudriashov and B. Ia. Sveshnikov

(Presented by Academician A.N. Terenin, February 21, 1957)

It is a basic assertion of the modern theory that fluorescence polarization depends on the viscosity and temperature of the solution as well as on the volume of the molecule and the duration of its excited state. Quantitative relations between these quantities, according to V.L. Levshin [1] and F. Perrin [2], are given by

$$\frac{1}{p}-\frac{1}{p_0}=\left(\frac{1}{p_0}-\frac{1}{3}\right)\frac{kT}{v\eta}\tau, \tag{1}$$

where $\underline{k}$ is the Boltzmann constant, T is the absolute temperature, η is the viscosity of the solution, $\underline{v}$ is the molecular volume, τ is the duration of the excited molecular state, $\underline{p}$ is the polarization and p_0 is the limit of polarization for $\eta \rightarrow \infty$ and $\tau \rightarrow 0$.

This formula has been tested by several investigators [1-3]. In some experiments the viscosity was varied by mixing different proportions of two solvents; in others the change of viscosity was accompanied by increased temperatures, and in some the duration of the excited molecular state was gradually varied by adding various amounts of a quencher or by heating the solution.

Most of the experiments yielded quite satisfactory results. However, we considered it necessary to perform a new test of (1) for fluorescence quenching by foreign substances. Following Perrin [2], in all experiments where fluorescence polarization is changed by quenching through foreign substances, it is customary to replace τ in (1) by $\frac{B}{B_0}\tau_0$, where B and B_0 are the fluorescence yields of the quenched and unquenched solutions, respectively. Thus, it is assumed that the duration is proportional to the yield. Yet during the past 20 to 25 years considerable experimental evidence has been accumulated showing that when the fluorescence of solutions is quenched by foreign substances the yield decreases considerably more rapidly than the duration of the fluorescence. Most investigators have explained this by assuming that in addition to the quenching which depends on the duration of the excited molecular state other quenching occurs which is practically instantaneous and thus independent of τ.

If this hypothesis were correct it is obvious that (1) should yield good results when the direct fluorometric measurements of fluorescence persistence are used instead of replacing τ by $\frac{B}{B_0}\tau_0$. Yet, according to the data of F. Perrin, S.I. Vavilov, I.M. Frank and A.N. Sevchenko the replacement of τ by $\frac{B}{B_0}\tau_0$ is more or less satisfactory while the insertion of fluorometric values of τ in (1) yields obviously poor results, as we shall show below.

This contradiction between experiment and theory results from the fact that in applying (1) to quenched solutions Perrin assumed exponential damping of the fluorescence. But both the theoretical and experimental investigations of fluorescence quenching in solutions by foreign substances [4] showed that the damping of the quenched solutions is nonexponential and that this causes the persistence and yield to change differently during the quenching of some solutions. Under such conditions, for the comparison of experimental and calculated results, (1) must be replaced by another formula in keeping with the nonexponential damping which takes place in connection with quenching by foreign substances. This is easily accomplished if in Perrin's derivation of (1) the damping law is suitably modified. For excitation by polarized light whose electric vector is parallel to the Z axis we thus obtain

$$I_x(t)\,dt = e^{-\alpha t - w\beta\sqrt{t}}\,\frac{dt}{3\tau}\left[(1+2e^{-6Rt})\,I_{x_0} + (1-e^{-6Rt})\,(I_{y_0}+I_{z_0})\right] \tag{2}$$

and similar results for $I_y(t)\,dt$ and $I_z(t)\,dt$.

In (2) $I_x(t)$, $I_y(t)$, $I_z(t)$ are the intensities of emission of the virtual linear oscillators along the OX, OY and OZ axes when Brownian rotation of the molecules occurs and $I_{x_0}(t)$, $I_{y_0}(t)$, $I_{z_0}(t)$ when this is absent; $R = \frac{1}{6}\,kT/v\eta$; the quenching constants α and β are defined by the familiar formulas [4]

$$\alpha = 4\pi w D r c + \tau_0^{-1}; \quad \beta = 8\pi^{1/2} D^{1/2} r^2 c, \tag{3}$$

where w is the probability of quenching in a single collision; c is the number of molecules of the quencher in one cm^3; r is the sum of the kinetic radii of the colliding molecules; D is the diffusion coefficient.

Integrating (2) from 0 to ∞, we obtain expressions for the light sums L_x, L_y, L_z emitted along each of the axes.

By the definition of fluorescence polarization

$$p = \frac{L_z - L_x}{L_z + L_x}, \tag{4a}$$

$$p_0 = \frac{L_{z0} - L_{x0}}{L_{z0} + L_{x0}}. \tag{4b}$$

Inserting in (4a) the values of L_z and L_x calculated from (2), we obtain after some simple transformations

$$\frac{1}{p} - \frac{1}{3} = \left(\frac{1}{p_0} - \frac{1}{3}\right)\left(\frac{kT}{v\eta}\,\frac{B}{B_0}\,\tau_0\delta_1 + 1\right)\frac{\delta_2}{\delta_1}, \tag{5}$$

where

$$\delta_1 = \left[1 - \sqrt{\pi}\,\gamma e^{\gamma^2}\left(1 - \int_0^{\gamma} e^{-z^2}\,dz\right)\right]^{-1}, \quad \gamma = \frac{w\beta}{2\sqrt{\alpha}} \tag{6}$$

and δ_2 is obtained from δ_1 through replacement of α by $\alpha + 6R$.

When $\beta = 0$, that is, with an exponential fluorescence damping law, $\delta_1 = \delta_2 = 1$ and (5) becomes the usual Levshin-Perrin formula; on the other hand in very strong quenching, when $\alpha \to \infty$, $p \to p_0$.

We tested Equation (5) for the quenching of fluorescence from aqueous solutions of fluorescein by means of potassium iodide. L.A. Kuznetsova, V.I. Shirokov and one of the present authors [4] showed that for this case the nonproportional changes of yield and persistence with increasing amounts of the quencher does not result from the existence of any additional static quenching but from the nonexponential damping of fluorescence in quenched solutions. Equation (5) was tested as follows: for each concentration of potassium iodide we calculated p_0 from (5), inserting into the formula the experimental values of B/B_0 and the values of δ_1 and δ_2/δ_1 which were calculated from (6).

We wished to compare our values of p_0 with the values obtained by other investigators from experiments in which the relation between polarization and viscosity was studied. But an examination of the literature showed that the maximum fluorescence polarization of fluorescein which different workers obtained from such experiments fluctuates from 0.36 to 0.44. This evidently results from the considerable leeway which one has in drawing the straight line of the graph relating $1/p$ to $1/\eta$.

Since we had available the fluorometric values of fluorescence persistence in water ($4.8 \cdot 10^{-9}$ sec), in glycerine ($4.5 \cdot 10^{-9}$ sec) and in glycol ($4.7 \cdot 10^{-9}$ sec), as well as the molecular volumes from Marinesco's data [5], we decided to repeat the experiments on the relation of p and η and to calculate the values of p_0 for each of our measured values of p.

All of the fluorescein solutions used for the experiments had a dye concentration of $5 \cdot 10^{-6}$ g/cm^3 and alkali concentration of $2 \cdot 10^{-2}$ g/cm^3. Excitation was produced by polarized filtered light from a mercury lamp (436 mμ), which was carefully stabilized by the method of V.I. Shirokov [6]. Observations were made with a filter crossed with the 436 mμ line and perpendicular to the exciting light; the degree of polarization was determined by successive measurements of fluorescence intensity for two positions of the Glan prism placed before the photomultiplier.*

For the purpose of testing the apparatus we determined the degree of polarization of fluorescence of an aqueous solution of fluorescein excited by both polarized and unpolarized light. In the latter case the measurements were made at temperatures of 20° and 60°. The respective polarization measurements were 1.8; 0.8 and 0.5%.

Table 1 contains our experimental values of p and the values of p_0 calculated from experiments on the relation of p to η. The average value of p_0 is 40.8%.**

TABLE 1

Experimental Values of the Degree of Polarization p and Calculated Values of the Polarization Limit p_0 for Mixtures of Water and Glycol ($\eta = 0.0144$-0.0994) and Mixtures of Water and Glycerine

η, poises	0.0144	0.0183	0.0259	0.0455	0.0994	0.872	0.91	1.56	4.55
p, %	3.3	3.7	5.00	8.00	12.8	30.0	31.5	33.8	37.7
p_0, %	44.6	44.0	43.7	42.9	40.0	36.5	38.4	38.0	39.4

Table 2 contains our values of p, B/B_0,*** τ/τ_0 for various concentrations of potassium iodide, the calculated values of δ_1 and δ_2/δ_1 and the values of the polarization limit p_0 calculated 1) from Formula (1) in which τ was replaced by $\frac{B}{B_0}\tau_0$; 2) from the same formula with τ replaced by fluorometric values of the fluorescence persistence and 3) from Formula (5).

A comparison of the last three columns shows that the best results are obtained from the calculation using (5); this produces a relatively small spread of the calculated values of p_0 while the mean value of p_0 is 41.2%, which is very close to the mean value of p_0 calculated from experiments on the relation of polarization to viscosity. The widely used method of calculation from (1) with τ replaced by $\frac{B}{B_0}\tau_0$ gives too low values of the polarization limit; also, when there is a large discrepancy between the changes of B/B_0 and τ/τ_0 this method has no theoretical justification. Finally, calculation using (1), in which the fluorometric values of τ are used for each concentration of potassium iodide, gives the worst results. The polarization limit in this case increases systematically and very rapidly with increased concentration of the quencher and thus the dependence of $1/p$ on the fluorometric values of τ cannot be represented by a straight line, as is required by (1).

Thus, it may be regarded as proved that for the fluorescence quenching in our investigation the nonproportional changes of the yield and persistence result from nonexponential damping of fluorescence in quenched solutions.

In conclusion, we consider it a pleasant duty to thank F.S. Cheremisin, who assisted us with the assembling

---

*A detailed description of the apparatus will be given elsewhere.

**We assumed that all values of p_0 which we obtained are of equal weight, although there may be some objections to this. However, it is very difficult to estimate the weights of the individual measurements.

***The tabulated data for the yield contain a small correction to account for the change of anisotropy of radiation through quenching [7].

TABLE 2

Experimental Values of the Degree of Polarization, the Yield and Persistence of Fluorescence in Solutions of Fluorescein Quenched by Potassium Iodide, and the Values of the Polarization Limit Calculated from Formulas (1) and (5)

C_{KI} m/l · 10	B/B_0	$\frac{\tau}{\tau_0}$	p, %	δ_1	δ_2/δ_1	$p_0\left(\frac{B}{B_0}\right)$	$p_0(\tau)$	p_0 from (5)
1.5	0.34	0.336	4.54	1.31	0.8416	36.6	36.3	39.2
3	0.192	0.21	7.15	1.57	0.763	35.8	38.2	39.2
6	0.095	0.128	11.43	1.96	0.7370	34.2	40.4	40.0
9	0.0518	0.085	15.85	2.225	0.7675	33.2	43.3	41.5
12	0.0351	0.066	19.55	2.485	0.7821	34.0	45.8	41.5
15	0.0261	0.052	22.83	2.73	0.7828	35.4	46.7	44.5
18	0.0189	0.041	26.0	2.975	0.7850	36.2	47.1	42.9

of the apparatus and with the calculations.

LITERATURE CITED

[1] V.L. Levshin, Z. Physik 26, 274 (1924); 34, 330 (1925).

[2] F. Perrin, Ann. Physique 12, 169 (1929); Thèse (Paris, 1929).

[3] V.L. Levshin, Photoluminescence of Liquids and Solids [in Russian] (1951); S.I. Vavilov and I.M. Frank, Z. Physik 69, 100 (1931); A.N. Sevchenko, Trudy GOI 14, 65 (1941); F. Perrin, Acta Phys. Polon. 5, 335 (1936).

[4] S.I. Vavilov, Acta Phys. Polon. 5, 417 (1936); B.Ia. Sveshnikov, Acta Physicochim. URSS 3, 257 (1935); Trudy GOI No. 108 (1938) [dissertation]; L.A. Kuznetsova, B.Ia. Sveshnikov and V.I. Shirokov, Optica i Spectr. 2, 5, 578 (1957).

[5] N.S. Marinesco, Adsorption sur les molecules dissoutes (Paris, 1927).

[6] V.I. Shirokov, Izv. Akad. Nauk SSSR, ser. fiz. 20, 605 (1956).

[7] B.Ia. Sveshnikov, Acta Physicochim. URSS 4, 354 (1936).

Received February 8, 1957

THE CHANGE OF CONDUCTIVITY OF KBr IN STRONG FIELDS AT TEMPERATURES FROM 300° to 450°

V. F. Pisarenko

(Presented by Academician A.N. Terenin, December 17, 1956)

It is known [1] that the electrolysis of heated alkali-halide salts under certain conditions can lead to increased conductivity of the crystals along with their coloration. In such cases the dielectrics become impurity semiconductors. The F-centers serve as the impurities which increase the conductivity. Crystal coloration occurs only when the electrons entering the crystal displace haloid ions.

We have been able to detect a sharp increase of conductivity by a factor of 100 to 1000 in heated KBr single crystals subjected to relatively strong fields (1000-10,000 v/cm) without coloration, with no formation of dendrites in the specimens.

We used the method described in Reference [2] with the difference that during electrolysis the specimens were connected in series with a "retarding" resistance of about 10^5 ohms to protect the specimens from breakdown. It was possible to observe increased conductivity between approximately 300° and 450°. At lower temperatures dendrites grow in the specimens; above 450° the specimens become colored.

Figure 1 shows the change of conductivity of a specimen with time at constant temperature, voltage and retarding resistance. It can be seen that for some time (depending on the field and the nature of the contact between the cathode and the specimen) the conductivity remains constant and then increases very rapidly by a factor of 100 to 1000. When the field is reversed the conductivity is reduced to its original value within one second, and when the field direction is restored the conductivity again increases rapidly. When the field is reversed for a long period the conductivity, after being reduced at first, increases for a time, after which a return to the original direction results in decreased conductivity. Control experiments showed that the increase of conductivity was not the result of heating of the specimens nor of the growth of dendrites.

The passage of a current through a crystal in such an "altered" state results in damage to the anode while the cathode is not affected (aluminum plates being usually used as electrodes); in ordinary electrolysis only the cathode is damaged.

The current-voltage characteristic of a crystal with increased conductivity is a loop which is not reproduced when the voltage cycle is repeated. The dependence of the conductivity on temperature at constant voltage also does not remain unchanged. From these measurements it is possible to estimate the activation energy at roughly about 0.6 ev, while in the normal state it is about 3 ev.

A highly conducting crystal which is cooled rapidly to room temperature reveals properties which differ from those which it possessed originally. After such treatment a thin layer (10μ) near the cathode is colored. The absorption spectrum contains F-, M-, U- and V-bands. The concentration of F-centers, estimated from the optical density, is of the order of 10^{18}-10^{19} cm^{-3}. The near-anode portion of the crystal is usually damaged but is not colored. The bulk of the crystal is not colored and its absorption spectrum is not appreciably changed from its original form. Nevertheless the specimen is photoconducting and its integral photosensitivity is comparable with the photosensitivity of x-rayed specimens with F-center concentrations of the order of 10^{16} cm^{-3}. Figure 2 shows the spectral distribution of photoconductivity of an "altered" and of an x-irradiated specimen; the spectral region of the first specimen is considerably broader. When the specimen is cooled to − 183° the photoconductivity disappears. The thermal conductivity of such crystals at room temperature is greater than normal by 2-3 orders of magnitude.

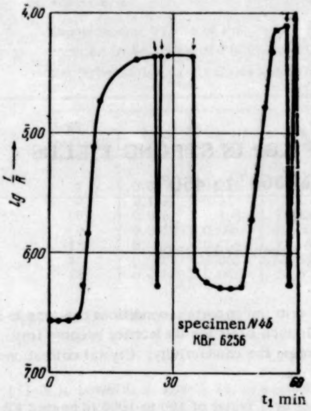

Fig. 1. Change of conductivity of a specimen of KBr in strong fields at 400°. $E_{init} = 1200$ v/cm.

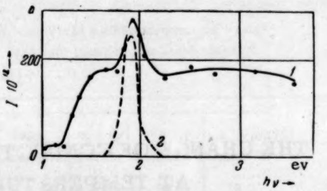

Fig. 2. Spectral distribution of photoconductivity of an "altered" KBr crystal (2). of an x-irradiated KBr crystal.

Altered specimens which are annealed at 400-500° for a few minutes return to their normal state.

The observed effects can be explained on the basis of the mechanism of electrolysis which was proposed by M.S. Kosman [2]. It is assumed that the electrons which enter the crystal when the boundary barrier is lowered by the potassium deposited on the cathode neutralizes the near-electrode space charge, forming a layer of higher conductivity; but because of the relatively low temperature the fields created in the crystal are not sufficiently strong to drive the Br^- ions to the anode, so that the electrons move in the conduction band through the entire crystal and accumulate in the near-anode layer. The field which is generated by this charge causes the release of Br at the anode. Only a very small fraction of the electrons are captured by the defects in the crystals. These acceptors presumably release their electrons to a metastable level when excited by light; thermal fluctuations then eject the electrons into the conduction band. Since the absorption by a specimen does not change appreciably in its transition to the altered state, the number of defects evidently does not exceed 10^{13} cm^{-3}. This small number of defects probably accounts for the high electron mobility in the specimen. However, it must be mentioned that we are still unable to explain the observed effects in all details.

A sharp unipolar change of conductivity in strong fields at high temperatures was previously observed by N.I. Shefer [3] for barium titanate.

In conclusion the author considers it his obligation to thank Professor M.S. Kosman for directing this work.

LITERATURE CITED

[1] P.S. Tartakovskii, The Photoconductive Effect in Dielectrics [in Russian] (Moscow-Leningrad, 1940); N. Mott and R. Gurney, Electronic Processes in Ionic Crystals (Clarendon Press, Oxford, 1950), 2nd Ed. [Russian translation, 1st Ed., Foreign Lit. Press, 1950]; R.W. Pohl, Physik Z. 39, 36 (1938).

[2] M.S. Kosman and V.F. Pisarenko, Doklady Akad. Nauk SSSR 115, 4, 693 (1957).*

[3] N.I. Shefer, Author's Abstract of Dissertation [in Russian] (Leningrad, 1953).

Received November 19, 1956

A.I. Herzen Leningrad State
Pedagogical Institute

---

*[This issue, p. 375.]

ON THE TEMPERATURE DEPENDENCE OF THE HEAT CAPACITY OF SOLIDS

Academician N. N. Sirota (Belorusskaia SSR)

The quantum theory of the specific heats of monoatomic solids was first developed by Einstein [1] on the assumption that all the atoms of a solid possess the same vibrational frequency. Using the Planck distribution to express the average energy of an oscillator as a function of temperature, Einstein obtained the following expression for the internal energy of a solid:

$$\Delta U_{\mathbf{e}} = 3N \frac{h\nu}{e^{h\nu/kT} - 1} .$$

The great fundamental significance of Einstein's work lay in the fact that he derived theoretically a temperature dependence of specific heat which resembled experimental findings, and also that he explained the fundamental role of the characteristic temperature $\theta_e = h\nu/k$, which is an important constant associated with many properties of solids.

In Debye's theory [2], which is now the generally accepted theory of the vibrational heat capacity of solid lattices, a spectral distribution of frequencies is assumed, which is described by the parabolic law $dz/d\nu = B\nu^2$ (Figure 1). In this connection the work of Born and Karman [3] and of Blackman [4] is very important.

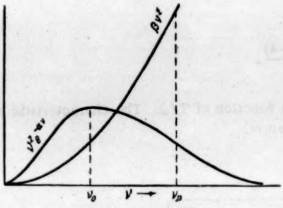

Fig. 1.

It follows from several considerations as well as from direct experiments and calculations [4] that the actual frequency distribution in solids is closer to the Gaussian than the Debye form; this was pointed out especially by A.F. Ioffe [5].

In the present paper we shall show the possibility of calculating the temperature dependence of the heat capacity of solids using a near-Gaussian frequency distribution. In an earlier note [6] we pointed out the need for taking the regularity of structural form into account in the frequency distribution; this was later considered by other writers [7, 8]. In our present approach to the problem of calculating the temperature dependence of heat capacities it is possible to include the structure, using expressions which have been derived, but we shall limit ourselves to isotropic solids.

Our frequency distribution subject to a certain approximation can be described by

$$\frac{dz}{d\nu} = A\nu^p e^{-\alpha\nu^n}. \tag{1}$$

For simplicity, without introducing a large error, we shall approximate the vibrational frequency distribution by using (Figure 1)

$$\frac{dz}{d\nu} = A\nu^p e^{-\alpha\nu}. \tag{1a}$$

As the total number z of vibrations per gram-atom of a solid is 3N we have

$$z = 3N = \int_0^\infty A\nu^p e^{-\alpha\nu}\, d\nu = A\,\frac{\Gamma(p+1)}{\alpha^{p+1}} \tag{2}$$

whence $A = 3N\alpha^{p+1}/\Gamma(p+1)$; the maximum frequency ν_0 on the curve, which we take as the characteristic frequency, is then given by $\nu_0 = p/\alpha$. Then the characteristic temperature θ is

$$\theta = \frac{h\nu_0}{k} = \frac{hp}{k\alpha}\,. \tag{3}$$

The total vibrational energy or internal energy of a solid is then

$$\Delta U = A\int_0^\infty \frac{h\nu\cdot\nu^p e^{-\alpha\nu}\, d\nu}{e^{h\nu/kT}-1}\,, \tag{4}$$

whence we obtain to a sufficient approximation

$$\Delta U = 3RT\left(\frac{T}{\theta}\right)^{p+1}\frac{p^{p+1}}{(pT/\theta+1)^{p+1}}\,. \tag{5}$$

Since for an isotropic solid we can assume $p \geq 2$, for $p = 2$ we have

$$\Delta U = 24RT\,\frac{(T/\theta)^3}{(2T/\theta+1)^3}\,. \tag{6}$$

On the basis of (5) we obtain for the temperature dependence of the heat capacity of a solid

$$C = 3Rp^{p+1}\,\frac{(T/\theta)^{p+1}\,[p\,T/\theta+p+2]}{(pT/\theta+1)^{p+2}}\,; \tag{7}$$

and for $p = 2$

$$C = 3R\,\frac{(T/\theta)^3\,(2T/\theta+4)}{(T/\theta+{}^1/_2)^4}\,.$$

Figure 2 shows the vibrational heat capacity of a solid as a function of T/θ. The characteristic temperature is approximately one-third the Debye characteristic temperature.

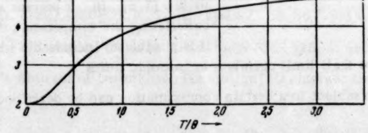

Fig. 2.

This expression is a good description of the experimental temperature dependence of the heat capacities of various solids. The simplicity of this law opens broad possibilities for its use in the most diversified thermodynamic and other physical calculations.

LITERATURE CITED

[1] A. Einstein, Ann. Physik 22, 180, 800 (1906); 34, 170 (1911).

[2] P. Debye, Ann. Physik 39, 789 (1912).

[3] M. Born and T. Karman, Physik Z. 13, 297 (1912); 14, 15 (1913).

[4] M. Blackman, Z. Physik 86, 421 (1933).

[5] A.F. Ioffe, Collection: Problems of the Theory and Investigation of Semiconductors and Semiconductor Metallurgy [in Russian] (Izd. AN SSSR, 1945), p. 5.

[6] N.N. Sirota, Doklady Akad. Nauk SSSR 47, 1, 40 (1945).

[7] V.V. Tarasov, Doklady Akad. Nauk SSSR 46, No. 1 (1945).

[8] I.M. Lifshits, J. Exptl.-Theoret. Phys. (USSR) 22, 471, 475 (1952).

Received March 25, 1957

EXPERIMENTAL STUDIES OF THE ALPHA DECAY OF MEDIUM-WEIGHT NUCLEI

Iu. A. Surkov

(Presented by Academician A.P. Vinogradov, March 7, 1957)

The alpha decay of elements with $A < 209$ has already been discussed in the literature [1] and it has been shown that all elements of mass number greater than approximately 150 are unstable against alpha decay. Intermediate elements ($N = 82$-126) are stable only because their disintegration energy is small and their lifetime correspondingly long. The detection of such alpha activity is mainly limited by the existing possible methods of measurement. However, in some instances careful investigations have revealed a number of natural alpha emitters.[2-6].

It follows from the theory of alpha decay that with reduced mass number of an isotope its alpha-disintegration energy increases. Thus, the lighter isotopes are less stable against alpha decay. This fact enables us to employ nuclear reactions induced by high-energy nucleons for the purpose of obtaining isotopes with large neutron deficiencies. But these isotopes are also unstable against K capture and β^+ decay, and in the investigated range these transitions are usually most probable; this hinders considerably the detection and study of alpha decay. Yet even for intermediate atoms alpha decay is in some instances the predominant process of radioactive transformation. Thus, for example, it is known from energy considerations that isotopes which are most unstable against alpha decay are those at the beginning of nucleon shell occupancy. A number of such isotopes containing 84 or 85 neutrons were observed and studied in Refs. [7-10]. The jump in the binding energy of nucleons at $N = 82$ is so large that the decay of isotopes with $N < 84$ cannot be observed. Moreover, among the heaviest intermediate nuclei with even a small neutron deficiency isotopes are unstable against alpha decay while K capture and β^+ decay are still of small probability. This accounts for the alpha activity of neutron-deficient isotopes of Au, Hg, Bi, Po, At and Rn.

From the systematics of experimental data on the alpha decay of medium-weight elements we determine the existence of the same laws of alpha decay which are observed in the case of heavy elements ($A > 209$). We are thus able to stipulate requirements concerning the conduct of experiments on alpha decay in medium-weight atoms.

In accordance with the foregoing we have performed an experimental investigation of alpha decay in isotopes with $N = 82$-126. Alpha-active isotopes were obtained through nuclear reactions when Er, Yb and Hf were irradiated in the synchrocyclotron of the Joint Institute for Nuclear Studies by protons from 70 to 660 Mev. For the investigation of short-lived alpha activity the elements were irradiated for two hours. Long-lived alpha activity was investigated in the products of nuclear reactions which were accumulated during 3 months of operation of the accelerator.

The elements which were produced by the nuclear reactions were separated chromatographically and were identified by their various forms of radioactive decay as published in the literature, and by the chromatographic scale of activated elements obtained in the chromatographic separation of nuclear reaction products. For the alpha-decay investigations we used only very pure chromatographically separated fractions of the elements. Special care was taken to obtain sufficiently complete separation; this was a very important aspect of the experiments.

Figure 1 contains chromatograms of the products of nuclear reactions formed in the bombardment of Er, Yb and Hf with 660-Mev protons. The beta and alpha activities were obtained simultaneously. The solid curves

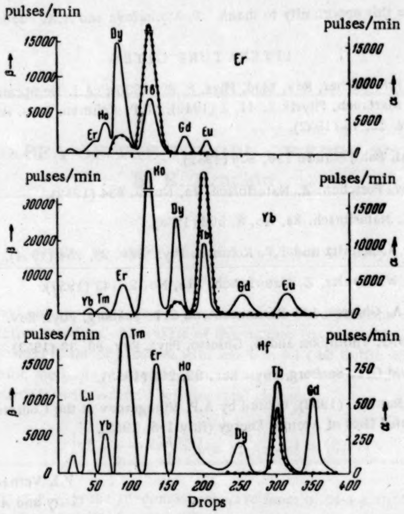

Fig. 1. Chromatograms of the products of bombarding Er, Yb and Hf with 660-Mev protons (separation by lactic acid on resin, D = 50 (X-12); pH 3.4-3.6; t = 85°; V ≈ 1 drop/min).

TABLE 1

Element	A	E_α Mev	T_α	From our data	
				E_α, Mev	T_α
Gd	148	3.3 ±0,2	~ 10^3 yrs calc.	3.27	> 35 yrs
Tb	149	4.06±0.05	4.3±0.2 hr	4.08	4.1 hr
Dy	152	3.66±0.08	3.2±0.3 hr	3.73	2.3 hr
Dy	(153)	3.3 ±0.2	~ 10 yrs calc.	—	—
Hf	—	3.5 ±0.2	~ 10^4 yrs. calc.	—	—

represent beta activity and the lines with dots represent alpha activity in pulses per minute as recorded by our counter. Alpha activity which was recorded only photographically is not shown here.

Table 1 gives all of the alpha-active isotopes which we observed in our investigation of the products of bombardment of intermediate elements. Some of these were known from earlier published work; we used the best data given in Ref. [8]. The isotopes $Dy^{(153)}$ and Hf (?) are presumed to be new. We did not obtain the mass numbers. The numbers in parentheses are the most probable values assigned to the given alpha activity according to the alpha-decay systematics. The alpha activity of hafnium is not entirely reliable because of the imperfect chemical method that was used. The alpha activities given in Table 1 were measured a few hours after irradiation of the target; the time of the measurement was dependent on the atomic number of the bombarded and investigated elements. We did not investigate elements with Z < 64.

For the isotopes Tb^{149} and Dy^{152} the energies were measured with an ionization chamber and a single-channel pulse-height analyzer. The corresponding half-lives were measured with a scintillation alpha counter. For Gd^{148}, $Dy^{(153)}$ and Hf (?) the energies were determined from the ranges in thin (50μ) photographic emulsions. The corresponding half-lives for alpha decay are rough estimates.

In addition to the apparatus and methods of registering alpha activity which have already been mentioned we used a luminescence gamma spectrometer, standard apparatus with end-window Geiger counters and a coarse magnetic beta analyzer.

In conclusion, I take this opportunity to thank L.P. Moskaleva and A.A. Pozdniakov for their assistance.

LITERATURE CITED

[1] H.A. Bethe and R.F. Bacher, Rev. Mod. Phys. 8, 82 (1936); A.J. Dempster, Phys. Rev. 53, 869 (1938); O. Hahn, S. Flügge and J. Mattauch, Physik Z. 41, 1 (1940); T.P. Kohman, Phys. Rev. 76, 448 (1949); S. Jha and G.P. Dube, Ind. J. Phys. 26, 15 (1952).

[2] G. Hevesy and M. Pahl, Nature 130, 846 (1932).

[3] W. Riezler and W. Porschen, Z. Naturforsch. 7a, No. 9, 634 (1952).

[4] E. Bodenstedt, Z. Naturforsch. 8a, No. 8, 502 (1953).

[5] E.C. Waldron, V.A. Schultz and T.P. Kohman, Phys. Rev. 93, 254 (1954).

[6] W. Porschen and W. Riezler, Z. Naturforsch. 11a, No. 2, 143 (1957).

[7] S.G. Thompson, A. Ghiorso, J.O. Rasmussen and G.T. Seaborg, Phys. Rev. 76, 1406 (1949).

[8] J.O. Rasmussen, S.G. Thompson and A. Ghiorso, Phys. Rev. 89, 33 (1953).

[9] D.C. Dunlavey and G.T. Seaborg, Phys. Rev. 92, 206 (1953).

[10] S.A. Baranov [in Russian] (1952), quoted by A.P. Vinogradov at the Conference of the Academy of Sciences USSR on the Peaceful Uses of Atomic Energy (July 1-5, 1955).

Received March 7, 1957

V.I. Vernadskii Institute of Geochemistry and Analytic Chemistry
Academy of Sciences, USSR

MATRIX ALGEBRA OF THE THEORY OF SPIN 3/2 PARTICLES

E. E. Fradkin

(Presented by Academician V.A. Fok, April 5, 1957)

1. In the matrix method one operates with the matrices in the wave equation as with abstract numbers, knowing only their commutation relations. The value of this method has been fully proved in the theory of spin 1/2 particles (the Dirac algebra) [1] and of particles with spin 0 and 1 (the Duffin-Kemmer algebra) [2]. In the present paper we shall establish the basic relationships in the algebra of the α^k matrices** which appear in the wave equation of spin 3/2 particles with positive definite total charge:

$$\left\{\alpha^k \frac{\partial}{\partial x_k} + i\varkappa\right\} \Psi(x_0, x_1, x_2, x_3) = 0, \tag{1}$$

where $\Psi(x_0, x_1, x_2, x_3) \equiv \Psi(t, x, y, z)$ is the 16-component wave function of a particle with spin 3/2; α^k are square matrices of order 16, whose specific form in different representations is given in Refs. [3-5]; $\varkappa$ is the mass of the particle.***

2. For particles of any spin Refs. [6, 7] give a general method of deducing the commutation relations from the minimal equation that is satisfied by the matrices. The minimal equation for the matrices of a particle of definite spin s is [6, 8]

$$(L^n)(L^2 - 1) = 0. \tag{2}$$

For particles with spins 1/2, 1, 3/2 or $2n = 2s - 1$.****

However, the commutation relations which follow from (2) are too general. Thus, for spin 1 particles, just as for particles of spin 0, we obtain the following commutation relations:

$$\sum_p \beta^k(\beta^l\beta^m - g^{lm}) = 0, \tag{3}$$

where g^{lm} is the metric tensor of the special theory of relativity; $g^{00} = -g^{11} = -g^{22} = -g^{33} = 1$; $g^{lm} = 0$ $(l \neq m)$; $\sum_p$ denotes summation over all possible permutations of the superscripts k, l, m. The commutation relations (3) are divided into two types of commutation relations which are symmetrical in two indices. One of these types, the Duffin-Kemmer commutation relations [2], is satisfied and determines the entire algebra of the matrix theory of particles with spins 0 and 1.

---

*Presented January 12, 1957 at the seminar of the theoretical laboratory of the Joint Nuclear Research Institute.

**Here and hereinafter the Latin indices assume the values 0, 1, 2, 3 and the Greek indices assume the values 1, 2, 3. As usual, a single index which appears twice in the same expression represents a summation.

***In this paper the Planck constant $\hbar$ and the velocity of light c are taken as unity.

****For particles of spin 2 the matrix L^0 constructed by the method of Gel'fand and Iaglom [3] satisfies the minimal equation $(L^0)^5 = (L^0)^3$.

3. For particles with spin 3/2 Equation (2) leads to the following commutation relations*:

$$\sum_p \alpha^i\alpha^k (\alpha^l\alpha^m - g^{lm}) = 0. \tag{4}$$

Here in $\sum\limits_p$ it is necessary to permute the four superscripts.

None of the three types of commutation relations with partial symmetry of two or three indices, nor their linear combination, is satisfied by the matrices α^k. On the other hand, the general commutation relations (4) are satisfied not only by the matrices α^k of the theory of spin 3/2 particles but also by the Dirac γ^k matrices, the Duffin-Kemmer β^k matrices, the matrices for particles with mass κ and two spin states 3/2 and 1/2 in Ref. [9] and many others. Therefore, in order to distinguish the algebra of matrices which describe spin 3/2 particles it is necessary to obtain some additional relations which will be satisfied, as well as (4), by the α^k matrices of interest. These new relations must fulfill the following requirements: (a) they need not be satisfied by Hermitian matrices, because in the theory of spin 3/2 particles with positive charge the α^k are nonHermitian [3]; (b) they must lead to additional conditions imposed on the wave function.

Such relations are of the form**

$$g_{mn}\{\alpha^m\alpha^j\alpha^n + \alpha^n\alpha^j\alpha^m + \alpha^j(\alpha^m\alpha^n + \alpha^n\alpha^m) - \\ -(\alpha^m\alpha^n + \alpha^n\alpha^m)\alpha^j\}\{\alpha^k\alpha^l + \alpha^l\alpha^k\} = 0. \tag{5}$$

The Relations (5) have been verified by us for the α^k in the parametric representation of Petras [5]. Consequently, they are also satisfied in other representations, since, as was shown in Ref. [11], matrices in the Petras representation are related by allowable linear transformations to the other known representations of the α^k matrices [3, 4].

For the complete construction of the algebra of spin 3/2 matrices it is essential that the infinitesimal transformations I^{kl} of the wave function Ψ, in

$$\Psi \to \Psi' = \Psi + {}^1/_2\, \varepsilon_{kl} I^{kl}\Psi \tag{6}$$

for the infinitesimal Lorentz transformation

$$x^i \to x'^i = x^i + g^{ik}\varepsilon_{kl}x^l \quad (\varepsilon_{kl} = -\varepsilon_{lk}) \tag{7}$$

be representable through antisymmetric combinations of the α^k matrices, as follows:

$$I^{kl} = {}^3/_4\{(\alpha^k\alpha^l - \alpha^l\alpha^k) + (\alpha^k\alpha^i\alpha_i\alpha^l - \alpha^l\alpha^i\alpha_i\alpha^k) - \\ - {}^3/_4(\alpha^i\alpha^k\alpha_i\alpha^l - \alpha^l\alpha^l\alpha_i\alpha^k) - {}^5/_4(\alpha^k\alpha^l - \alpha^l\alpha^k)\alpha^i\alpha_i + \\ + {}^7/_4(\alpha^k\alpha^i\alpha^l\alpha_i - \alpha^l\alpha^i\alpha^k\alpha_i)\}. \tag{8}$$

The α^k matrices satisfy the necessary relation for Lorentz invariance of the theory [3]:

$$\alpha^k I^{lm} - I^{lm}\alpha^k = g^{kl}\alpha^m - g^{km}\alpha^l. \tag{9}$$

---

*We note that the matrices of order 20 which were obtained in Ref. [10] and which can also be applied to spin 3/2 particles only satisfy the minimal Equation (2) with n = 3 and thus do not satisfy the commutation relations (4).

**It must be noted that the 16th-order matrices for spin 3/2 particles are for (5) the representation of lowest order, as it was shown in Ref. [3] that these matrices are unique and cannot be of lower order. We did not investigate the question of higher-order representations of (5).

The transformation T for the reflection

$$x^0 \to x^0, \quad x^\nu \to -x^\nu, \tag{10}$$

is given by

$$T = {}^3/_4 \{\alpha^l \alpha_l \alpha^0 + \alpha^0 \alpha^l \alpha_l - {}^8/_3 \alpha^0 - 4 (\alpha^0)^3\}, \quad T^2 = 1. \tag{11}$$

4. In order to construct a real invariant Lagrangian it is necessary to determine the basic invariant Hermitian bilinear form $\Psi^+\Psi = \Psi^*\eta\Psi$.[*] Harish-Chandra [9] has shown that the Gram metric matrix η which satisfies the conditions

$$\begin{gathered} (\alpha^h)^* \eta - \eta\alpha^h = 0, \quad I^{0\mu}\eta - \eta I^{0\mu} = 0, \\ T\eta - \eta T = 0, \quad I^{\nu\mu}\eta - \eta I^{\nu\mu} = 0 \end{gathered} \tag{12}$$

must be obtained in the form

$$\eta = \Lambda T, \tag{13}$$

where Λ is a certain scalar matrix, that is, $I^{ik}\Lambda - \Lambda I^{ik} = 0$, $T\Lambda - \Lambda T = 0$. In our case Λ is a linear combination of the two scalar matrices I and $\alpha^i\alpha_i$,[**] as follows:

$$\Lambda = (7 - 4\sqrt{3})(I - {}^3/_2 (2 + \sqrt{3})\, \alpha^l \alpha_l). \tag{13'}$$

Here it must be remembered that the α^k are not Hermitian.

$$(\alpha^h)^* = \varepsilon^h \left\{\alpha^h - \frac{3\sqrt{3}}{2}\left(\alpha^l\alpha_l\alpha^h - \alpha^h\alpha^l\alpha_l - \frac{2}{\sqrt{3}}\, \alpha^l\alpha^h\alpha_l\right)\right\}, \tag{14}$$

where ϵ^k is the sign function: $\epsilon^0 = 1$, $\epsilon^1 = \epsilon^2 = \epsilon^3 = -1$.

It must be remembered that the expressions for η and $(\alpha^k)^*$ in terms of α^k are true only in the Petras representation, because when we go over to the other representations which are related to the Petras representation by allowable but nonunitary transformations [11] η and $(\alpha^k)^*$ transform differently than α^k.

5. When we construct the Lagrangian, introduce the interaction with the electromagnetic field in the usual way and perform the variation we obtain the equation for a spin 3/2 particle in an external electromagnetic field:

$$(\alpha^l \pi_l + i\varkappa)\Psi = 0, \tag{15}$$

where $\pi_l = \partial/\partial x_l - ie\varphi_l$; φ_l is the four-dimensional potential of the electromagnetic field and $\underline{e}$ is the charge.

By using (5) we can obtain two kinds of supplementary conditions for the wave function. In order to derive the first kind of supplementary conditions, which relate the components of the wave-function among themselves, we obtain from (15) the following second-order equation:

$$\left\{\frac{1}{2}(\alpha^k\alpha^l + \alpha^l\alpha^k)\pi_k\pi_l - \frac{i}{4} e (\alpha^k\alpha^l - \alpha^l\alpha^k) F_{kl} + \varkappa^2\right\}\Psi = 0. \tag{16}$$

We have here used the commutation relations for the π_k $\qquad \pi_k\pi_l - \pi_l\pi_k = -ieF_{kl}$, where $F_{kl} = \partial\varphi_l/\partial x_k - \partial\varphi_k/\partial x_l$ is the electromagnetic field tensor.

---

[*] Here and hereinafter an asterisk denotes the Hermitian conjugate form.

[**] The numerical coefficient in (13') was taken from the condition that the metric matrix η has 12 eigenvalues equal to ± 1 in the representation for spin 3/2.

Multiplying (16) by the matrix vector

$$A^j = \alpha^i\alpha^j\alpha_i + \alpha^j\alpha^i\alpha_i - \alpha^i\alpha_i\alpha^j, \tag{17}$$

by virtue of (5) we obtain the supplementary conditions in the form

$$\left\{\frac{1}{4i}\left(\frac{e}{\varkappa^2}\right)Q^{jkl}F_{kl} + A^j\right\}\Psi = 0, \tag{18}$$

containing the antisymmetric tensor of rank 3

$$Q^{jkl} = A^j(\alpha^k\alpha^l - \alpha^l\alpha^k) = (\alpha^i\alpha^j\alpha_i + \alpha^j\alpha^i\alpha_i - \alpha^i\alpha_i\alpha^j)\,(\alpha^k\alpha^l - \alpha^l\alpha^k). \tag{19}$$

In order to derive supplementary conditions with derivatives of the wave function, (15) must be multiplied by the second-rank matrix tensor

$$R^{jk} = A^j\alpha^k = (\alpha^i\alpha^j\alpha_i + \alpha^j\alpha^i\alpha_i - \alpha^i\alpha_i\alpha^j)\,\alpha^k. \tag{20}$$

By virtue of (5) we obtain the relativistically covariant relations for Ψ:

$$\left\{\frac{1}{2i}\left(\frac{1}{\varkappa}\right)Q^{jkl}\pi_l + R^{jk}\right\}\Psi = 0. \tag{21}$$

Since $Q^{jkl} = -Q^{jlk}$, we have $Q^{jkk} = 0$ (not summed over k) and in (21) the term with π_k is absent. For $k = 0$, the term with the time derivative is absent, and (21) assumes the character of supplementary conditions which relate the wave function with its spatial derivatives.

For a free particle $\varphi_l = 0$ and $F_{kl} = 0$ and the supplementary conditions (18) and (21) become

$$A^j\Psi = 0, \quad \left\{\frac{1}{2i}\left(\frac{1}{\varkappa}\right)Q^{jkl}\frac{\partial}{\partial x_l} + R^{jk}\right\}\Psi = 0. \tag{22}$$

In conclusion the author sincerely thanks S.V. Izmailov for his constant interest and Iu.A. Iappa for valuable discussions.

LITERATURE CITED

[1] F. Sauter, Z. Physik 63, 803 (1930); 64, 296 (1930).

[2] H. Kemmer, Proc. Roy. Soc. A 173, 91 (1939).

[3] I.M. Gel'fand and A.M. Iaglon, J. Exptl.-Theoret. Phys. (USSR) 18, 703 (1948).

[4] S.H. Gupta, Phys. Rev. 95, 1334 (1954).

[5] M. Petras, Czechoslov. J. Phys. 5, 160 (1955).

[6] H.I. Bhabha, Rev. Modern Phys. 21, 451 (1949).

[7] Iu.A. Iappa, Dissertation (Leningrad State University, 1953).

[8] V.I. Karpman, Dissertation (Physical Institute, Academy of Sciences USSR, 1954).

[9] Harish-Chandra, Proc. Roy. Soc. A 192, 195 (1948).

[10] E.S. Fradkin, J. Exptl.-Theoret. Phys. (USSR) 20, 27 (1950).

[11] E.E. Fradkin and S.V. Izmailov, Doklady Akad. Nauk SSSR 114, 2, 277 (1957) [Soviet Physics – Doklady, p.232].

Received March 27, 1957

A.I. Herzen Leningrad State
Pedagogical Institute

THE OPTICAL ANISOTROPY OF SOME CHAIN MOLECULES CONTAINING BENZENE RINGS

V. N. Tsvetkov and S. Ia. Magarik

(Presented by Academician A.A. Lebedev, February 19, 1957)

We know that the investigation of birefringence in a streaming polymer solution is the most direct method of determining the optical anisotropy of the molecules.

When a polymer consisting of linear chain molecules and its solvent have the same refractive index so that the so-called "form effect" is absent [1, 2], the statistical theory [3] leads to the following relation between the characteristic viscosity [η] of the solution and its dynamic optical constant [n]:

$$[n] = \lim_{\substack{c \to 0 \\ g \to 0}} \left(\frac{\Delta n}{gc\eta}\right) : \frac{[n]}{[\eta]} = 0,195 \frac{(n^2 + 2)^2}{nkT} (\alpha_1 - \alpha_2). \qquad (1)$$

Here n is the refractive index of the solvent, η is its viscosity, k is the Boltzmann constant, T is the absolute temperature, c is the concentration and Δn is the difference between the two principal refractive indices of the solution observed in laminar flow with velocity gradient g, $\alpha_1 - \alpha_2$ is the difference between the two principal polarizabilities (along and perpendicular to the direction orientation of the chain) of a chain segment, which is a portion of the chain of sufficient length so that its direction does not depend on the directions of the two adjoining segments.

Thus, the measurement of [n] and [η] in the solution enables us to determine the anisotropy $\alpha_1 - \alpha_2$ of a segment.

On the other hand, the anisotropy of a segment is determined by the chemical structure of the polymer chain. When its structure is sufficiently well known (both with respect to the stereochemistry of a monomer link and rotation around the valence bonds of the chain) the theory [4] makes it possible to calculate the difference between the polarizabilities of a segment from the known polarizabilities of the bonds of a monomeric link.

Most frequently we have to deal with polymer chains of complex structure, the details of which are not known. Under such conditions it is impossible to determine a quantitative relation between the anisotropy of a segment and the anisotropy of a monomeric link. However, even in such cases the experimental value of $\alpha_1 - \alpha_2$ sometimes makes it possible to draw qualitative conclusions regarding the structure of a monomeric link of the chain. Thus, experiment shows that the difference between the polarizabilities of a monomeric link (along and perpendicular to the direction of the chain of principal valence bonds) agrees in sign with the anisotropy of the segment.

In the present work this fact has been utilized for a comparative study of the structure of polymer chains containing benzene rings.

The following four polymers were investigated: (1) polystyrene (Π_1), (2) poly-n-tertiary butyl phenyl methacrylate (Π_2), (3) poly-1,4-diisopropenyl benzene (Π_3) and (4) poly-4,4'-diisopropenyl diphenylethane (Π_4). The second substance was produced by M.M. Koton, T.V. Sheremet'eva and M.G. Zhenevskaia [5] and the third and fourth by Iu.V. Mitin and N.A. Glukhov [6]. All four polymers were unfractionated. The average molecular weights, which were determined from light scattering by V.G. Aldoshin, are given in Table 1.

For the purpose of obtaining the difference $\alpha_1 - \alpha_2$ from (1) we performed dynamo-optical and viscosimetric measurements of the polymers in solvents where the form effect was excluded. For Π_2 chlorobenzene was used; for the other three polymers bromoform was used. The viscosities, which were obtained with an ordinary Ostwald viscosimeter, are listed in the third column of the table.

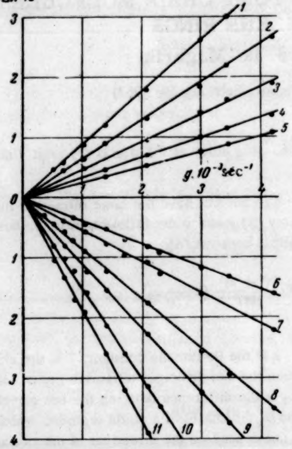

Fig. 1. Birefringence as a function of velocity gradient. Poly-1,4-diisopropenyl benzene: 1) C = 7.70; 2) C = 5.80; 3) C = = 4.20; 4) C = 2.60; 5) C = 2.10. Polystyrene: 6) C = 0.22; 7) C = 0.28; 8) C = 0.42; 9) C = 0.51; 10) C = 0.65; 11) C = 0.79.

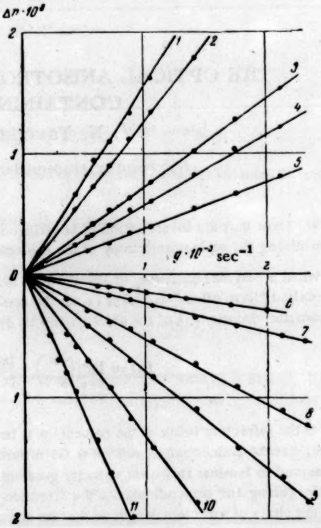

Fig. 2. Birefringence as a function of velocity gradient. Poly-d,4'-diisopropenyl diphenylethane: 1) C = 1.00; 2) C = 0.80; 3) C = 0.48; 4) C = 0.35; 5) C = 0.22. Poly-n-tertiary-butyl phenylmethacrylate: 6) C = 0.52; 7) C = 0.69; 8) C = 1.15; 9) C = 1.48; 10) C = 2.03; 11) C = 2.50. The concentrations C in Figs. 1 and 2 are given in g/100 milliliters.

Dynamic birefringence was measured in a dynamic optimeter with inside rotor. The rotor length was 3 cm and the gap width 0.26 mm; the critical gradient $g_k = 4.9 \cdot 10^5 \frac{\eta}{\rho}$ (where η is the viscosity and ρ is the density of the solvent) was nowhere exceeded. The birefringence was measured with an elliptical compensator and additional half-shade device. The path difference of the compensator was $\delta = 0.027\lambda$, where $\lambda = 5.5 \cdot 10^{-5}$ cm.

The measured dependence of the birefringence on the velocity gradient is shown in Figure 1 for the polymers Π_3 and Π_1, and in Figure 2 for Π_4 and Π_2. Figure 3 shows the extrapolated dependence of $\Delta n/gc\eta$ on concentration; the values of the dynamic optical constant are given in the fourth column of the table. In all calculations the birefringence of the solvents was suitably added or subtracted; for both bromoform and chlorobenzene this is given by $\Delta n/g = 1 \cdot 10^{-12}$.

The fifth column of Table 1 contains the values of the optical anisotropy of a statistical segment, $\alpha_1 - \alpha_2$, which were calculated from Equation (1).

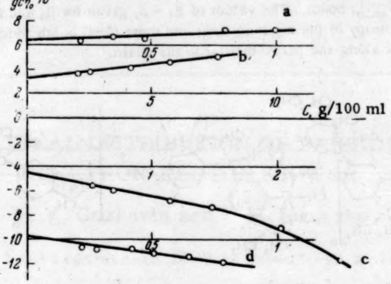

Fig. 3. $\Delta n/gc\eta$ as a function of concentration: a) poly-4,4'-diisopropenyl phenylethane; b) poly-1,4-diisopropenyl benzene ($\Delta n/gc\eta \cdot 10$); c) poly-n-tertiary butyl phenylmethacrylate; d) polystyrene.

The data show that the difference of the polarizabilities ($\alpha_1 - \alpha_2$) of a statistical segment is a large positive quantity for Π_3 and Π_4, and a large negative quantity for Π_1 and Π_2.

In interpreting the results it must be kept in mind, first of all, that the optical anisotropy of these chain molecules must be determined to a considerable extent by the position of the phenyl groups whose polarizability in the plane of the ring is considerably greater than normal to the ring. Therefore we can expect positive values of $[n]/[\eta]$ and, correspondingly, of $\alpha_1 - \alpha_2$ for polymers containing benzene rings in the chain of principal valence bonds, and negative values for the same quantities in the case of chains where the phenyl nuclei are contained in side groups. Therefore the results contained in Table 1 show that Π_3 and Π_4 belong to the first group and Π_1 and Π_2 to the second group of polymers. In polymers Π_1 and Π_2, the structure of which is well known and shown in Figure 4c, d, the phenyl groups are radicals of side groups.

TABLE 1

Polymer	$M \cdot 10^{-4}$	$[\eta]$	$[n] \cdot 10^{10}$	$(\alpha_1 - \alpha_2) \cdot 10^{25}$	$(\beta_1 - \beta_2) \cdot 10^{25}$
Polystyrene (Π_1)	27	0.82	−9.7	−190	−26
Polyparatertiary butyl phenylmethacrylate (Π_2)	37	0.85	−4.5	− 90	−15
Poly-1,4-diisopropenyl benzene (Π_3)	0.7	0.066	0.32	78	30
Poly-4,4'-diisopropenyl diphenylethane (Π_4)	78	0.70	6.20	142	24

The structure of the new polymers Π_3 and Π_4 is not yet well known. However, on the basis of the polymerization reaction scheme given in [6] the arrangement of the benzene cycles in the Π_1 and Π_2 chains can be represented in the form shown in Figure 4a, b.

By using the structures depicted in Figure 4 it is possible to calculate the anisotropy of a monomeric link in these polymers. The results are given in the last column of Table 1; these are the values of $\beta_1 - \beta_2$, the difference between the polarizabilities along and perpendicular to the chain of principal valence bonds for a single C−C bond around which rotation is possible. These values were calculated according to the scheme of additivity of polarizabilities of bonds, and the numerical values of the polarizabilities and valence angles were taken from Stuart's book [7]. The calculations for Π_1 were made on the assumption of a planar arrangement of the benzene rings normal to the chain of principal valence bonds. The value of $\beta_1 - \beta_2$ given for Π_2 refers to a rigid plane configuration of a side chain with completely free rotation of the plane of the benzene ring around the $C_{aliph} - C_{arom}$ and $O - C_{arom}$ bonds. The values of $\beta_1 - \beta_2$ given for Π_3 and Π_4 are rough estimates, taking into account only the anisotropy of the benzene rings and those C−C bonds which can give considerable difference of the polarizabilities along and perpendicular to the chain.

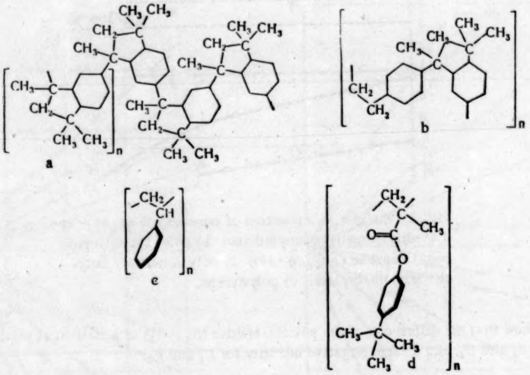

Fig. 4. Scheme of the polymer structures: a) poly-1,4-diisopropenyl benzene; b) poly-4,4'-diisopropenyl diphenylethane; c) polystyrene; d) poly-n-tertiary-butyl phenylmethacrylate.

We see that the difference of the polarizabilities of chain links ($\beta_1 - \beta_2$) obtained in this way agrees in sign in all instances with the experimental values of $\alpha_1 - \alpha_2$ and has fully permissible absolute values a few times smaller than $\alpha_1 - \alpha_2$.

Thus, the measured values of the dynamic optical constants of the investigated polymers are in good agreement with their structural formulas in Figure 4 and are thus a confirmation of the correctness of these formulas.

LITERATURE CITED

[1] V.N. Tsvetkov and E.V. Frisman, Doklady Akad. Nauk SSSR 97, 647 (1954)

[2] E.V. Frisman and V.N. Tsvetkov, Doklady Akad. Nauk SSSR 106, 42 (1956).*

[3] H. Kuhn, F. Moning and W. Kuhn, Helv. Chim. Acta 36, 731 (1953).

[4] Iu.Ia. Gotlib, M.V. Vol'kenshtein and E.K. Biutner, Doklady Akad. Nauk SSSR 99, 935 (1954).

[5] M.M. Koton, T.V. Sheremet'eva and M.G. Zhenevskaia, Bull. Acad. Sci. USSR, Div. Chem. Sci. 826 (1957).

[6] Iu.V. Mitin and N.A. Glukhov, Doklady Akad. Nauk SSSR 115, No. 1 (1957).

[7] H.A. Stuart, Die Struktur des freien Molekūls, 1952.

Received February 19, 1957

---

*[Soviet Physics — Doklady, p. 12].

ON THE LATERAL DISTRIBUTION OF PARTICLES IN AN ELECTRON-PHOTON SHOWER

V. V. Guzhavin and I. P. Ivanenko

(Presented by Academician D. V. Skobel'tsyn April 9, 1957)

In Reference 1 we proposed a method of calculating the angular and lateral distributions of electrons in the maximum of a cascade shower. In the present paper we propose a method of calculating a broader class of functions when their moments are known.

Let us consider the function $\Phi(r, s)$ which depends on the parameter s (and a number of other parameters) and is defined in the interval $0 \leq r < \infty$; it is known that for $r \to 0$

$$\Phi(r, s) = \frac{1}{r^{2-s}} \varphi(r, s); \tag{1}$$

here $\varphi(r, s) \underset{r \to 0}{=} \text{const} \neq 0$; $0 < s \leq 2$.

The r-moments of $\Phi(r, s)$, defined by

$$\overline{r^n_\Phi}(s) = \int_0^\infty \Phi(r, s)\, r^n r\, dr \Big/ \int_0^\infty \Phi(r, s)\, r\, dr, \tag{2}$$

are assumed to be known. It is easily seen that

$$\overline{r^n_\Phi}(s) = \overline{r^{n+s-1}_\varphi}(s), \tag{3}$$

where $\overline{r^m_\varphi}(r) = \int_0^\infty \varphi(r, s)\, r^m\, dr \Big/ \int_0^\infty \varphi(r, s)\, dr$ is the m-th moment of $\varphi(r, s)$.

We note that in all cases of practical interest it is not possible to obtain an explicit analytic expression for the moments $\overline{r^n_\Phi}(s)$. One can ordinarily obtain numerical values for only the first few moments of the sought distribution function. Therefore for the calculation of $\Phi(r, s)$ from its moments it is more practical to approximate it by using another function whose first few moments coincide with the exact moments of the sought function.

We shall approximate $\varphi(r, s)$ by summing the polynomials $R_n(\alpha r, s)$:

$$\varphi(r, s) = e^{-\alpha r^\beta} \sum_{n=0}^{N} a_n(s)\, R_n(\alpha r, s). \tag{4}$$

The polynomials $R_n(\alpha r, s)$ are orthogonal in the interval $[0, \infty]$ with the weight function $e^{-ar^{\beta}}$. We determine the coefficients $a_n(s)$ from the orthogonality of the polynomials:

$$a_n(s) = \int_0^\infty \varphi(r, s)\, R_n^+(r, s)\, dr \Big/ \int_0^\infty e^{-\alpha r^\beta} R_n(\alpha r, s)\, R_n^+(r, s)\, dr. \tag{5}$$

The coefficients $a_n(s)$ can be expressed in terms of the moments of the sought distribution function. It is reasonable to assume that the n-th coefficient is a linear combination of the first n nonvanishing moments; therefore $R_n^+(r, s)$ (taking (3) into account) can be expressed by the formula

$$R_n^+(r, s) = \sum_{m=0}^{n} c_m(s)\, r^{m+s-1}.$$

It is then easy to write down the conditions which determine $R_n(\alpha r, s)$ and $R_n^+(r, s)$:

$$\int_0^\infty r^{s+{}'kn-1} e^{-\alpha r^\beta} R_n(\alpha r, s)\, dr = \begin{cases} 0 & \text{for } n' < n, \\ \text{const} \neq 0 & \text{for } n' = n\ ; \end{cases} \tag{6a}$$

$$\int_0^\infty e^{-\alpha r^\beta} R_{n'}(\alpha r, s)\, R_n^+(r, s)\, dr = \delta_{n, n'}. \tag{6b}$$

Here $\delta_{n, n'}$ is the Kronecker symbol; k is an integer. The coefficients α and β are determined from the asymptotic behavior of $\varphi(r, s)$ for $r \to \infty$. If the behavior of $\varphi(r, s)$ for $r \to \infty$ is unknown α and β are determined from the equality of the two highest moments of the weight function used in (4) to the corresponding moments of the sought function, that is,

$$\int_0^\infty e^{-\alpha r^\beta} r^k\, dr \Big/ \int_0^\infty e^{-\alpha r^\beta}\, dr = \overline{r^k_\Phi}. \tag{7}$$

We note that when β 1, $k = 1$, $s = 2$ the conditions in (6) define polynomials which coincide with Laguerre polynomials. Placing α equal to the minimum value of the total photon absorption coefficient $\sigma_{\min}(E)$ we find that (4) coincides with the approximate formula used in Reference 2 in calculating the depth and energy dependence of the numbers of electrons and photons for a cascade shower in light and heavy matter. We believe that the proposed method of approximating the functions from their known moments (see Equations (4), (5), (6) and (7)) can be applied successfully to the solution of a broad range of problems. In the present paper we shall use the method to calculate the lateral distribution of particles in an electron-photon shower. It is known (see [3], for example) that the distribution function $N_p(E_0, E, t, r)dt\,dr$, which gives the number of shower electrons of energies greater than E at depth t to t + dt and passing between r and r + dr from the axis* which result from a primary particle of energy E_0, is proportional for $r \to 0$ to

$$N_p(E_0, E, t, r) \sim \frac{1}{r^{2-s}}, \tag{8}$$

---

* The axis of the shower is a linear continuation of the direction of motion of the primary particle which initiates the shower.

where s is the cascade parameter.

We introduce the function $N_p(E, r, s) = N_p(E_0, E, t, r)/N_p(E_0, E, t)$ where $N_p(E_0, E, t)$ is a function which describes the longitudinal development of the shower [4]. It is easily shown that $N_p(E, r, s) = N_p(x, s)$, where $x = Er/E_s$, $E_s = 21$ Mev.

Taking (8) into account we represent $N_p(x, s)$ in the form

$$N_p(x, s) = \frac{1}{x^{2-s}} f(x, s). \tag{9}$$

Using (5), (4) and (6), we shall compute the function $f(x, s)$, assuming that the moments of $N_p(E_0, E, t, r)$ are known. As a result we obtain the following expressions for $R_n(\alpha x, s)$ and $R_n^+(x, s)$:

$$R_0(\alpha x, s) = \frac{\beta}{\varphi_0(s)} \alpha^{s/\beta}; \; R_1(\alpha x, s) = \frac{\beta}{\varphi_1(s)} \alpha^{(s+2)/\beta} [-\Gamma_1 + \varphi_0(s) \alpha^{1/\beta-1} \alpha x]; \tag{10}$$

$$R_2(\alpha x, s) = \frac{\beta}{\varphi_2(s)} \alpha^{(s+4)/\beta}[(\Gamma_1\Gamma_4 - \Gamma_2\Gamma_3) - (\Gamma_0\Gamma_4 - \Gamma_2\Gamma_2)\alpha^{1/\beta-1}\alpha x + \varphi_1(s)\alpha^{2/\beta-2}(\alpha x)^2],$$

$$\text{где } \Gamma_n = \Gamma\left(\frac{s+n}{\beta}\right); \; \varphi_0(s) = \Gamma_0; \; \varphi_1(s) = \Gamma_0\Gamma_3 - \Gamma_1\Gamma_2; \; \varphi_2(s) = \Gamma_0(\Gamma_3\Gamma_6 - \Gamma_4\Gamma_5) -$$

$$- \Gamma_2(\Gamma_1\Gamma_6 - \Gamma_2\Gamma_5) + \Gamma_4(\Gamma_1\Gamma_4 - \Gamma_2\Gamma_3);$$

$$R_0^+(x, s) = x^{s-1}; \quad R_1^+(x, s) = -\frac{\Gamma_2}{\varphi_0(s)} \alpha^{-2/\beta} x^{s-1} + x^{s+1};$$

$$R_2^+(x, s) = \frac{1}{\varphi_1(s)}(\Gamma_5\Gamma_2 - \Gamma_3\Gamma_4)\alpha^{-4/\beta}x^{s-1} + \frac{1}{\varphi_1(s)}(\Gamma_1\Gamma_4 - \Gamma_0\Gamma_5)\alpha^{-2/\beta}x^{s+1} + x^{s+3}. \tag{11}$$

Using (5), (10) and (11) we obtain expressions for $a_n(s)$:

$$a_0(s) = 1; \; a_1(s) = -\frac{\Gamma_2\alpha^{-2/\beta}}{\varphi_0(s)} + \overline{r^2};$$

$$a_2(s) = \frac{\Gamma_5\Gamma_2 - \Gamma_3\Gamma_4}{\varphi_1(s)} \alpha^{-4/\beta} - \frac{\Gamma_1\Gamma_4 - \Gamma_0\Gamma_5}{\varphi_1(s)} \alpha^{-2/\beta}\overline{r^2} + \overline{r^4}, \ldots \tag{12}$$

The coefficients α and β were determined from (7); for β the value ~ 0.5 was obtained. In Reference 5 it was shown that when $r \to \infty$ we have $N_p(E_0, E, r, t) \sim e^{-\alpha\sqrt{x}}$; therefore in the numerical computations we assumed $\beta = 0.5$ while α was determined from (7). N in (4) was assumed to be equal to n /2, where n is the index of the highest moment in the expansion.

By a method similar to that utilized in (6) we obtained algebraic recurrence relations for the calculation of the n angular and lateral moments of the particle distribution function without allowing for ionization losses. From these formulas we obtained numerical values of $\overline{r^2}$, $\overline{r^4}$ and $\overline{r^6}$ for the lateral distribution function of electrons with the cascade parameter s varying from 0.4 to 2.0;* we used these values in our computations from (4).

The values of the spatial distribution function $x^{2-s} N_p(x, s)$** are given in Table 1. The values of $N_p(x, s)$ were obtained by using $\overline{r^2}$, $\overline{r^4}$ and $\overline{r^6}$.

---

* We note that our calculated values of $\overline{\theta^2}$, $\overline{\theta r}$ and $\overline{r^2}$ for s from 1.1 to 1.9 differ by a few percent from the values obtained by Borsellino [7].

** $N_p(x, s)$ was normalized as follows: $\int_0^\infty N_p(x, s)\, x\, dx = 1.$

TABLE 1

x \ s	0,4	0,6	0,8	1,1	1,3	1,5	1,7	1,9
0	1.72	4.04	7.34	$1.21\cdot10^{1}$	$1.38\cdot10^{1}$	$1.36\cdot10^{1}$	$1.21\cdot10^{1}$	9.87
0.0001	1.59	3.79	6.96	1.16	1.33	1.32	1.17	9.58
0.0002	1.55	3.70	6.82	1.14	1.31	1.30	1.16	9,46
0.0005	1.46	3.52	6.52	1.10	1.27	1.26	1.13	9.23
0.001	1.37	3.33	6.21	1.06	1.22	1,22	1.09	8.98
0.002	1.25	3.08	5.80	1.00	1.16	1.16	1.05	8.62
0.005	1.06	2.64	5.08	8.93	1.05	1.06	9.62	7.97
0.01	$8.94\cdot10^{-1}$	2.24	4.36	7.87	9.35	9.56	8.73	7.29
0.015	7.91	1.98	3.89	7,13	8.56	8.82	8.12	6.81
0.02	7.17	1.80	3.53	6,56	7.93	8.25	7.62	6.43
0,04	5.42	1.32	2.63	5,08	6.28	6,68	6,28	5.36
0.06	4.43	1.08	2.10	4.16	5.24	5.67	5.41	4.67
0.1	3.24	$7.48\cdot10^{-1}$	1.48	3.04	3.93	4.37	4,23	3.74
0.15	2.36	5.39	1.04	2.21	2.94	3.36	3.34	2.99
0.2	1.79	4.09	$7.87\cdot10^{-1}$	1.69	2.31	2.69	2.72	2.47
0.6	$3.20.10^{-2}$	$9.26\cdot10^{-2}$	1.55	$3.81\cdot10^{-1}$	$6.05\cdot10^{-1}$	$7.65\cdot10^{-1}$	$8.65\cdot10^{-1}$	$8.57\cdot10^{-1}$
1.0	$6.55\cdot10^{-3}$	2.79	$5,75\cdot10^{-2}$	1.33	2.16	3.10	3.80	4.03
1.5	1.88	$8.18\cdot10^{-3}$	1.94	$4.59\cdot10^{-2}$	$7.71\cdot10^{-2}$	1.22	1.56	1.84
2.0	$5.08\cdot10^{-4}$	2.71	$7.52\cdot10^{-3}$	1.85	3.21	$5.39\cdot10^{-2}$	$7.76\cdot10^{-2}$	$9.44\cdot10^{-2}$
2.5	1.54	$9.73\cdot10^{-4}$	3.17	$8.29\cdot10^{-3}$	1.41	2.55	3.95	5.12
3.0	$5.12\cdot10^{-5}$	3.67	1.42	4.00	$6.80\cdot10^{-3}$	1.27	2.10	2.90
3.5	1.85	1.46	$6.61\cdot10^{-4}$	2.04	3.32	$6.50\cdot10^{-3}$	1.15	1.73
4.0	$7.19\cdot10^{-6}$	$5.81\cdot10^{-5}$	3.16	1.11	1.75	3.40	$6.44\cdot10^{-3}$	1.01
4.5	3.03	2.37	1.54	$6.30\cdot10^{-4}$	$9.23\cdot10^{-4}$	1.81	3,65	$6.14\cdot10^{-3}$
5.0	1.38	1.01	$7.59\cdot10^{-5}$	3.72	5.26	$9.79\cdot10^{-4}$	2.08	3.77
5.5	$6.81\cdot10^{-7}$	$4.42\cdot10^{-6}$	3.76	2.28	3.04	5.25	1.19	2.33
6.0	3.59	2.08	1.86	1.45	1.92	2.87	$6.74\cdot10^{-4}$	1.45

The series of moments of (4) defines a function of which only the first few moments coincide with the exact moments, the higher moments being different from the exact moments. But in consideration of the fact that the asymptotic behavior of (4) coincides with the asymptotic behavior of the exact function for $x \rightarrow \infty$, it can be expected that the higher moments of (4) will not differ appreciably from the exact moments and that (4) differs from the exact function by not more than a few percent over a broad range of values of $\underline{x}$. Using $N_p(x, s)$ as calculated from the 3 even moments we have calculated $\overline{r^8}$ and $\overline{r^{10}}$ for $s = 1$; the numerical values of $\overline{r^8}$ and $\overline{r^{10}}$ agree with the exact values within 10%. It is reasonable to assume that the values for $\overline{r^n}$ are mainly determined by some finite interval of values of $\underline{x}$ depending on $\underline{n}$. Therefore by comparing the values of $N_p(x, s)$ constructed from 2 or 3 of the first even moments of the function, for example, we can determine the limits of applicability of the approximation (4) with respect to $\underline{x}$. An investigation shows that even when only the first 2 moments are used (4) enables us to calculate $N_p(x, s)$ in the range of $\underline{s}$ from ~ 0.4 to ~ 2 and of $\underline{x}$ from 0 to ~ 6 with an error not exceeding 10%.

In Reference [6], $N_p(x, s)$ was constructed from moments for $s = 0.6$; 1; 1.5 by obtaining graphically a function whose first few moments agree with the exact moments. In constructing $N_p(x, s)$, Eyges and Fernbach made essential use of Moliere's exact calculation of the lateral distribution for small $\underline{x}$ and $s = 1$. In Reference 1 the comparison of the $N_p(x, s)$ which were obtained in Reference 6 with our calculations for $s = 1$ showed that the functions agree within 10%. In constructing $N_p(x, s)$ for $s = 0.6$ and 1.5 it was assumed in Reference 6 that the behavior of $N_p(x, s)$ for $x \rightarrow 0$ differs little from the behavior for $x \rightarrow 0$ and $s = 1$, and it was also considered that the character of the singularity for $x \rightarrow 0$ and the given value of $\underline{s}$ does not affect the behavior of the function for $x > 0.2$-0.4.

A comparison of the values of $N_p(x, s)$ with $s = 0.6$ and 1.5 in Reference 6 and those calculated from Equation (4) shows that they differ by a factor of about 2. The functions constructed from (4) for $s = 0.6$ and 1.5 on the assumption that $N_p(x, s) \sim 1/x$ are in much better agreement with the functions obtained in Reference 6.

The authors wish to express their gratitude to N. S. Strunina for assistance with the numerical calculations.

M. V. Lomonosov Moscow State University Received April 2, 1957.

LITERATURE CITED

[1] V. V. Guzhavin and I. P. Ivanenko, Doklady Akad. Nauk SSSR 113, 3, 533 (1957).*

[2] I. P. Ivanenko, J. Exptl.-Theoret. Phys. (USSR) 31, 86 (1956);** Doklady Akad. Nauk SSSR 107, 819 (1956). [Soviet Physics – Doklady, p. 231].

[3] I. Ia. Pomeranchuk, J. Exptl.-Theoret. Phys. (USSR) 14, 1252 (1944); A. B. Migdal, J. Exptl.-Theoret. Phys. (USSR) 15, 313 (1945).

[4] S. Z. Belen'kii, Cascade Processes in Cosmic Rays [In Russian] 1948.

[5] B. A. Chartres and H. Messel, Proc. Phys. Soc. A 67, 158 (1954).

[6] L. Eyges, Phys. Rev. 82, 23 (1951); L. Eyges, and S. Fernbach, Phys. Rev. 82, 288 (1951).

[7] A. Borsellino, Nuovo Cim. 7, 323 (1950).

[8] G. Moliere, Cosmic Radiation, (N. Y., 1946).

---

*[See Soviet Physics – Doklady, p. 131].

**[See Soviet Physics – JETP, p. 55].

ON THE INTERACTION OF HIGH-ENERGY PARTICLES WITH NUCLEI

A. P. Zhdanov, I. B. Berkovich, K. I. Ermakova, F. G. Lepekhin,
N. V. Skirda and Z. S. Khokhlova

(Presented by Academician A. F. Ioffe April 4, 1957)

At the present time we have no theory which satisfactorily describes the mechanism of the production of elementary particles in nucleon-nucleus interactions at 10^{11}-10^{13} ev. The experimental investigation of such interactions is therefore of great importance. In this paper we present preliminary results of an analysis of seven jets containing a relatively large number of shower particles that were produced through interactions of nucleons with emulsion nuclei.

After scanning part of a stack of Ilford G-5 emulsions irradiated for 7 hours at about 30 km we selected jets that were initiated by neutral and charged particles. From the analysis of these cases we obtained very reliable data only about the number of shower particles and their angular distribution. The angles between the direction of motion of the primary particle and the tracks of the secondary particles were measured with an MBI-8 microscope by the coordinate method [1]. The characteristics of these disintegrations are shown in Table 1.

TABLE 1

Characteristics of the Disintegrations*

No. cases	n_λ	N_Γ	Z_{init}	$\theta_{1/2}$ in radians	φ in deg.	l μ	Type
1	28	8	0	$1.9 \cdot 10^{-2}$	14	760	1
2	18	10	$\leqslant 2$	$3.2 \cdot 10^{-2}$	6	500	1
3	27	9	0	$3.4 \cdot 10^{-2}$	13	900	1
4	46	16	$\leqslant 2$	0.13	4	1000	2
5	52	37	$\leqslant 2$	0.23	3	320	2
6	46	9	0	0.20	8	130	2
7	17	27	$\leqslant 2$	0.155	17	100	3

---

*Notation: n_λ is the number of shower particle tracks; N_Γ is the number of black and gray tracks; Z_{init} is the suggested charge of primary particle; $\theta_{1/2}$ is the angle containing half of the shower particle tracks; φ is the angle of inclination of shower axis to the plane of the emulsion; l is the distance from beginning of shower to point where measurements were made.

As a graphic representation of the angular distribution of shower particles in a jet we have plotted $\frac{1}{N}\int\limits_0^\theta N(\theta)d\theta$ against θ in radians in the laboratory system. The jets were divided into three types. Jets of type I are characterized by a tight cone and a symmetrical integral representation (Fig. 1). Type II (Fig. 2) contains jets with a much larger cone and a larger number of charged particles. Each curve of this type divides clearly into two parts one of which is similar to the curves of Figure 1 while the other is not symmetrical. Figure 3 represents the angular distribution of shower particles for a jet which shows no symmetry even at small angles.

Any theoretical examination of the mechanism of elementary particle production [2, 3] is based on the symmetrical ejection of the produced particles in the center-of-mass system. As was shown in Reference 4 such a distribution in the center-of-mass system can be obtained when the integral angular distribution in the laboratory system possesses a certain kind of symmetry. In such cases the curve possesses a point with respect to which the following relation is satisfied:

$$\ln\theta_f = -\ln\theta_{1-f}.$$

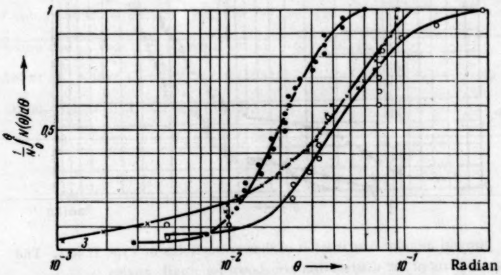

Fig. 1. Integral angular distribution of shower particles in jets of Type I (laboratory system).

In three cases which are shown in Figure 1 such symmetry is observed experimentally. The point of symmetry corresponds approximately to the angle which includes half of the observed shower particles. Thus we can apply to these cases the basic propositions of the Fermi-Landau theory; we can calculate the energy of the primary particle, determine the multiplicity and construct the angular distribution in the center-of-mass system. The calculated primary particle energies and the multiplicities (Table 2) are in good agreement with theory [3]. With the exception of jet 3 (Fig. 4) the angular distribution in the center-of-mass system was isotropic. This disagrees with the predictions of Landau's theory but agrees with other experimental data [5-7].

TABLE 2

Primary Particle Energy and Multiplicity for Jets of Types I and II

No. cases	F_{lab} from $\theta_{1/2}$, in ev	$k = N_{exp}\gamma^{-1/4} A^{-0.19}$	F_{lab} from symmetrical part of curve, in ev	k from symmetrical part of curve
1	$5.2\cdot10^{12}$	1.4	$5.2\cdot10^{12}$	1.4
2	$1.8\cdot10^{12}$	1.2	$1.8\cdot10^{12}$	1.2
3	$1.6\cdot10^{12}$	2.4	$1.6\cdot10^{12}$	2.4
4	$1\cdot10^{11}$	7	$1\cdot10^{13}$	2.0
5	$4\cdot10^{10}$	5	$1\cdot10^{12}$	3.6
6	$4\cdot10^{10}$	4	$2\cdot10^{12}$	2.9

The next three cases are characterized by a wide cone. The energy which is calculated from the angle $\theta_{1/2}$ is small and does not agree with the rough estimate of the energy threshold from the total number of particles. The multiplicity is large (Table 2). The experimental value of the multiplicity cannot be considered too high because the contribution of electron-positron pairs can be neglected, as the distance at which angles were measured was considerably smaller than the radiation length unit in the emulsion. As was indicated above, all three curves are divided into two parts. This is evidence of a more complex angular distribution of shower particles from nucleon-nucleus interactions than is predicted by the theory [3]. It is evident that the primary particle energy can be evaluated by a more valid kinematic method if only the symmetrical parts of the curves are used, because it follows from both theory and experimental findings [8] that most of the energy of the primary particle is carried off by shower particles in a very narrow cone. However, when the primary particle energies obtained in this manner are used to compute the multiplicity the values (Table 2) are somewhat greater than those usually assumed: k = 1.2-2.3. This fact and the observed angular distribution in Type II jets can be interpreted as evidence that when shower particles interact with nuclear matter they are not only scattered but produce new particles. It is clear that the production mechanism in jets of this type is more complicated than the multiple production mechanism.

In the last case the angular distribution of the shower particles appears to us to be even more complicated, as they can be seen to form two cones. There is small probability of the observation of this effect from the

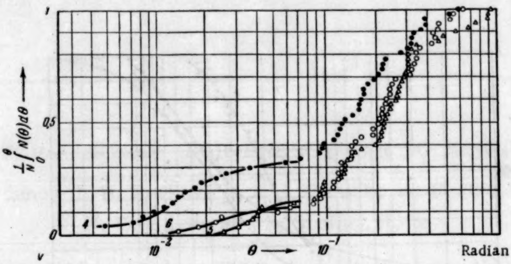

Fig. 2. Integral angular distribution of shower particles in Type II jets. The symmetrical parts of the distribution are shown for small angles.

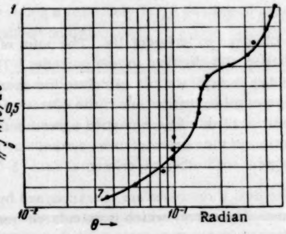

Fig. 3. Integral angular distribution of shower particles in case 7 of Table 1.

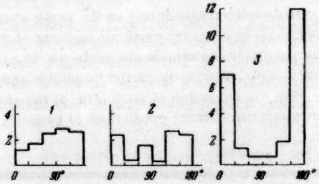

Fig. 4. Angular distribution of shower particles in the center-of-mass system for disintegration cases 1, 2 and 3 of Table 1.

collision of a nucleon with even a heavy nucleus at 10^{13} ev and higher. The kinematic method cannot be applied to this case for determination of the primary particle energy, but a rough estimate can be obtained from consideration of the constriction of the jet with increasing primary energy. By using this criterion it was possible to establish that the primary particle energy in Case 7 was lower than in Cases 1-3 of Table 1. The primary energy, angular distribution and number of particles produced show that the theory of multiple production of elementary particles cannot explain this case. In the last four cases the number of shower particles and their angular distribution could be explained by multiple-plural production. Additional experimental data will make it possible to obtain a more definite idea of the production mechanism of elementary particles in nucleon-nucleus interactions at high energies.

V. G. Khlopin Radium Institute,
Academy of Sciences USSR

Received March 26, 1957.

LITERATURE CITED

[1] P. A. Zhdanov, I. B. Berkovich, F. G. Lepekhin, N. V. Skirda and Z. S. Khokhlova, Experimental Instruments and Techniques, No. 4, [In Russian] (1957).

[2] E. Fermi, Uspekhi Fiz. Nauk 46, 71 (1952) [Russian translation].

[3] S. Z. Belen'kii and L. D. Landau, Uspekhi Fiz. Nauk 61, 3 (1955).

[4] M. F. Kaplon and D. M. Ritson, Phys. Rev. 88, 386 (1952).

[5] G. Bertolino and D. Pescetti, Nuovo Cim. 12, No. 5 (1954).

[6] A. Engler et al., Nuovo Cim. 12, No. 6 (1954).

[7] G. Bertolino, Nuovo Cim. 3, No. 1 (1956).

[8] M. Schein et al., Nuovo Cim. 1, No. 3 (1955).

ON A METHOD OF CALCULATING QUANTUM DISTRIBUTION FUNCTIONS

R. L. Stratonovich

(Presented by Academician N.N. Bogoliubov, April 10, 1957)

Systematic methods of calculating quantum distribution functions for thermodynamic equilibrium must use the well-developed methods and concepts of quantum field theory because in both instances we are concerned with the quantum theory of many particles. In Ref. [5] the methods of field theory were applied to the calculation of the free energy of interacting particles. In the present paper we shall derive relations for distribution functions in a form which resembles the results obtained by the theory of propagation functions.

We shall limit ourselves to a single-component model of a non-relativistic Bose gas, although the method can, of course, be extended to other cases. The Hamiltonian of the system is given by

$$H = \int \left[\psi^*(x')\, T_{x'x} \psi(x) + \frac{1}{2} \psi^*(x') \psi(x') \Phi(x' - x) \psi^*(x) \psi(x) \right] dx'\, dx \equiv$$
$$\equiv \psi^* T \psi + \frac{1}{2} n \Phi n. \qquad (1)$$

The right-hand side is the abbreviated notation which we shall use hereinafter: $n(x) = \psi^*(x)\psi(x)$; $T = p^2/2m \equiv T_p$; $\Phi(x' - x) = \Phi(x - x')$ is the interaction potential; $\psi(x)$ is the second-quantized wave function in three-dimensional space which satisfies the commutation rules

$$[\psi, \psi] = 0, \quad [\psi^*, \psi^*] = 0, \quad [\psi, \psi^*] = 1$$

that is, $\psi(x)\psi^*(x') - \psi^*(x')\psi(x) = \delta(x - x')$.

The quantum distribution functions $f_r(x_1, x'_1; \ldots; x_r, x'_r)$ are functional derivatives at the point $v = 0$ of the generating functional

$$L[v] = \left\langle N \exp \int \psi^*(x')\, v_{x'x} \psi(x)\, dx'\, dx \right\rangle \equiv \left\langle N e^{\psi^* v \psi} \right\rangle, \qquad (2)$$

where N is Wick's symbol for the normal product.

The Functional (2) is a quantum generalization [4] of the classical generating functional [2, 3]. Wigner's transformation can take us from x, x' in (2) to the phase coordinates x, p. By setting $v_{xx'} = v_x \delta(x - x')$ the investigation will be confined to distribution functions in the x-configuration space.

Using the operator identity

$$\exp \psi^* u \psi = N \exp \psi^* (e^u - 1) \psi, \qquad (3)$$

which holds true under the above-indicated commutation rules for ψ and ψ^*, we can transform (2) to the form

$$L[v] = \mathrm{Tr}\, \{R \exp [\psi^* \ln (v + 1) \psi]\}. \qquad (4)$$

Here ln(v + 1) must be understood as an operator which is an analytic function of the operator v. The state operator R for thermodynamic equilibrium at temperature $kT = 1/\lambda$ and with uniform mean spatial particle density n_0 is

$$R = \exp(\lambda\Psi - \lambda H + \mu\psi^*\psi). \tag{5}$$

In our abbreviated notation $\psi^*\psi = \int \psi^*\psi\,dx$ is the operator of the total number of particles: $\Psi = \int \varphi\,dx$ is the free energy (φ is its density); μ/λ signifies the chemical potential. The magnitudes of φ and μ are determined from the conditions

$$\operatorname{Tr} R = 1; \quad \lambda\frac{\partial\varphi}{\partial\mu} = -n_0 \tag{6}$$

where the latter is equivalent to $\langle n\rangle = n_0$.

When the operator $e^{-\lambda H}$, using Feynman's ordering subscript $\underline{s}$ [1], is written as

$$\exp\left\{-\lambda\psi^*T\psi - \frac{\lambda}{2}n\Phi n\right\} = \exp\left\{-\int_0^\lambda \left[(\psi^*T\psi)_s + \frac{1}{2}(n\Phi n)_s\right]ds\right\}, \tag{7}$$

we need not attend to the order in which the operator is written because the order in which it acts is completely determined by the values of $\underline{s}$.

We now transform the interaction term in (7). For this purpose we introduce $\xi_s(x)$, a Gaussian random function of $\underline{x}$ and $\underline{s}$, with the correlation function

$$M\xi_{s_1}(x_1)\,\xi_{s_2}(x_2) = \Phi(x_1 - x_2)\,\delta(s_1 - s_2) \tag{8}$$

and zero average value $M\xi_s(x) = 0$. Here M denotes statistical averaging over the ensemble of realizations of the random function. From the familiar rules for writing the characteristic function of a Gaussian random process we obtain

$$\exp\left\{-\frac{1}{2}\int_0^\lambda ds \iint n_s(x')\,\Phi(x' - x)\,n_s(x)\,dx'\,dx\right\} = M\exp\left\{i\int_0^\lambda ds \int \xi_s(x)\,n_s(x)\,dx\right\}. \tag{9}$$

Keeping (4), (5), (7) and (9) in mind we have

$$L[v] = e^{\lambda\Psi} M \operatorname{Tr}\exp\left\{(\psi^*\ln(1+v)\,\psi)_0 + \mu\psi^*\psi - \int_0^\lambda (\psi^*T\psi)_s\,ds + i\int_0^\lambda (\psi^*\xi_s\psi)_s\,ds\right\}. \tag{10}$$

Thus, by means of a continuous Fourier transformation the problem is reduced to the investigation of non-interacting particles in a fluctuating external field. The symbol M enables us to avoid writing out the implied continuous transformation with the weight $\text{const}\cdot\exp\left\{-\int \xi_s\Phi^{-1}\xi_s\frac{ds}{2}\right\}$.

Calculation of the trace with respect to ψ^*, ψ yields the result

$$L[v] = e^{\lambda\Psi} M\exp\{-\operatorname{Tr}\ln|1 - K - vK|\}, \tag{11}$$

where $K = \exp\left[\mu - \int_0^\lambda T_s\,ds + i\int_0^\lambda \xi_s\,ds\right]$, and Tr refers to the operators $\underline{v}$, T, ξ_s.

Expanding the functional (11) with respect to $\underline{v}$, we obtain

$$\lambda\Psi = -\ln f^{(0)}; \quad f_1(x, x') = \frac{f^{(1)}_{xx'}}{f^{(0)}}; \quad f_2(x, x'; y, y') = \frac{f^{(2)}_{xx'yy'} + f^{(2)}_{xy'yx'}}{f^{(0)}}; \ldots \tag{12}$$

$$f^{(r)}_{x_1x_1'\dots x_rx_r'} = M\exp\{-\mathrm{Tr}\ln|1-K|\}\left(\frac{K}{1-K}\right)_{x_1x_1'}\cdots\left(\frac{K}{1-K}\right)_{x_rx_r'}. \tag{13}$$

In the absence of an interaction K becomes $K_0 = e^{\mu-\lambda T}$, and $f^{(r)}$ becomes the corresponding ideal gas function which we shall denote by $f^{0(r)}$. We shall examine the departure of $f^{(r)}$ from ideal values as a result of interactions. The functions $F^{(r)}$ describe this departure as follows:

$$f^{(0)} = f^{0(0)}F^{(0)}; \quad \frac{f^{(1)}}{f^{(0)}} = \frac{f^{0\,(1)}}{f^{0\,(0)}} + \frac{F^{(1)}}{F^{(0)}};$$

$$\frac{f^{(2)}_{xx'yy'}}{f^{(0)}} = \frac{f^{0\,(2)}_{xx'yy'}}{f^{0\,(0)}} + \frac{f^{0\,(1)}_{xx'}}{f^{0\,(0)}}\frac{F^{(1)}_{yy'}}{F^{(0)}} + \frac{F^{(1)}_{xx'}}{F^{(0)}}\frac{f^{0\,(1)}_{yy'}}{f^{0\,(0)}} + \frac{F^{(2)}_{xx'yy'}}{F^{(0)}};\ \dots \tag{14}$$

It follows from (11) and (12) that the functions defined in this way can be represented by the sum

$$\mathrm{Tr}\,[F^{(r)}v_1\dots v_r] = M\sum_{j=0}^{\infty}\ \sum_{m_1,\dots,m_{j+r}=1}^{\infty}\frac{1}{m_1\dots m_j}\mathrm{Tr}\,[(kB)^{m_1}]\dots$$

$$\dots\mathrm{Tr}\,[(kB)^{m_j}]\,\mathrm{Tr}\,[v_1B(kB)^{m_{j+1}}]\dots\mathrm{Tr}\,[v_rB\,(kB)^{m_{j+r}}], \tag{15}$$

where $k = K - K_0$; $B = (1 - K_0)^{-1}$; $r = 0, 1, 2, \dots$

Each term of this sum corresponds to a diagram with j closed loops and r unclosed lines. On each line there are m_α k-vertices. A line segment which connects two vertices or goes from a vertex to the edge of the diagram corresponds to the operator B, which in the momentum representation becomes $\left(1 - e^{\mu-\lambda T}\right)^{-1} = f_0(p) + 1$. Before averaging M the vertex which lies between the segments with momenta p and p' corresponds to the operator

$$k_{p'p} = ie^{\mu}\int_0^{\lambda} ds\exp\{(s-\lambda)T_{p'} - sT_p\}\,\xi_{sp'p} +$$

$$+ i^2e^{2\mu}\int_0^{\lambda} ds\int_0^{s} dt\int\exp\{(s-\lambda)T_{p'} + (t-s)T_q - tT_p\}\,\xi_{sp'q}\,\xi_{tqp}\,dq + \dots \tag{16}$$

It is known that the moments of the Gaussian random function can be expressed in terms of the correlation function. This means that in averaging M all operators ξ are paired in all possible ways; in the diagram such connections of vertices are indicated by dashed interaction lines. In the momentum representation (8) becomes

$$M\xi_{sp'p}\,\xi_{tk'k} = \delta(p' + k' - p - k)\,\nu(p' - p)\,\delta(s - t);$$
$$\left((\nu(\varkappa) = (2\pi)^{-3}\int e^{i\varkappa z}\Phi(z)\,dz\right). \tag{17}$$

Therefore each interaction line corresponds to $\nu(\kappa)$ and can be interpreted as the exchange of an interaction quantum with conservation of momentum.

The number of interaction lines in a diagram determines the order of the given term according to the power of the square of the interaction constant, or the power of the interaction potential Φ. Calculation of the terms corresponding to diagrams of given order enables us to obtain the exact terms of the expansion of the distribution function as a power series in Φ.

The first correction resulting from interaction is linear in ν and is described by diagrams containing only one interaction line. In Figure 1 diagrams a, b and c are all the possible diagrams that describe the first correction to $F^{(0)}$, which is given by the sum in (15) with $r = 0$. Diagrams b and c can be eliminated by consideration

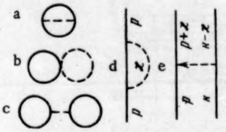

Fig. 1.

of the normalization of the chemical potential. The b term is proportional to $\int \nu(\kappa)d\kappa = \Phi(0)$ and describes the self-stress of a particle. The c term is proportional to $\nu(0)$ and describes the average thrust of the gas as a whole. Nonvanishing $\Phi(0)$ and $\nu(0)$ can be eliminated from $\Phi(x)$ if we replace them with an additional uniform external potential $\Phi(0) + \int \Phi n_0 dx$, and include the latter in the chemical potential by the substitution $\mu/\lambda - \Phi(0) - \Phi n_0 dx \rightarrow \mu/\lambda$. Therefore, in calculating the first correction one need keep in mind only the a diagram for $F^{(0)}$ and only d and e for $F^{(1)}$ and $F^{(2)}$, respectively. When (16) is inserted in (15) in this approximation it is sufficient to take into account only the first term. After averaging, by virtue of (17), we have

$$F^{(1)}_{p'p} = -\delta(p'-p)\lambda f_0(p)\,[f_0(p)+1]\int f_0(p+\varkappa)\,\nu(\varkappa)\,d\varkappa; \qquad (18)$$

$$F^{(2)}_{p'pk'k} = -\delta(p'+k'-p-k)\,\nu(p'-p)\,f_0(p')\,f_0(k')\,f_0(p)\,f_0(k)\times$$
$$\times\frac{e^{\lambda T_{p'}+\lambda T_{k'}}-e^{\lambda T_p+\lambda T_k}}{T_{p'}+T_{k'}-T_p-T_k}\,e^{-2\mu}. \qquad (19)$$

The function which is the cofactor of $\delta(p'-p)$ in (18) is the correction to the unperturbed momentum distribution $f_0(p)$.

In our diagrams only a few interaction lines can start at a single vertex. In this they differ from the diagrams of Ref. [5] and result from the breaking-up of the latter. Thus, the diagram in Ref. [5] which looks like a of Figure 1 is nothing but the sum of our diagrams a and b.

LITERATURE CITED

[1] R.P. Feynman, Phys. Rev. 84, 108 (1951).

[2] N.N. Bogoliubov, Problems of Dynamical Theory and Statistical Physics (Moscow-Leningrad, 1946) [In Russian].

[3] P.I. Kuznetsov and R.L. Stratonovich, Bull. Acad. Sci. USSR, Math. Ser. 20, 167 (1956).

[4] R.L. Stratonovich, J. Exptl.-Theoret. Phys. (USSR) 31, 1012 (1956).•

[5] T. Matsubara, Progr. Theoret. Phys. 14, 351 (1955).

Received April 9, 1957

M.V. Lomonosov Moscow State University

•[Soviet Physics – JETP, p. 891.]

ON THE CHANGE OF ELECTRICAL RESISTIVITY IN ELEMENTARY DISLOCATION GENERATION

E. D. Shchukin, V. N. Rozhanskii and Iu. V. Goriunov

(Presented by Academician P.A. Rebinder, April 12, 1957)

During the stretching of zinc single crystals the ratio between the increase of electric resistance and the elongation, $\delta R/\delta l$, for discontinuous deformations of ~ 0.5-20μ is smaller than the analogous ratio $\frac{R - R_0}{l - l_0}$ of the total increase of resistance to the total elongation of the specimen. It has been suggested that this lower value is associated with the appearance of dislocation avalanches at various points in the single crystal [1]. Of most interest, however, are similar measurements for "elementary" dislocations of ~500-2000A localized in a single slip zone. For this purpose the resolving power of the channel for recording deformations was reduced to 50A and for the recording of resistance jumps to $(3$-$5) \cdot 10^{-9}$ ohms [2].

The experiments were performed on single crystals of cadmium (of 0.75 mm diameter) and of zinc (of 0.5 mm diameter), 15-20 mm long, at room temperature with the initial angle 30° between the hexagonal axis and the direction of stretching. Stretching occurred under a constant load to 3-5% elongation at an average rate of $(0.03$-$0.6) \cdot 10^{-4}$ cm/sec. 1% stretching was ordinarily observed at intervals of 1 to 2 hours. Before and after stretching the cross sections of the specimens were measured within 1%. The total increase of resistance that was calculated from these data agreed with the measurement of $R - R_0$ by a precision potentiometer; thus for such small and slow deformations the total increase of resistance was not measurably higher than the result from the geometry.

It is easily shown that for a small deformation jump located in the cross section where the deformation has reached ϵ the geometrical increase of resistance is given by $\delta R \approx \delta l \cdot 2r_0 \cdot (1 + \epsilon)$, where r_0 is the resistance of unit length of the undeformed specimens.* If the entire resistance increase in jumps had purely geometrical causes the experimental values of $q = \frac{\delta R}{\delta l \cdot 2r_0} \cdot 100$ should lie in the interval from 100% to $100\% + \epsilon_{\max}$.**

Figure 1 contains the results of careful measurements of about 300 of our oscillograms of jumps of $\delta l =$ $= 350$A and greater lasting 1 to 30 millisec in single crystals of cadmium and zinc. The dot-dash lines bound this band, because from 150 to 350A, although the jumps are fully distinguishable in the oscillograms they could not usually be measured with sufficient accuracy.

Our data show that the band of actual values of q (indicated by the solid lines in Figure 1) is S-shaped with a bend in the region of $\delta l \approx 500$-1000A and with an overall reduction up to 30% compared with the geometrical values for $\delta l > 1000$A; for the given orientations this corresponds to a shift of ~500 interatomic distances in the slip direction, that is, 500 **b**, where **b** is Burger's vector. In other words, the large jumps, which are dislocations which exceed a certain critical value, are associated with a restoration of order and reduction of structural defects in the slip zone, while for small jumps of $\delta l < 500$A this is not observed or the reverse effect occurs.

Of special interest are paired jumps separated by 40-80 millisec. In such cases q for the second jump very frequently shows a sharp reduction compared with the average values (Figure 2, second jumps). Points represent-

---

*For cadmium, which possesses intrinsic anisotropy of electrical resistance, an additional small correction must be made here to allow for the change of orientation.

**Local deformations in our case reached $\epsilon_{\max} = 30$-40% for cadmium and 40-45% for zinc specimens.

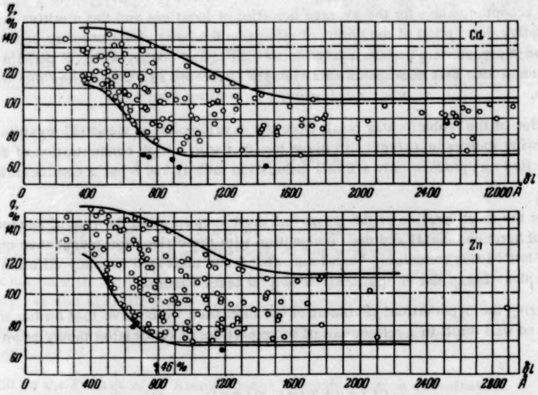

Fig. 1. Experimental values of q for discontinuous deformations in cadmium and zinc single crystals.

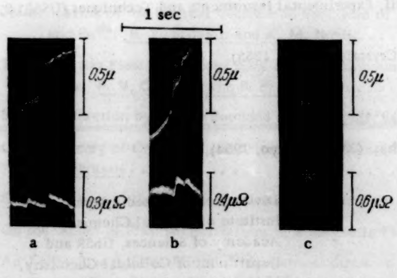

Fig. 2. Oscillograms of paired jumps with considerable reduction of q for the second jump in single crystals of a) cadmium, b) zinc and c) tin.

ing some jumps of this type are indicated separately in Figure 1.

This effect can be explained as follows. A jump of ~500 **b** corresponds to a small avalanche of dislocations which can accumulate in the region of a single slip plane accompanied by the greatest possible disorder for such a cluster, which in turn determines considerable electron scattering. During a jump a rapid discharge of this cluster takes place, lasting a few milliseconds. In the region of this slip plane the normal structure is largely restored and the added dislocation resistance disappears. A jump of ~500 **b** must evidently be regarded as the maximum elementary jump. Large jumps > 1000 **b** can be regarded as the discharge of prepared avalanches in several slip zones immediately following a single elementary "initiating" jump. The observed reduction of δR compared with the geometrical value is then composed additively of the reductions in individual zones; therefore for large δl the values of q form a horizontal band (Figure 1).

For elementary jumps which are smaller than the maximum the associated variation of the electron scattering cross section declines with greater than linear rapidity, resulting in the bend of the q-band. Such jumps correspond to the discharge of a cluster which is smaller than the maximum possible in a single zone or to the incomplete discharge of a maximum cluster. The explanation of the shape of the q-band requires a nonlinear relation between the cross section σ for scattering of electrons by the cluster and the number n of dislocations, such as $\sigma = An^k$; in the first case $k \approx 2$, in the second case $k \approx 1/2$. The considerable reduction of q for second jumps must be treated differently in the two cases. The first of the mechanisms mentioned seems more likely.

A certain rise of the q-band above the geometrical values for the very smallest jumps can only be associated with an entirely different process – the sudden activation of dislocation sources functioning according to the Frank-Read scheme, for example, and the resulting further disordering of structure in the slip zone. But this rise lies almost at the limit of accuracy of our experiments and requires further experimental confirmation.

The currently accepted values for the average densities of locations and the resulting resistances [3, 4] do not permit a quantitative description of the observed effects on the basis of the ordinary concepts of dislocation theory. The observed decreases of $\underline{q}$ require a large local dislocation density which is perhaps caused by some new type of dislocation source that corresponds to a strongly disordered slip zone before the jump and its restoration during the jump.

A partial solution of the problem may result from the development of views [5] regarding the preparation of an avalanche by many sources in a single slip plane together with a high concentration of dislocations in this plane; their annihilation can produce only a small dislocation such as 500 **b** but a considerable reduction of the jump δR.

Finally, despite the short duration of the jumps one must keep in mind the role of vacancies in the increase of resistance of hardened metal and their connection with the dislocation mechanism of deformation. It is also possible that Mott's ideas concerning "local annealing" and increased vacancy diffusion in the slip zone [6] will lead to an explanation of the sharp reduction of $\underline{q}$ for second jumps.

While emphasizing the hypothetical character of our discussion we believe that further investigation of the shape of the q-band will result in a refinement of some portions of dislocation theory as an explanation of plastic deformation.

LITERATURE CITED

[1] V.N. Rozhanskii, Iu.V. Goriunov and E.D. Shchukin, Physics of Metals and Metallography (USSR) 3, 113 (1956).

[2] E.D. Shchukin, N.V. Pertsov and V.N. Rozhanskii, Experimental Instruments and Techniques (USSR) 2, 98 (1957).

[3] A.H. Cottrell, Dislocations and Plastic Flow in Crystals (Oxford, 1953).

[4] T. Broom, Adv. in Phys. 3, 27 (1954).

[5] G. Leibfried and P. Haasen, Z. Physik 137, 67 (1954).

[6] N.F. Mott, Proc. of the Intern. Conf. Theoret. Phys. (Kyoto-Tokyo, 1954), p. 565.

Received April 3, 1957

Division of Dispersed Systems,
Institute of Physical Chemistry,
Academy of Sciences, USSR and
Department of Colloidal Chemistry,
M.V. Lomonosov Moscow State University

SOVIET PHYSICS – "DOKLADY" VOL. 2 NO. 4 JULY-AUGUST, 1957

(Translation of all papers in the "Physics" Sections of the Proceedings of the
Academy of Sciences of the USSR, Vol. 115, Nos. 1-6, Published by the
American Institute of Physics, May, 1958).

CONTENTS

		Russian	
	Page	Issue No.	Page
Measurement of the Primary Cosmic-Ray Flux at 31° N Latitude. K. I. Alekseeva, S. I. Brikler, N. L. Grigorov F. D. Savin and N. A. Shcherbakov	303	1	71
On the Lines Associated with the $L\alpha_{1,2}$ and $L\beta_1$ Lines of the Germanium Spectrum. G. P. Borovikova and M. I Korsunsky	308	1	75
On New Possibilities to Raise the Efficiency of Charged-Particle Accelerators. E. M. Moroz	311	1	78
Isotope Separation on the Passage of an Atomic Beam Through a Region of Ionization. K. D. Sinelnikov B. G. Safronov, G. G. Aseev and Yu. S. Azovsky	313	1	80
Inelastic Interaction Cross Section of Carbon Nuclei for Protons Above 7 Bev. K. I. Alekseeva and N. L. Grigorov	317	2	259
Identification of the Internal Conversion Spectrum of the Long-Lived Isotopes Eu^{152} and Eu^{154}. B. V. Bobykin and K. M. Novik	322	2	263
Theory of Gas Flow in a Porous Body Near the Knudsen Region. Pseudomolecular Flow. B. V. Deriagin and S. P. Bakanov	326	2	267
Sound Diffraction by a Thin Bounded Elastic Cylindrical Shell. L. M. Liamshev	332	2	271
On the Theory of Concentration Quenching of Fluorescence in Solutions. B. Ia. Sveshnikov	336	2	274
On the Theory of the Decay of a Quasi-Stationary State. L. A. Khalfin	340	2	277
On the Modes of Plasma Oscillations in a Magnetic Field. S. I. Braginskii	345	3	475
An X-Ray Study of the Effect of Mechanical Stress on the Structure of Polycrystalline Barium Titanate. I. G. Ismailzade	350	3	479
Coloration of $BaTiO_3$ Single Crystals. M. S. Kosman and E. V. Bursian	354	3	483
The Microwave Spectrum of 1,2-Fluorochloroethane. I. A. Mukhtarov	357	3	486
The Natural Shape of Energy Levels. B. I. Stepanov and P. A. Apanasevich	359	3	488
Concentration Dependence of the Sign of Birefringence in a Streaming Polymer Solution. E. V. Frisman and E. N. Arkhipova	363	3	491
The Interaction Between Lead Nuclei and Cosmic Ray Protons at about 10^{10} ev. L. T. Baradzei, V. I. Rubtsov Iu. A. Smorodin, M. V. Solov'ev, B. V. Tolchakev and Z. I. Tulinova	367	4	685
The Interaction of Molecular and Lattice Vibrations in Crystals and the Infra-Red Spectrum. E. F. Gross and A. A. Shultin	371	4	689
Near-Electrode Effects in Alkali-Halide Crystals at High Temperatures. M. S. Kosman and V. F. Pisarenko	375	4	693
Lowest Excited Levels of Axially Symmetric Even-Even Nuclei. G. F. Filippov	378	4	696

CONTENTS (Continued)

	Page	Russian Issue No.	Russian Page
Calculation of the Magnetization of a Uniaxial Ferrite at Low Temperatures. L. N. Iakovlev	381	4	699
Dispersion Relations for Weak Interactions. N. N. Bogoliubov, S. M. Bilen'kii and A. A. Logunov	384	5	891
On the Theory of the Polarization of Fluorescence of Solutions. P. I. Kudriashov and B. Ia. Sveshnikov	387	5	894
The Change of Conductivity of KBr in Strong Fields at Temperatures from 300° to 450°. V. F. Pisarenko	391	5	898
On the Temperature Dependence of the Heat Capacity of Solids. N. N. Sirota	393	5	901
Experimental Studies of the Alpha Decay of Medium-Weight Nuclei. Iu. A. Surkov.	396	5	904
Matrix Algebra of the Theory of Spin 3/2 Particles. E. E. Fradkin	399	5	907
The Optical Anisotropy of Some Chain Molecules Containing Benzene Rings. V. N. Tsvetkov and S. Ia. Magarik	403	5	911
On the Lateral Distribution of Particles in an Electron-Photon Shower. V. V. Guzhavin and I. P. Ivanenko	407	6	1089
On the Interaction of High-Energy Particles with Nuclei. A. P. Zhdanov, I. B. Berkovich, K. I. Ermakova, F. G. Lepekhin, N. V. Skirda and Z. S. Khokhlova.	412	6	1093
On a Method of Calculating Quantum Distribution Functions. R. L. Stratonovich	416	6	1097
On the Change of Electrical Resistivity in Elementary Dislocation Generation. E. D. Shchukin, V. N. Rozhanskii and Iu. V. Goriunov	420	6	1101

SIGNIFICANCE OF ABBREVIATIONS MOST FREQUENTLY ENCOUNTERED IN SOVIET PHYSICS PERIODICALS

AN SSSR	*Academy of Sciences, USSR*
FIAN	*Physics Institute, Academy of Sciences USSR*
GITI	*State Scientific and Technical Press*
GITTL	*State Press for Technical and Theoretical Literature*
GOI	*State Optical Institute*
GONTI	*State United Scientific and Technical Press*
Gosenergoizdat	*State Power Press*
Gosfizkhimizdat	*State Physical Chemistry Press*
Gozkhimizdat	*State Chemistry Press*
GOST	*All-Union State Standard*
Goztekhizdat	*State Technical Press*
GTTI	*State Technical and Theoretical Press*
GUPIAE	*State Office for Utilization of Atomic Energy*
IF KhI	*Institute of Physical Chemistry Research*
IFP	*Institute of Physical Problems*
IL	*Foreign Literature Press*
IPF	*Institute of Applied Physics*
IPM	*Institute of Applied Mathematics*
IREA	*Institute of Chemical Reagents*
ISN (Izd. Sov. Nauk)	*Soviet Science Press*
IIaP	*Institute of Nuclear Studies*
Izd	*Press (publishing house)*
KISO	*Solar Research Commission*
LETI	*Leningrad Electrotechnical Institute*
LFTI	*Leningrad Institute of Physics and Technology*
LIM	*Leningrad Institute of Metals*
LITMiO	*Leningrad Institute of Precision Instruments and Optics*
Mashgiz	*State Scientific-Technical Press for Machine Construction Literature*
MATI	*Moscow Aviation Technology Institute*
MGU	*Moscow State University*
Metallurgizdat	*Metallurgy Press*
MOPI	*Moscow Regional Institute of Physics*
NIAFIZ	*Scientific Research Association for Physics*
NIFI	*Scientific Research Institute of Physics*
NIIMM	*Scientific Research Institute of Mathematics and Mechanics*
NII ZVUKSZAPIOI	*Scientific Research Institute of Sound Recording*
NIKFI	*Scientific Institute of Motion Picture Photography*
OIIaI	*Joint Institute of Nuclear Studies*
ONTI	*United Scientific and Technical Press*
OTI	*Division of Technical Information*
OTN	*Division of Technical Science*
RIAN	*Radium Institute, Academy of Sciences of the USSR*
SPB	*All-Union Special Planning Office*
Stroiizdat	*Construction Press*
URALFTI	*Ural Institute of Physics and Technology*

NOTE: Abbreviations not on this list and not explained in the translation have been transliterated, no further information about their significance being available to us.—*Publisher.*

The expanded program of the American Institute of Physics comprises translation of four leading Soviet physics journals, as listed below. These translations, by competent, qualified scientists, provide all research laboratories and libraries with accurate and up-to-date information of the results of research in the U.S.S.R.

Soviet Physics — Technical Physics

A translation of the "Journal of Technical Physics" of the Academy of Sciences of the U.S.S.R. The translation began with the 1956 issues, and is being continued. Twelve issues per year, approximately 3,000 Russian pages. Annually $90.00 domestic, $95.00 foreign.

Soviet Physics — Acoustics

A translation of the "Journal of Acoustics" of the Academy of Sciences of the U.S.S.R. The translation began with the 1955 issues. Four issues per year, approximately 400 Russian pages. Annual price, beginning with the 1957 issues, $12.00 domestic, $14.00 foreign. Prices for each volume prior to 1957, $20.00 domestic, $22.00 foreign.

Soviet Physics — "Doklady"

A translation of the "Physics Section" of the Proceedings of the Academy of Sciences of the U.S.S.R. The translation began with the 1956 issues. Six issues per year, approximately 900 Russian pages. Annually $25.00 domestic, $27.50 foreign.

Soviet Physics — JETP

A translation of the "Journal of Experimental and Theoretical Physics" of the Academy of Sciences of the U.S.S.R. Translation began with the 1955 issues. Twelve issues per year, approximately 4,000 Russian pages. Annual price, beginning with the 1957 issues, $75.00 domestic, $79.00 foreign. Prices for back volumes may be obtained from the American Institute of Physics upon request.

Subscriptions should be addressed to the American Institute of Physics, 335 East 45th Street, New York 17, N. Y.